HOMOGENISATION OF TITANIUM - 6 ALUMINIUM - 4 VANADIUM (Ti-6Al-4V) POWDER BLENDS DURING SINTERING

Varaidzo Amanda Churu

A dissertation submitted to the Faculty of Engineering and the Built Environment in full fulfilment of the requirements for the degree of Master of Science in Materials Engineering

December 2022

PLAGIARISM DECLARATION

I know the meaning of plagiarism and declare that all the work in the dissertation, except for that which is properly acknowledged, is my own both in concept and execution. The acknowledgements were performed according to the *Energy materials: materials science and engineering for energy systems* style referencing. This thesis has been submitted to the Turnitin module and I confirm that my supervisor has seen my report and any concerns revealed by such have been resolved with my supervisor.

Name: Varaidzo Churu

Student number: CHRVAR001

Signature: Signed by candidate

Date: 06/02/2022

ACKNOWLEDGEMENTS

The financial assistance of the National Research Foundation (NRF), the Council for Scientific and Industrial Research (CSIR) and the Department of Science and Technology (DST) towards this research is hereby acknowledged. Opinions expressed and conclusions arrived at, are those of the author and not necessarily to be attributed to the aforementioned.

The author would like to acknowledge the following for their help and support throughout her studies:

- To my parents and siblings for their love and support throughout the undertaking of this project.
- To my supervisor, Professor RD Knutsen, for his support and guidance with the project.
- To the students and staff at the Centre for Materials Engineering (CME) for their help.
- To the UCT mechanical engineering workshop for their assistance with many aspects of this project.
- I would also like to convey my sincere gratitude to Dr Deborah Blaine from the University of Stellenbosch, for her help and assistance during this project.
- To the Electron Microscope Unit (EMU) for all their assistance with the SEM.
- To the Department of Mechanical Engineering at the University of Cape Town for affording me the opportunity to undertake the current research.

DEDICATION

To my beloved parents:

Mr Zvinechimwe and Mrs Miriam Churu

Thank you for your material, emotional and spiritual support.
Most importantly for your unconditional love.

ABSTRACT

Titanium alloys have received significant attention in recent years primarily within the aerospace sector due to their superior material properties, high strength to weight ratios and high resistance to corrosion. However, high processing costs associated with the alloys have hindered their usage in other fields such as the automotive industry. The powder metallurgy (PM) method is an emerged method that may lower processing costs. The blended elemental (BE) route to produce titanium alloys has been identified as the cheapest process by which the PM process can be applied.

The powder metallurgy method has a few limitations, one of the associated limitations is that elemental powder blends must be homogenized in terms of chemical composition for them to meet the same quality standards as ingot processed titanium alloys. To combine cost-effectiveness with good mechanical property attainment, the sintering process should be optimized at the lowest temperatures and shortest duration. In the current study, Ti-6Al-4V alloys were synthesized by the blended elemental press and sinter powder metallurgy route. This was carried out using three different powder blends comprising of Ti (100µm) and TiH_2 (63µm) as base powders, blended with either Al (75µm), V (25 µm) or a 60Al-40V (40µm) master alloy powder (MA). The powder blends made from the powders were namely TiH_2 + MA, TiH_2 + Al+ V and CpTi + MA. The average particle sizes in each case are indicated in parentheses.

As a precursor to mechanical property measurement, the relative degree of homogenization that occurs during sintering of powders shaped by uniaxial pressing was investigated at sintering temperatures of 1000 - 1350^{o}C under vacuum at times ranging from 0.5 hours to 4 hours. The homogenization was evaluated via scanning electron microscopy (SEM) and energy dispersive X-ray analysis (EDS) and X-ray diffraction (XRD). The density was measured using the Archimedes method. The EDS approach was used at a specific length scale (100µm× 100µm) to assess the degree of elemental mixing that occurs during the limited sintering exposure. A combination of SEM/EDS analysis and XRD was successfully used to measure homogenization progress of the powder blends.

The different powder blends reached different levels of homogeneity at different temperature and time. The TiH_2 + MA powder blend became fully homogeneous after sintering at 1350°C for 2 hours with a relative density of 98% ± 1. Three stable beta peaks coinciding with the wrought titanium spectra were also shown after sintering at 1350°C for 2 hours . The CpTi + MA powder did not reach full homogeneity as the TiH_2 + MA powder blend at any of the sintering temperature and times but after sintering at 1350°C for 4 hours the samples demonstrated reasonable homogeneity, although still significantly less homogeneous than the wrought alloy. There were some peaks that had peak broadening and peak splitting also shown that were closely related to the beta peaks of the wrought titanium shown in the XRD spectra but were not fully stable and a relative density of 97% ±1. The TiH_2 + Al + V powder blend also did not reach homogeneity at any of the sintering temperature and time, there was however an improvement in diffusivity of aluminium and vanadium after sintering at 1350°C for 4 hours, with a relative density of 96% ± 1, no beta peaks were shown in the XRD spectra.

The factors that mainly affected homogeneity besides time and temperature were the type of base powder as well as alloying elements. From the experiments, it was noticed that when Al and V are added as elemental alloys there was a 2-hour increase in sintering time for relative homogeneity to improve due to aluminum diffusing faster than vanadium at lower temperatures and stabilizing the alpha titanium phase. Whereas when vanadium and aluminum were added as a master alloy it resulted in a faster diffusion of both elements, therefore, reaching homogeneity earlier. The combination of TiH_2 + MA powder blend had the lowest temperature and time reaching homogeneity at 1350°C after 2 hours of sintering.

SYMBOLS AND ACRONYMS

α	Alpha phase
β	Beta phase
SEM	Scanning electron microscope
EDX/EDS	Energy Dispersive X-Ray spectroscopy
BEPM	Blended Elemental Powder Metallurgy

Table of Contents

LIST OF FIGURES

LIST OF TABLES

CHAPTER 1: INTRODUCTION

1.1 Subject of dissertation

The subject of this dissertation is:

1. To compare the progress in homogenization for different powder blends during the solid-state sintering operation.
2. To determine the process route that leads to optimum alloy homogenization during sintering whilst optimizing cost effectiveness.
3. To measure density development to obtain near theoretical density for mechanical property improvement.

1.2 Background to research

Ti-6Al-4V is the most widely used titanium alloy. It has a variety of properties namely high corrosion resistance, high strength and toughness.[1] These properties give titanium wide applications and it is therefore used in aerospace vessels, surgical instruments and pressure systems.[2] Titanium alloys are very costly; this is because the extraction and processing of titanium requires a lot of energy and therefore becomes expensive. Titanium is also 10 times more costly to machine compared to aluminum.[3] Powder metallurgy of titanium is a technology that is emerging in the processing of titanium because it introduces cost reduction. There are two types of titanium alloy powder metallurgy namely Pre-alloyed and blended elemental.[4] Pre-alloyed is made from powder that has been formed from an ingot of the specified metal alloy, whereas blended elemental is made from blending master alloy powders or elemental alloy powders with the base titanium powder. The achievement of cost-effective titanium alloys would allow their use to spread out from their limited application in the aerospace industry, into industries such as the automotive industry, where with increasing fuel prices, low weight vehicles will become a priority. This research intends to optimize the homogenization practice of Ti-6Al-4V powder blends by performing solid state sintering at different times and temperatures. All avenues are explored to reduce process cost.

1.3 Objectives of thesis

This research aims to achieve the following:

I. To create powder compacts of the different powder blends:
   - CP-Ti + Al-V master alloy
   - TiH_2 + Al +V elemental powder
   - TiH_2 +Al-V master alloy

II. Sinter the different powder blends at different conditions (time and temperature).

III. Analyze the compositional evolution of the sintered powder compacts.

IV. Measure the changes in density of the powder compacts as a result of sintering

V. Follow the progress in homogenization during the solid-state sintering.

1.4 Scope and limitations of dissertation

The pressing of the powder compacts operations was kept constant throughout the pressing of all compacts of the different blends, therefore the influence of this step was not measured. The solid-state sintering was performed at temperatures of 1000^oC-1350^oC and times ranging 0.5 - 4 hours, with furnace cooling, in the same furnace always. The effect of the changes in time and temperature for the different blends was evaluated using X-Ray Diffraction (XRD) and Energy Dispersive X-Ray spectroscopy (EDS). The relative densities calculated in this dissertation were calculated as a percentage of the theoretical density of ($4.43g/cm^3$) and the Archimedes principle was used to measure the density. Due to material limitations, mechanical testing was not performed on any of the powder compacts.

1.5 Plan of development

The dissertation will be organized in 7 chapters. Chapter 2 will explore the literature that has been written to support and explain the experimental procedure, results, and discussion in the following sections. Chapter 3 will describe the experimental methodology followed to obtain results. Chapter 4 will show the results obtained after sintering and analysis and the discussions that follow describing the results obtained. In Chapter 5, the conclusions of this research are given, followed by Chapter 6 with recommendations for future work and a list of references in chapter 7.

CHAPTER 2: LITERATURE REVIEW

2.1 Titanium

Titanium was first discovered in 1791 by a clergyman and mineralogist by the name William Gregor. It was only in 1910 that titanium was isolated by Matthew Hunter when he heated titanium tetrachloride with sodium. Significant quantities of titanium were produced in 1932 when Justin Kroll produced titanium by combining $TiCl_4$ with magnesium. This process was then named the 'Krolls process' and to this day it is the most widely used process in the commercial production of titanium.[2]

Titanium is the ninth most abundant element on the earth's crust following aluminum, iron and magnesium and is mostly found in ilmenite ($FeTiO_3$) and rutile (TiO_2) minerals.[51] Titanium (Ti) alloys are successfully applied in several sectors due to their outstanding properties. The exceptional combination of properties that titanium alloys exhibit, such as high strength-to weight ratio, excellent corrosion resistance, low density and good biocompatibility justifies their successful application in the aerospace, chemical, dental, and medical industries.[51]

2.2 The metallurgy of Titanium

Titanium is an allotropic element; this means that it can exist in more than one stable crystallographic form at different temperatures. In titanium two forms exist in different conditions; at room temperature titanium has a hexagonal close packed (hcp) crystal structure which is commonly referred to as the alpha phase.[5] At 888°C the titanium structure transforms from the hcp structure to a body-centered cubic structure (bcc) which is called the beta phase. The ease of plastic deformation increases from the hcp structure to the bcc structure.[5] The number of slip systems which is equal to the number of dislocation glide opportunities in a crystal lattice is only 3 for the hcp structure while it is 12 for the bcc structure.[5] This means that the hcp structure would have a higher strength compared to the bcc structure because it impedes or reduces dislocation motion.

2.3 Alloying elements in Titanium

Titanium may undergo selective addition of alloying elements to enable a wide range of physical and mechanical properties to be obtained. Alloying additions like aluminium and interstitials for example oxygen, carbon and nitrogen stabilize the alpha phase. They raise the temperature at which the alloy will be transformed to the beta phase which is namely the beta transus temperature.[1] Chromium, niobium, copper, iron, manganese, molybdenum, tantalum and vanadium stabilize the beta phase by lowering the temperature of transformation from alpha to beta.[1] Tin and zirconium behave as neutral solutes and do not affect the transformation temperature but rather act as strengtheners of the alpha phase. Therefore, titanium alloys can be separated into four different categories depending on their alloy composition, namely:

- Alpha
- Near-Alpha
- Alpha-Beta
- Beta

2.3.1 Alpha alloy

This is an alloy with an α phase and does not form β when it is heated. These alloys exhibit good weldability.[6] They usually have high aluminium content which assures high strength characteristics and oxidation resistance at high temperatures. These alloys cannot be heat treated to give higher strength as they are single phase.

2.3.2 Alpha-beta alloy

The addition of beta-stabilizing alloying elements causes some beta phase to be present below the beta transus temperature, down to room temperature resulting in a two-phase system.[7] Even small amounts of beta stabilizers will stabilize the beta phase at room temperature. A group of alloys designed with high amounts of alpha stabilizers and with a small amount of beta stabilizers are alpha-beta alloys, usually called high alpha or near alpha alloys.[7] As larger amounts of beta stabilizers are added, a higher percentage of the beta phase is retained at room temperature. Such two-phase titanium alloys can be significantly strengthened by heat treatment quenching (which would form martensite) from a temperature

high in the alpha-beta range, followed by an aging cycle at a somewhat lower temperature. The transformation of the beta phase which would normally occur on slow cooling is suppressed by the quenching. The aging cycle causes the precipitation of fine alpha particles from the metastable beta, imparting a structure that is stronger than the annealed alpha-beta structure.[7]

2.3.2.1 Titanium 6- Aluminum 4- Vanadium

The most popular and widely used α + β titanium alloy is Ti-6Al-4V which consists of 6 wt.% aluminium, 4 wt.% vanadium and the balance being made up of titanium.[1] It is an alloy that has been widely used in the aerospace industry due to its high specific strength to weight ratio.[4] Figure 1 below shows a pseudo binary phase diagram for Ti-6Al and V. The Beta transus temperature is shown at 1000^{o}C, with the dashed line on the 4wt. % V composition. When Ti-6Al-4V is an α + β alloy, at temperatures below the β transus temperature, the alloy exists as a mixture of both α and β phases. Vanadium has a higher solubility in the BCC β phase titanium while aluminium is more soluble in the HCP α phase, elemental partitioning exists between equilibrium α and β phases in the alloy, meaning the β phase will be rich with vanadium and the alpha phase will be depleted in vanadium as compared to the bulk composition of the alloy.[7] The opposite would be true for aluminium.

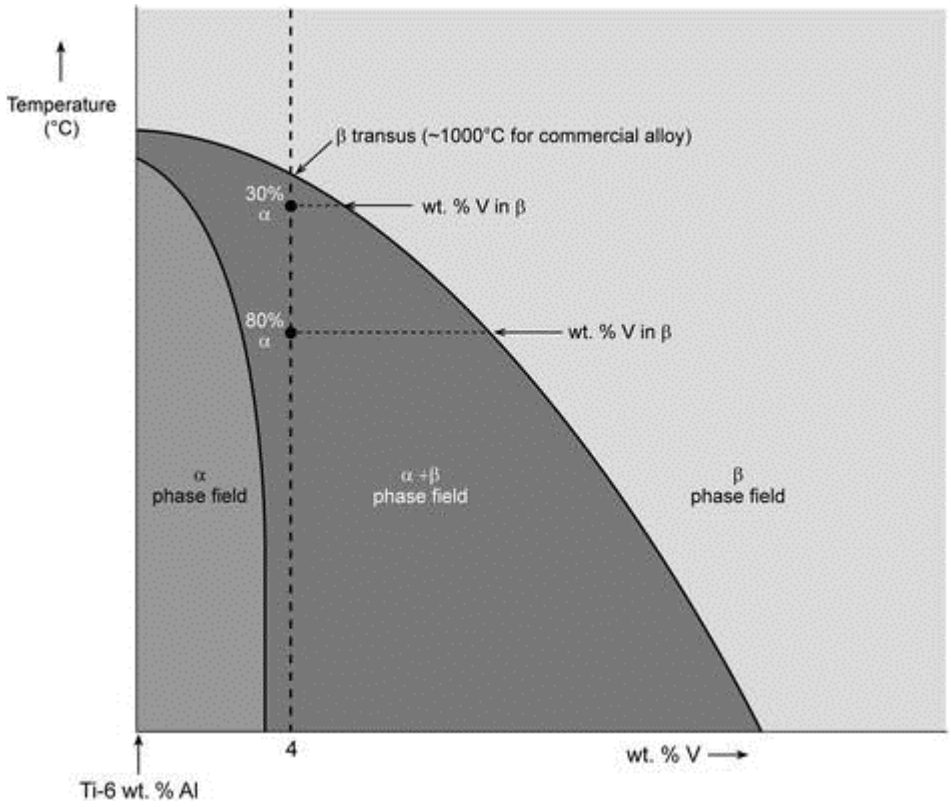

Figure 1: The pseudo binary phase diagram of Ti-6Al and V [7]

2.3.3 Beta alloy

β-Alloys have more β-stabilizer and less α-stabilizer than α/β-alloys. The alloys have high hardenability with the β-phase being retained completely during air cooling of thin sections and water quenching of thick sections. These alloys have good forgeability and good cold formability in the solution-treated condition.[8] After solution treatment, aging is performed to transform some β-phase to α-phase. The strength level of these alloys can be greater than that of α/β-alloys, a result of finely dispersed α-particles in the β-phase. These alloys have relatively higher densities, and generally lower creep strengths than the α/β-alloys. The fracture toughness of aged β-alloys at a given strength level is generally higher than that of an aged α/β-alloy, although crack growth rates can be faster.[8]

2.4 Powder metallurgy

Powder metallurgy is a process of producing metal finished or unfinished objects from fine metal powders. Powder metallurgy is most chosen because it can be used to produce near net shapes. It can, however, also be used to produce material that can be further processed. For desirable mechanical properties to be achieved, final products produced through powder metallurgy should have a homogeneous chemical composition and a density greater than 98 %.[9] The press and sinter method is the most cost-effective method for production.

The steps involved are shown in Figure 2 below and consist of powder production, blending where the parent material is mixed with alloys using a mechanical blender at various speeds, compaction by cold isostatic pressing (CIP), in which the powder is subjected to equal pressure from all directions, followed by machining. Cold isostatic pressing is commonly used for parts that are too large to be pressed in uniaxial presses and that do not require high precision in the sintered state.[9] Mechanical press is when a machine tool is used to the shape of a workpiece by the application of pressure. Vacuum sintering is heating the pressed powders at a controlled pressure at different temperatures and time in a furnace. Cold work and anneal, hot isostatic press, forging and coining are all methods to further improve strength and density of the sintered powder blends.[10]

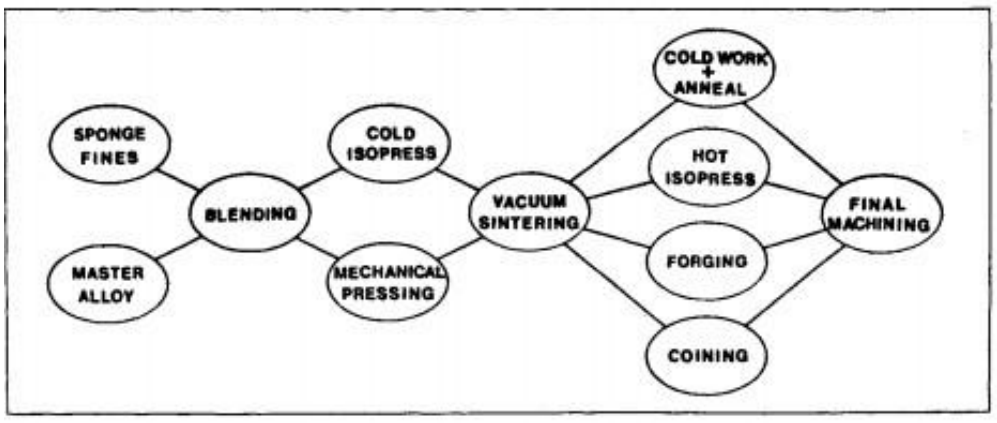

Figure 2: Process route of metal powder[10]

2.4.1. Powder Production:

The raw materials used in powder metallurgy are powders, these powders can be pure elements or pre-alloyed. The methods used in powder production are:

- Atomization which is used to produce both ferrous and nonferrous powders like stainless steel and Titanium alloy powders.
- Reduction of compounds which produces iron, copper, and tungsten.
- Electrolysis which produces copper, iron and silver powders.[11]

Due to the different process routes used to make powders, this results in the powders produced having different shapes and sizes; some of the different shapes are shown in Figure 3. Depending on the process route, individual powder particles can have very different shapes. Figure 3 shows different particle shapes and their names. The easiest particle shapes to quantify the size of is the spherical shape because it requires only a single dimension which is the diameter to completely define the particle. As the particle shape becomes more irregular, defining its size becomes more difficult.

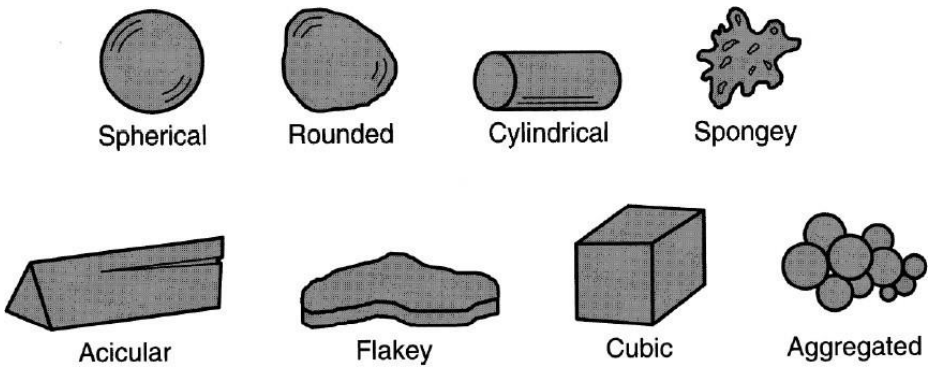

Figure 3: The different powder shapes formed during powder production[10]

Screening is the most common technique for describing the particle size of a powder and works by passing the powder through a series of screens or sieves. The screens consist of square openings created by orthogonal wires of a standard thickness (52µm) and are described by a "mesh" number, which is the number of wires in an inch perpendicular to the wire direction.[10] As such, an increasing mesh number results in smaller openings.

The powder that passes through a specific mesh is designated by a - sign and a powder that fails to pass through a mesh is designated by a + sign; for example a powder described as -200 mesh will pass through a 200-mesh screen, a powder described as +200 mesh will not pass through a 200-mesh screen and powder described as -100 +200 mesh will pass through a 100-mesh screen but not through a 200-mesh screen.[10] This technique is carried out by stacking screens with increasing mesh numbers (from top to bottom) on top of one another and placing a sample of the powder in the top screen and then agitating the screen stack for 15 minutes. Table 1 shows the different mesh size openings for mesh size.

Table 1: The size of the mesh openings in the mesh screens for different mesh size[10]

Mesh Size	Openings (µm)	Mesh Size	Openings (µm)
18	1000	100	150
20	850	120	125
25	710	140	106
30	600	170	90
35	500	200	75
40	425	230	63
45	355	270	53
50	300	325	45
60	250		
70	212		
80	180		

There are several other particle size measurement techniques available in powder metallurgy, but each has its own limitations. Table 2 classifies some of the common methods of particle size determination and their limits of applicability.

Table 2: The common methods of particle size determination and their limits of applicability[10]

Class	Method	Approximate useful size range (microns)
Sieving	Sieving using mechanical agitation or ultrasonic induced agitation and screens	44–800
Microscopy	Micromesh screens	5–50
	Visible light	0.2–100
	Electron microscopy	0.001–5
Sedimentation	Gravitational	1–250
	Centrifugal	0.05–60
Turbidimetry	Turbidimetry (light intensity attenuation measurements)	0.05–500
Elutriation	Elutriation	5–50
Electrolytic resistivity	Coulter counter	0.5–800
Permeability	Fisher sub-sieve sizer	0.2–50
Surface area	Adsorption from gas phase	0.01–20
	Adsorption from liquid phase	0.01–50

2.4.1.1 Powder Impurities

Metal powders are characterized for their chemical characteristics namely composition and purity. The chemical composition of a powder is important to know as it affects further processing such as compaction, ease of ejection and the degree of densification.[4] Chemical analysis must be able to give the amount of metallic and non-metallic impurities. The impurities may be in an elemental form or dissolved in the powder. The purity of a powder and the number of impurities depends on the production method; for example, electrolytic powders may contain dissolved oxygen or compounds containing oxygen.[4] Oxygen is the most common impurity either in the dissolved state or as compounds.[4] The need to analyse and find out the presence of impurities comes from the fact that difficulties arise during compaction because of the oxides which are abrasive, non-metallic inclusions can also lead to non-uniform sintering of the compact leading to poor properties.

2.4.1.2. Compaction

Compaction occurs to form a green compact with enough strength to withstand any further processes it will encounter. Strength of a green compact would then be related to its density, the higher the density after compaction the higher the strength.[13] There are several ways to compact powders but the most used are uniaxial compaction and cold isostatic pressing. Uniaxial compaction and cold isostatic pressing (CIP) were compared to determine which compaction method would yield the highest green density.[13] As shown from Figure 4 the two compaction methods were used on two different Titanium alloys; Ti-6Al-4V and NiTi and the CIP method yielded a higher green density for both the metal powders.

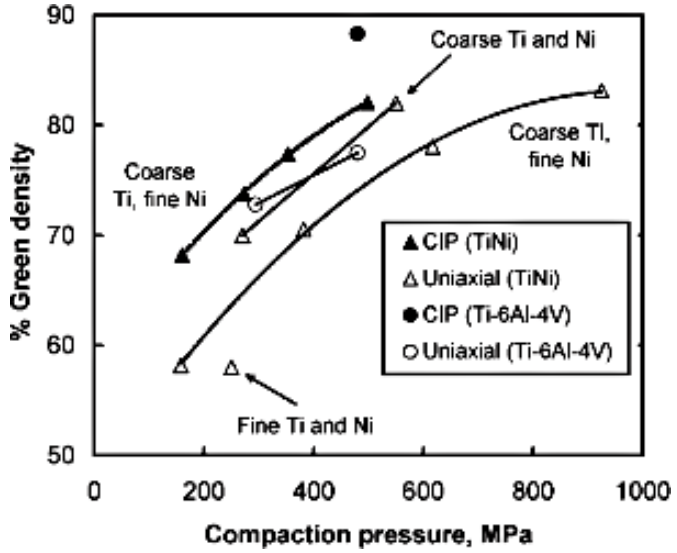

Figure 4: Effect of different methods of compaction on TiNi and Ti-6Al-4V[13]

In cold compaction the blended powders are pressed in a rigid steel or carbide die under pressure from 150-1000MPa to yield a green compact as shown in Figure 5. Figure 5 shows a force is applied to the powder to ensure a green compact is formed.

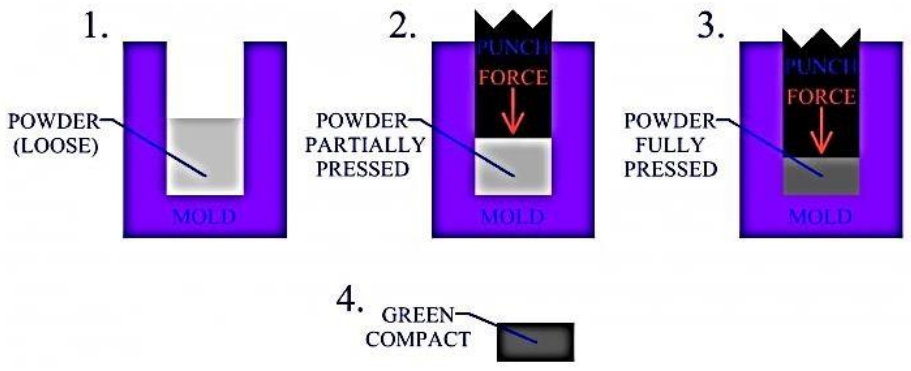

Figure 5: Illustration of the cold compaction pressing process used to form green compact[14]

As shown in Figure 6, in the first stage of powder pressing the density is increased by the rearrangement of the individual powder particles. The density is increased due to the more efficient packing of the particles as spaces, bridges and gaps are eliminated. In this initial stage there is little resistance and therefore the density of the powder rapidly increases with applied pressure. Physical contact of the powders is also made at this stage. As compression continues, increasing forces act between these contact points. Cold pressure welding, which is a type of bonding that happens during powder pressing, occurs at contact points between particles. It helps give the green compact structural integrity so that it may be processed further.

The second stage of the powder pressing then occurs (it is not distinctive on the graph in Figure 6) where plastic deformation of the particles begins and the stress between the powder particle contact points cause material deformation. The cold pressure welding results in the contact areas being increased, interlocking and the plastic flow of the powder particles then occurs. This results in a further volume decrease and an increase in the density.[10] In this stage as the pressure continues to rise the density does not increase as rapidly as in the initial stage (note how the rate of density increase drops off between the initial repacking stage and the second plastic deformation stage) because material movement is increasingly opposed by friction and the work hardening of the powder. The density will continue to increase until the maximum green density is reached. The green compact will contain pores.

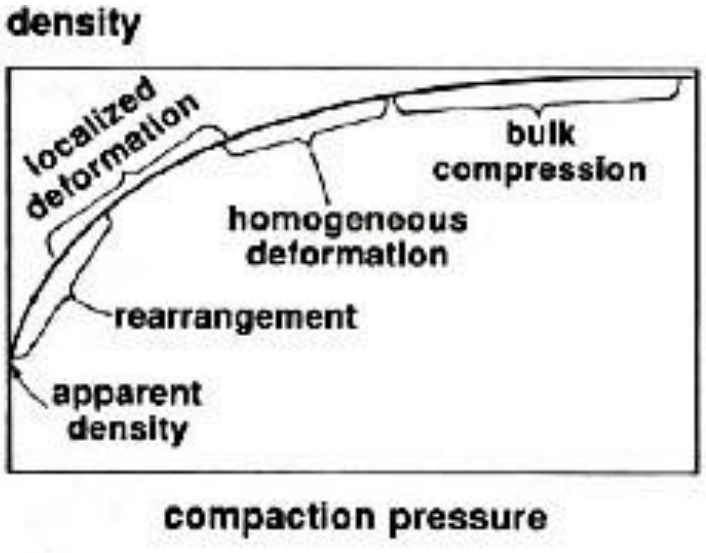

Figure 6: Stages of powder compaction that result with a green compact[10]

2.4.2 Sintering

Sintering is a heat treatment that is applied to a powder compact for it to gain strength and solidity.[11] The temperature used in sintering should be below the melting point of the major element of the powder blend to avoid liquid diffusion which causes a high porosity in the compacts. During compaction cold welds are formed which hold together neighboring powder particles which give enough green strength so that the compact may be handled. At sintering temperature, diffusion processes occur that cause necks to form and grow at these contact points formed during compaction.[13]

There are two processes that must occur before solid sintering starts which are the removal of the lubricant used during pressing by evaporation and the reduction of oxides found on the surface of oxides of the powder particles in the compact.[11] These processes and the sintering are done in one furnace by controlling the atmosphere of the furnace as well as the temperature.

2.4.2.1 Solid state sintering

Solid state sintering is the bonding and, usually, densification of particles by the application of heat below the melting point of a material. The densification occurs by the atomic diffusion of the powder particles. The main driving force for this densification to occur is the reduction in excess surface energy which is provided by the powder particles. Various transport mechanisms namely surface transport and grain boundary transportation reduce pores by transporting material from different areas.[10]

Densification results in mechanical property change like improvements in hardness, strength, toughness, physical properties like electrical, thermal conductivity and magnetic properties. The process of sintering only stops when the free surface energy of the system is zero; this is when the full densification would have occurred. To achieve low surface energy, high energy solid-vapor interfaces are replaced with low energy solid-solid interfaces which must be maximized to prevent grain growth.

The theory of sintering is shown for spherical particles in figure 7. The first step is for contacting particles to bond together, forming a neck between them. This bond between the

particles will enlarge as sintering progresses. If infinite time is allowed, the theory suggests that the two spheres will completely coalesce into a single sphere, having a diameter 1.26 times that of the original particles.[10]

In a green compact, any individual powder particle has several contacts with neighbouring particles and bonds will develop between all of them. Grain boundaries will initially form along the particle boundaries, replacing the solid-vapor interface and during the latter stages of sintering, when porosity is less, it is common for these grains to grow. The rate of sintering varies greatly over the process. The initial rate of sintering is quick and involves rapid growth of the interparticle neck. Later, when grain growth is occurring, isolated porosity can hinder the grain growth and slow the sintering process. The final stage of sintering will feature isolated spherical pores which, if filled with gas, will limit the final attainable density; thus, vacuum sintering can produce high final densities.[10]

Pore elimination occurs as powder compacts are sintered for longer or at increasing temperatures. Figure 8 shows how the density of the compacts increases with the sintering temperature. As shown in Figure 8 the green specimens that were not exposed to heat maintained a theoretical density of 70% whereas the density of the sintered specimens increased with increase in sintering temperature. There was an increase in density because with increase in temperature surface diffusion was enabled which resulted in pore elimination and subsequent increase in density.

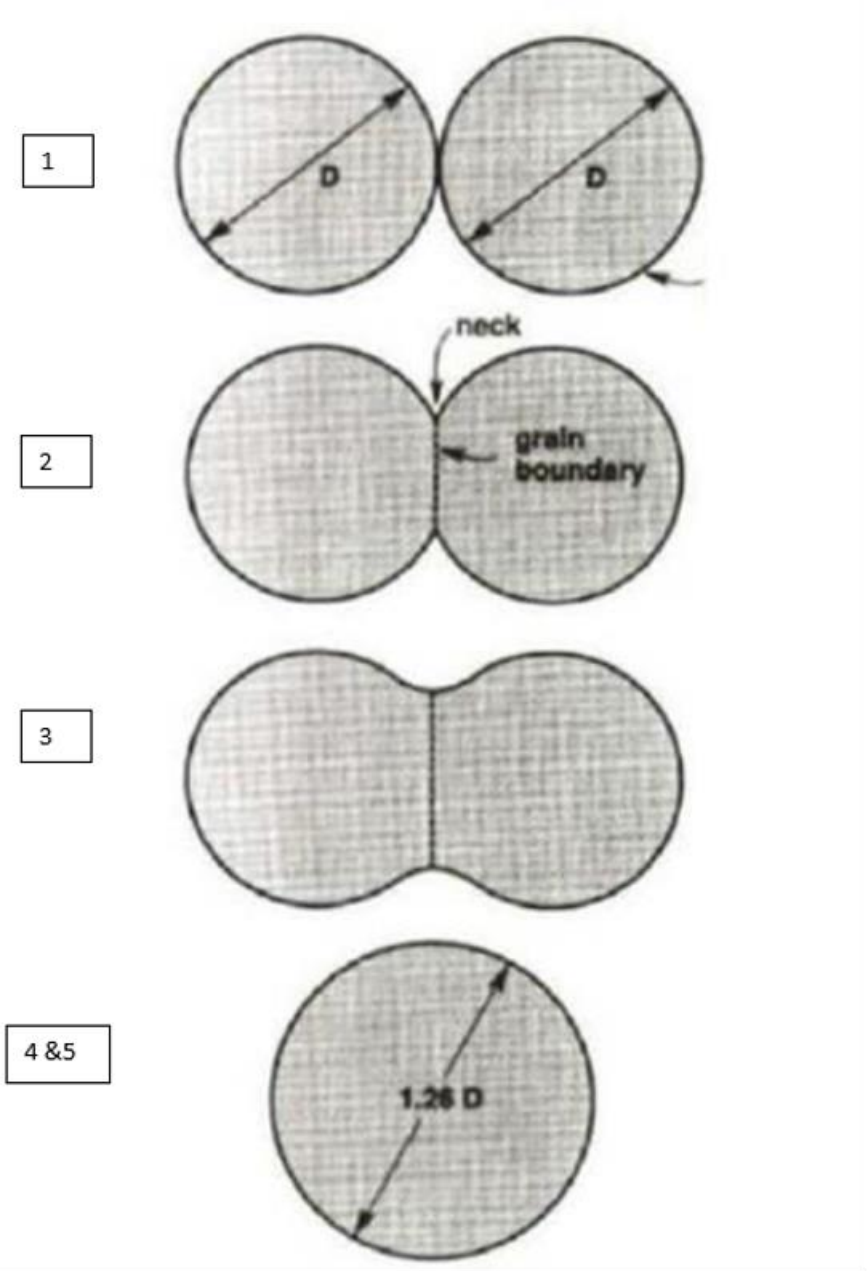

Figure 7: The two-sphere sintering mechanism illustrates various stages of metal powder sintering can be classified in the following sequence: 1) initial bonding; 2) neck growth; 3) Pore closure; 4) Densification or shrinkage; 5) Pore coarsening[10]

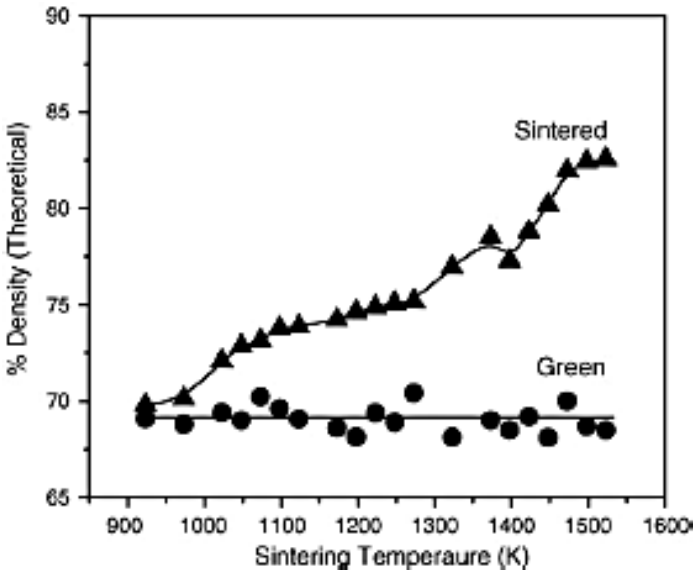

Figure 8: Density as a function of sintering temperature[12]

2.5 Titanium hydride

Studies have shown that, high sintered densities can be reached using hydrogenated titanium powder as the main element of the powder blends.[15] The use of titanium hydride instead of commercially pure titanium powder (CpTi) as the base element in powder blends with elemental powders or master alloys improves the sinter ability of the powder blends providing a higher sintered density with better homogeneity of the alloys that are made.

A study by Ivasishin et al.[15] showed that base powders with a higher hydrogen content resulted in higher sintered density. The study also showed that when there was a high initial hydrogen content the samples that were compacted with different pressures had the same sintered density.[15] In particular a hydrogen content of 3.9% resulted in attainment of nearly equal final relative densities of 98.5% (at 320 MPa) to 99% (at 960 MPa), i.e. difference in density at minimal and maximal pressures was within 0.5%.[15] This finding showed that there was no need to increase compaction pressure as the sintered density would not change when compacting titanium hydride with high hydrogen content.

Research by Ivasishin et al.[19] showed that titanium hydride had a higher sintered density compared to commercially pure titanium as shown in Table 3 and Figure 9. Lee et al.[6] discovered that this was because titanium hydride formed a uniform network of pores when compacted which easily healed upon sintering and the $TiH_2 \rightarrow Ti+2H$ phase transformation which accelerated the synthesis and caused a reduction of surface oxides by atomic hydrogen

evolution as shown in Figure 10 below, promoted better mass transfer through the inter particle boundaries. The sintering behaviour of commercially pure titanium powder has no oxide reduction occurring therefore there are more surface oxides present and reducing mass transfer.[6]

The reaction of the released hydrogen atom with the oxides decreased the free energy of the system by -200kJ/mole.[18] This decrease in energy then made the hydrogen atoms that were released, catalysts that stimulated reduction of the surface oxide, leading to the formation of oxide free boundaries shown in Figure 10 and stimulated the initiation of sintering.[6] During sintering hydrogen was evolved and therefore the end mechanical properties of the alloys were not degraded. The release of hydrogen from the compacts also resulted in shrinkage which increased the surface area and contributed to a higher rate of surface diffusion. Volume change from phase transformation also increased lattice defects which promoted volume diffusion and decreasing pore size, thereby resulting in TiH_2 powders having higher sintered densities than CpTi powder blends as shown in Figure 9.[19]

Table 3: Properties of the powder mixtures[19]

Mixture	Description	Methods of addition
1	Ti, −100 µm, 1% impurities, including 0.29%O	Elemental powders Al: 98%, −100 µm V: 99%, −100 µm
2	Ti, +100–200 µm, 0.7% impurities, including 0.29%O	Elemental powders Al: 98%, −100 µm V: 99%, −100 µm
3	TiH_2, −100 µm, 1% impurities, including 0.30%O	Elemental powders Al: 98%, −100 µm V: 99%, −100 µm
4	Ti, −100 µm, 1% impurities, including 0.29%O	Elemental powders Al: 95%, −20 µm V: 98%, −40 µm
5	TiH_2, −100 µm, 1% impurities, including 0.30%O	Elemental powders Al: 95%, −20 µm V: 98%, −40 µm
6	Ti, −100 µm, 1% impurities, including 0.29%O	Master alloy powders Ti-35Al: 98.5%, −100 µm V-25Al: 98.3%, −100 µm
7	TiH_2, −100 µm, 1% impurities, including 0.30%O	Master alloy powders Ti-35Al: 98.5%, −100 µm V-25Al: 98.3%, −100 µm

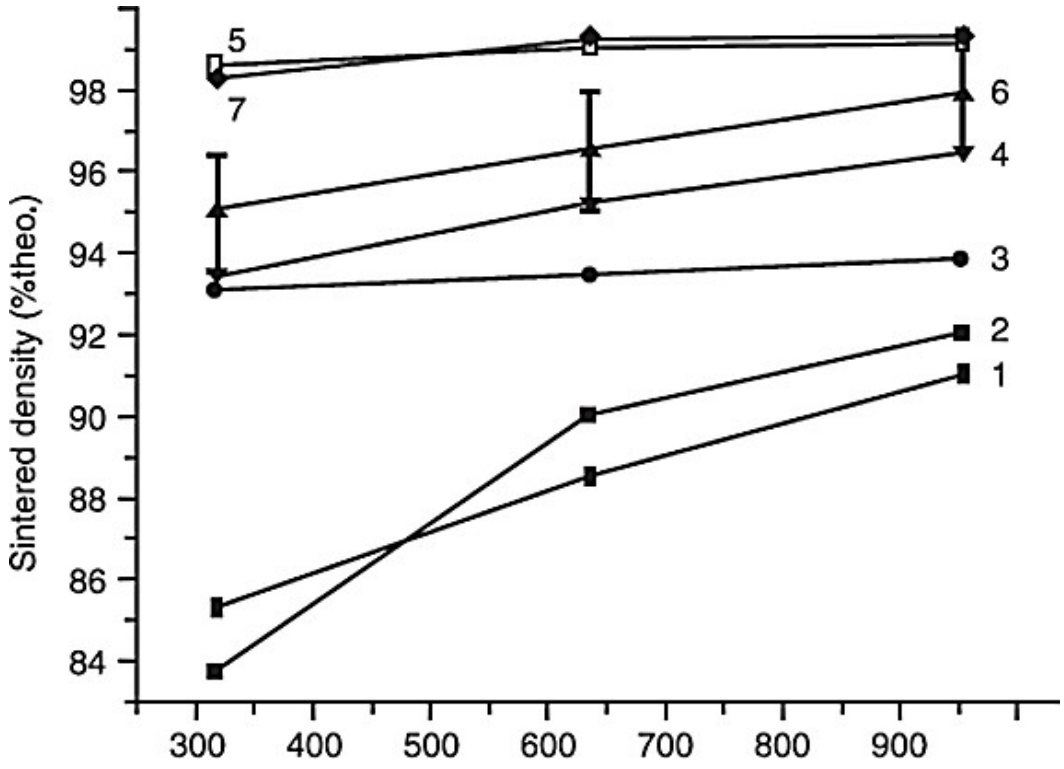

Figure 9: Comparison of sintered density of TiH_2 and CpTi [19]

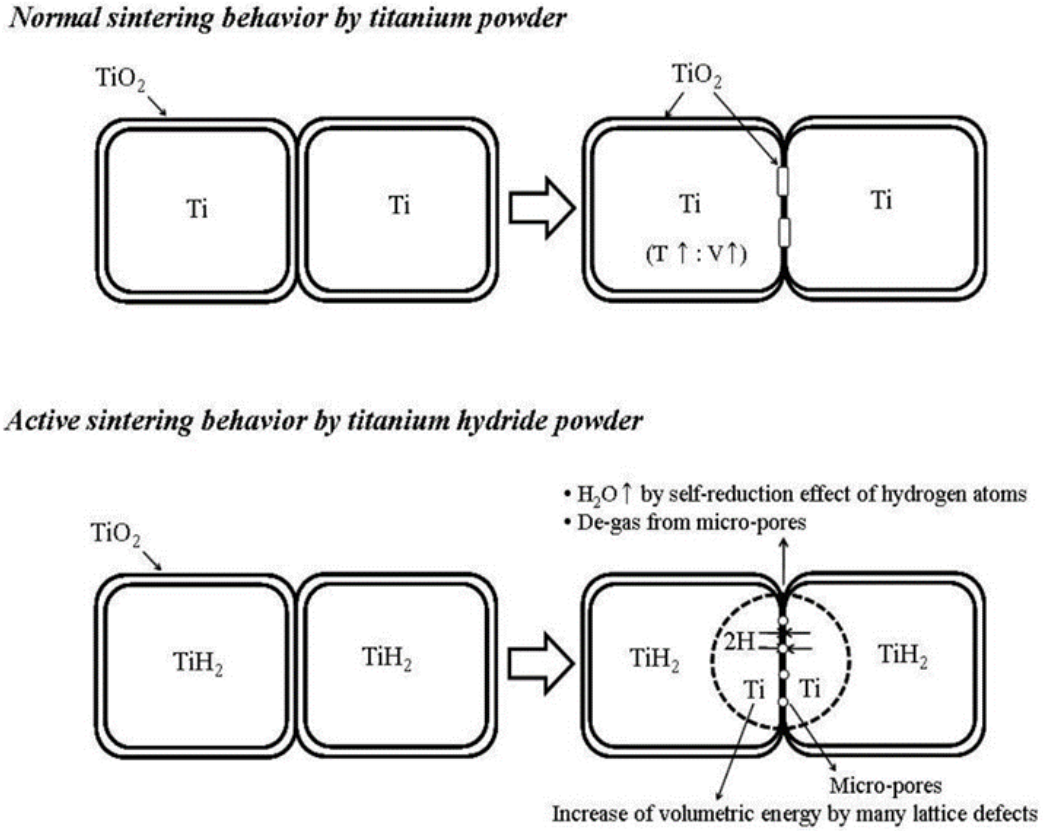

Figure 10: Comparison of the sinter ability of CpTi and TiH_2 [6]

2.6. Alloying powders

Alloying powders that are introduced play a major role on the densification of titanium-based alloys. The diffusion dissolution of alloying particles into the titanium matrix also causes formation of pores (shown by arrows) at the alloying particle or matrix interfaces as shown in Figure 11 which shows the synthesis of Ti-6Al-4V using 60%Al-40%V MA powder.[15] The difference in diffusion mobility of the Titanium atoms penetrating the master alloy and that of the Al and V atoms moving towards the Titanium matrix result in vacancies being initially formed and pores thereafter which reduce the density of the sintered compacts.

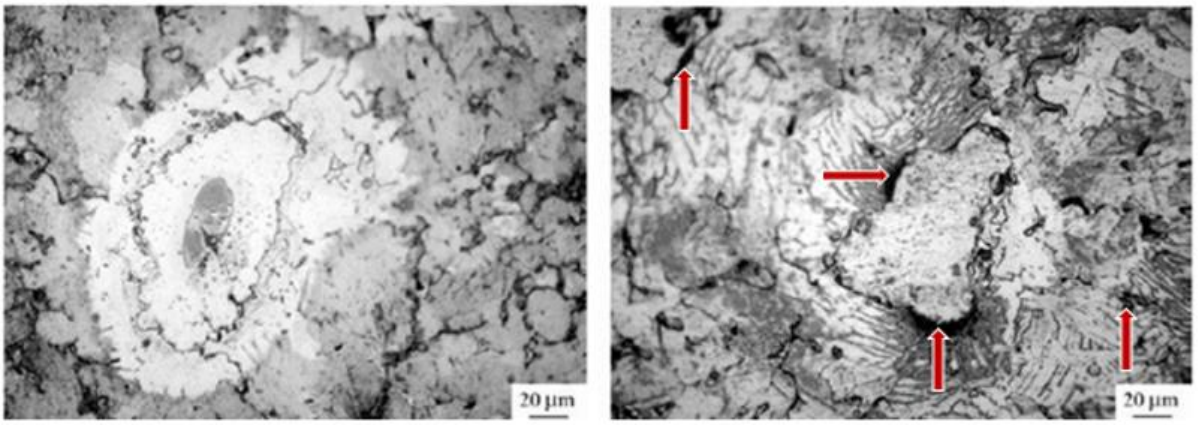

Figure 11: The microstructure evolution during dissolution of 60Al-40V in the Titanium matrix.[15]

In a study by Ivasishin et al.[13], the use of the Al-V master alloy gave a lower green density and a higher sintered density compared to elemental Al and V when producing Ti-6Al-4V. The low green density that the master alloy gives is because the master alloy has a higher hardness compared to the elemental powders.[13] The particle size of the alloying elements also plays a significant role in densification. Reducing the size of elemental Al particles is as effective as using a master alloy. This is because alloying particles are usually finer than titanium particles. If aluminium is unalloyed when the sintering temperature reaches the melting point 660^{o}C, it reacts rapidly to form $TiAl_3$ causing swelling to occur, and this should be avoided.[13]

In a study by Ivasishin et al.[13] they found out that manipulating the particle size of alloying powders had a greater impact than manipulating the size of the Titanium powder. They observed that after using finer elemental Al and V a higher sintered density of Ti-6Al-4V was

achieved and a lower sintered density and homogeneity when a coarse master alloy was used as shown in

This reiterated by another study by Ivasishin[15] where they used a fine and coarse Al: V master alloy and compared the rate of homogenization at the same temperature.

As shown in Figure 12, the compact with a finer master alloy had a faster homogenization with a nearly dense and fine-grained material already at a low temperature of 1100^{o}C after 2 hours. Whereas the compact with the coarse alloying powder had chemical inhomogeneity and large pores which would result in it requiring a longer exposure time or higher temperature leading to grain growth which is undesirable.

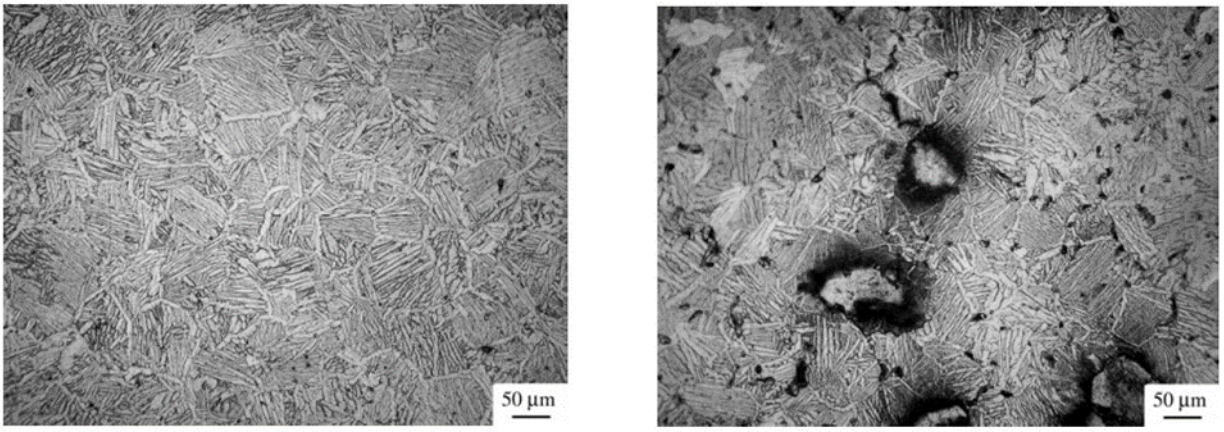

Figure 12: Microstructure of Ti-6Al-4V BEPM (Blended Elemental Powder Metallurgy) materials synthesized following the same temperature regime using a) fine and b) coarse 60%Al-40%V MA powder.[15]

2.7 Homogenization practices

The time needed for homogeneous redistribution of the alloying elements in the titanium matrix during alloy synthesis depends on a few things namely diffusion mobility of alloying elements, the type of alloying elements, their synergistic influence, and phase-composition.[15, 21] Titanium is allotropic having two phases, the alpha and beta phase. Alpha stabilizers have a higher solubility in the titanium alpha phase and are contained mainly in the alpha phase, the beta stabilizers mainly in the beta phase.

This solubility in different phases then gives rise to problems in homogenization as the introduction of alpha or beta alloying elements separately as two powders results in the stabilization of the phases having areas rich with alpha or beta elements due to diffusion of the alloying powders into the matrix.[15, 21] Homogenization is then hindered because the alpha stabilizers would have a difficult time penetrating the β phase and vice versa. Therefore, for elemental alloying powders to reach full homogenization there should be an increase in temperature to allow alpha to beta phase transformation in aluminium rich areas and very long exposure times to allow aluminium to penetrate the β phase. The increase in temperature results in high porosity because of melting of range eutectic compositions and longer exposure time would make the process expensive. [15, 21]

To avoid this the alloying elements are added as master alloys which would contain alpha and beta stabilizers. Master alloys also have their own problems; aluminium possesses a higher solubility in the alpha phase than vanadium and starts to penetrate the titanium matrix before vanadium as soon as the heating starts.[15] This then results in aluminium saturating the matrix around the master alloy and the titanium alpha phase. This leaves the β titanium unalloyed when the temperature rises above the β transus as the alpha rich areas of aluminium act as barriers for the diffusion of vanadium. This results in mutual diffusion of aluminium and titanium and a very low diffusion of vanadium as its diffusion rate is lowered as it will still have high concentrations in the locations of the former master alloy particles. The formation of a homogenous alloy will then be determined by the slow vanadium redistribution which will also require a long exposure time or increased temperature.[15] Independent of the alloying approach, homogenization of Ti-6Al-4V is controlled by the redistribution of vanadium which

only begins at 1200^{o}C. Heterogeneous microstructure is also sometimes seen due to the uneven distribution of vanadium even after heating to 1350^{o}C.[21]

Bolzoni et al.[22] conducted a study to show that the use of a master alloy was a suitable means to produce a well-developed Ti-6Al-4V alloy with the right composition. They did this by blending hydride-dehydride (HDH) elemental titanium powder with an Al:V master alloy. They exposed the Titanium powder blends at a fixed dwell time of 2 hours and used a sintering temperature ranged between 900^{o}C and 1400^{o}C. The dehydrogenation of the TiH_2, sintering and chemical homogenization of the heterogenous compacts happened in one heating cycle. This is important to note as this results in the low processing costs which this study is focusing on achieving.

Solid state diffusion is a key phenomenon in determining chemical homogenization of powder compacts which results in high temperature transformation resulting into a bulk uniform alloy. The melting point of the alloying powders had to be taken note of to prevent formation of melts and porosity that would follow. As mentioned earlier the diffusion of vanadium is the most limiting in homogenization of Ti-6Al-4V powder blends due to the huge difference in diffusion mobility. The diffusivity of titanium in vanadium is as low as $1.7x10^{-15}$ m^2/s, while vanadium in titanium is three orders of magnitude higher - $2.0x10^{-12}$ m^2 /s.[11, 23] Aluminium was introduced as master alloys only to avoid formation of melts up to 1250- 1350^{o}C.
Bolzoni et al.[22] obtained the results in Figure 13 and 14, via EDS chemical analysis. The powder blend compact was sintered up till 900^{o}C and analysed. The Al: V master alloy particle in position 1 showing 80 wt. % of V and 20 wt. % of Al which is not in relation to the starting composition of Al: V master alloy, 60:40 wt. %. This was mainly due to the fast diffusion of aluminium towards the titanium matrix compared to vanadium. This was shown by the darker zone depicted by position 2 having 30 wt. % of aluminium and 6 wt. % of vanadium. Moreover, the faster diffusion of aluminium compared to vanadium and titanium leaves some pores inside the master alloy particle due to the kirkendall effect. The content of vanadium already found in the titanium matrix, which corresponds to approximately 4.6 wt.%, justifies the presence of two-phase zones since the maximum solubility of vanadium in α-Ti is about 3wt. %.[22] At 30 µm away from the centre of the master alloy particle (position 3), it can be seen

that there is practically no diffusion of the alloying elements since their percentage is approximately zero and it is due to the lower sintering temperature which does not supply sufficient thermal energy to promote a longer diffusion range.

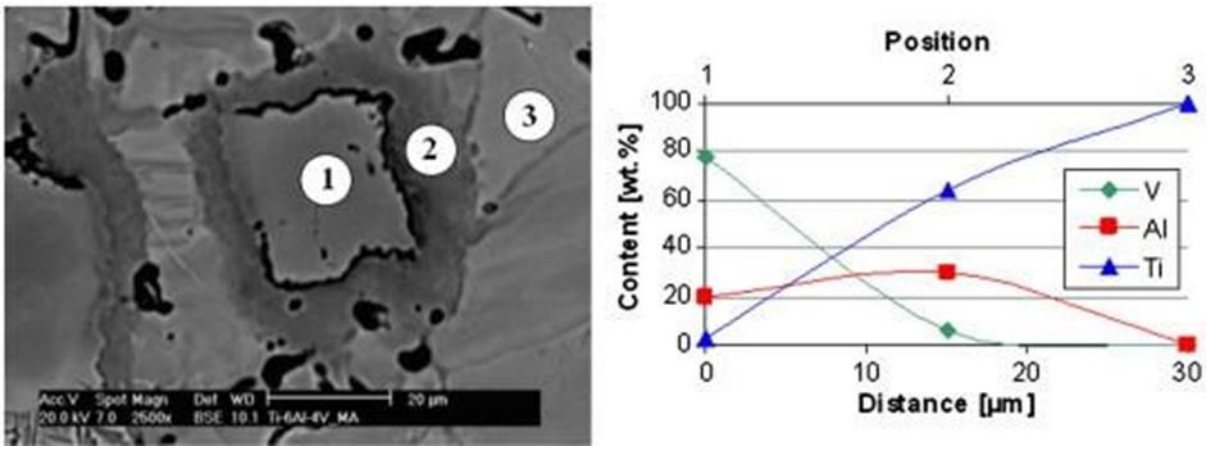

Figure 13: The diffusion of the alloying elements from an Al:V master alloy and the relative EDS composition change at 900°C.[22]

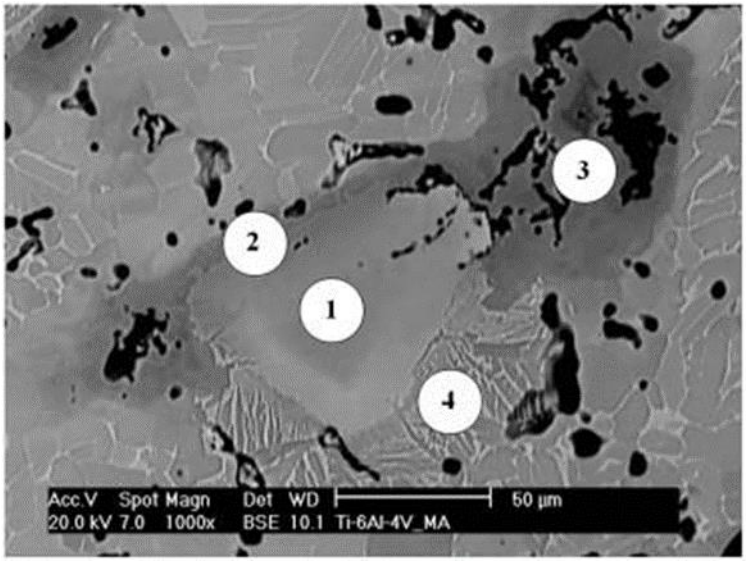

Figure 14: Diffusion of the alloying elements from an Al: V master alloy at 1000°C[22]

Figure 14 above shows that the EDS analysis of the dark grey zone (position 2 in Table 4) highlights the diffusion of the alloying elements towards the titanium matrix where the faster diffusion of aluminium is clearly visible since the percentage of aluminium is similar to that of the master alloy whilst the amount of vanadium is approximately one third. On the other side, the darkest zone (position 3), it is a more Al rich zone as the EDS chemical analysis reveals. This could correspond to the intermetallic compound that forms during the reaction between

the elemental aluminium and elemental titanium at 660 °C which is decomposing. The intermetallic that forms is the $TiAl_3$ whereas the composition found seemed to resemble much more to the Ti_3Al since the ratio in atomic percentage of Ti:Al found by EDS is approximately 65:35 and the compositional range of atomic percentage of aluminium for Ti_3Al at 1000 °C ranges between 24 and 37at%.[22] Finally, the chemical analysis of the two- phase zone (position 4) confirms that where diffusion has already taken place and the amount of vanadium is locally high enough, the β phase gets stabilized.

Table 4: EDS chemical composition of the features that characterized the microstructure of the master alloy addition Ti-6Al-4V alloy sintered at 1000°C.[22]

Position	Composition (wt.%)		
	Ti	Al	V
1 (Al:V particle)	2.34	20.38	77.28
2 (Dark grey zone)	55.45	18.96	25.59
3 (Darkest grey zone)	75.20	23.17	1.63
4 (Lamellae)	78.42	7.60	13.98

Table 5 shows the effect on homogenization with an increase in temperature where the fluctuation of the percentage of the alloying elements are influenced by the relative percentage of the α and β phase of the zone analyzed. Figure 15 shows the microstructural evolution of the CpTi-6Al-4V as the sintering temperature increased. From temperatures 900 - 1100°C, it is shown that homogeneity was not achieved. The pore structure of the sintered powder compacts has interparticle boundaries still visible, the diffusion of the alloying elements is not completed, and fine two-phase islands can be found by more spherical and isolated pores, but angular and elongated pores are still present. At 1200°C, there are less spherical pores and diffusion has occurred resulting in two phase islands disappearing. This then means that at a temperature as low as 1200°C homogeneity can be achieved and due to less pores, the mechanical properties of the sintered specimens would be good.

Table 5: The composition determined by EDS as a function of the sintering temperature for the Ti–6Al–4V alloy.[22]

Temperature (°C)	Composition (wt.%)		
	Ti	Al	V
1100	92.55	4.49	2.96
1200	90.40	6.07	3.53
1300	90.30	6.59	3.11
1400	89.64	6.21	4.15

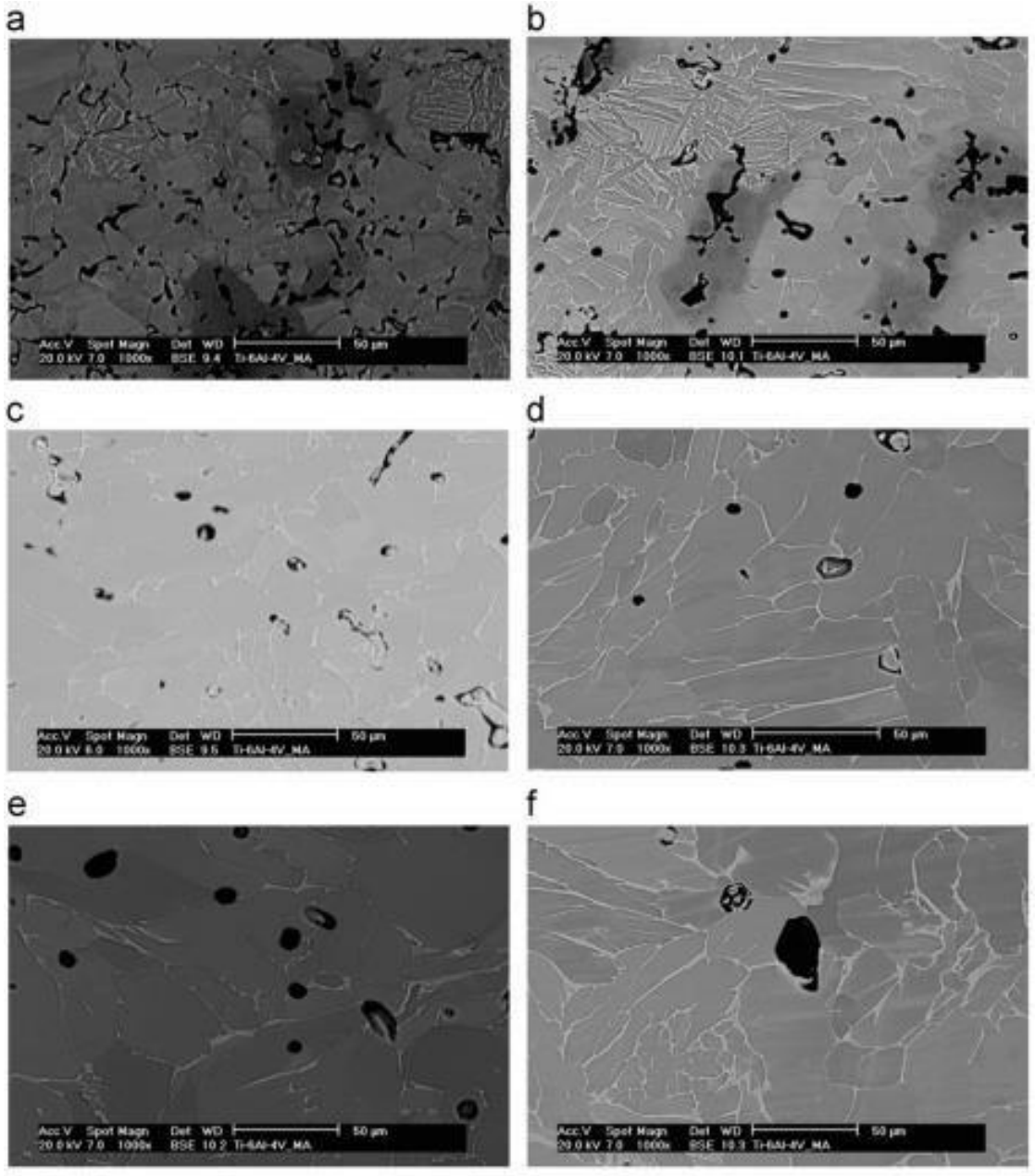

Figure 15: Microstructural evolution of the master alloy addition CpTi–6Al–4V alloy sintered under high vacuum: (a) 900°C , (b) 1000°C, (c) 1100°C, (d) 1200°C, (e) 1300°C and (f) 1400°C.[22]

3. EXPERIMENTAL METHODS

3.1 General Experimental Methodology

This chapter outlines the methods used in measuring the progress in homogenization for different powder blends, different sintering processes and influence of a deformation step.

3.1.1 Material

The three different materials used in this study were:

I. TiH_2 + Master Alloy
II. TiH_2 + Elemental Al + Elemental V
III. CpTi + Master Alloy

The details of the powders are as follows:

I. Ti (100µm) and TiH_2 (63µm) as base powders
II. Al (75µm)
III. V (25 µm)
IV. 60Al-40V (40µm) master alloy powder (MA)

3.2 Powder Processing

3.2.1 Blending and compacting

The blended elemental Ti-6Al-4V used in this work was blended from separate powders namely, CpTi, TiH_2, elemental aluminium, elemental vanadium and the 60Al40V Master Alloy. These powders were blended at Stellenbosch University (South Africa) for a total of 15 minutes at a speed of 65 rpm using a custom-made blending machine. Green compacts were produced by uniaxial pressing at the University of Stellenbosch using a custom made 200KN press. The floating die set used produced a cylindrical compact with a diameter of 10.10 mm. Specimens were made by compacting 2.60 g of powder at 375 MPa. These parameters produced samples with a mean height of 10.95 mm.

3.2.2 Sintering

The sintering conditions were chosen based on the aim of the dissertation which is to measure homogenization progress whilst optimizing cost. In current literature[22], sintering CpTi-6Al-4V (CpTi + Aluminium-vanadium Master alloy) at 1200°C for two hours gives a homogenized microstructure as well as a high relative density of 95%. The temperature ranges from 1000°C to 1350°C would be suitable to measure homogeneity.

Figure 16 shows a graphical representation of the sintering process. The heating rate of all the samples was 5 ˚C.min^{-1} followed by different dwell times in the range of 0.5 – 4 hours followed by furnace cooling to room temperature. The sintering times and temperature conditions are shown in the Table 6.

A furnace that could allow vacuum was important to use during the sintering as all the experiments performed were under vacuum. Cracker valves for safety, which open at an over pressure of 10kPa, and a correct exhaust system as seen in Figure 17 were set. All the samples underwent sintering in the vacuum of approximately 10^{-4} Pa shown in Figure 17. The horizontal vacuum sintering furnace was manufactured by ELITE TSH and was of the model 15/75/610. The heating rate used for all sintering procedures was the same and the samples were furnace cooled after the sintering treatment was complete.

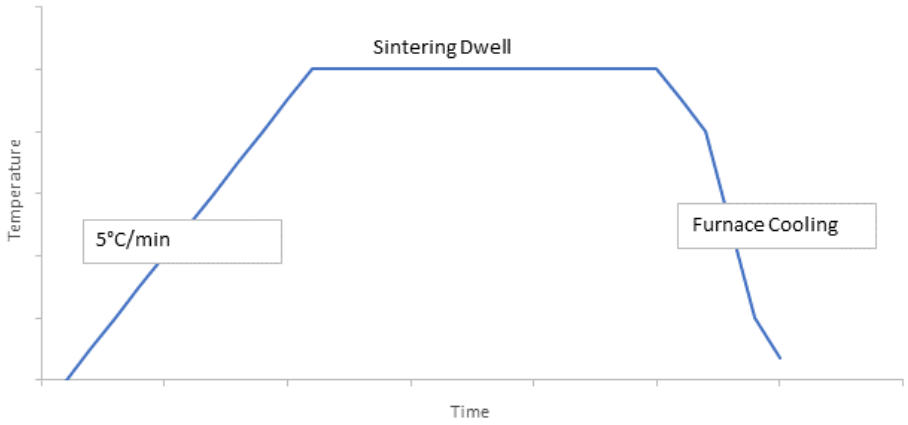

Figure 16: Graphical representation of the sintering process for all powder compacts

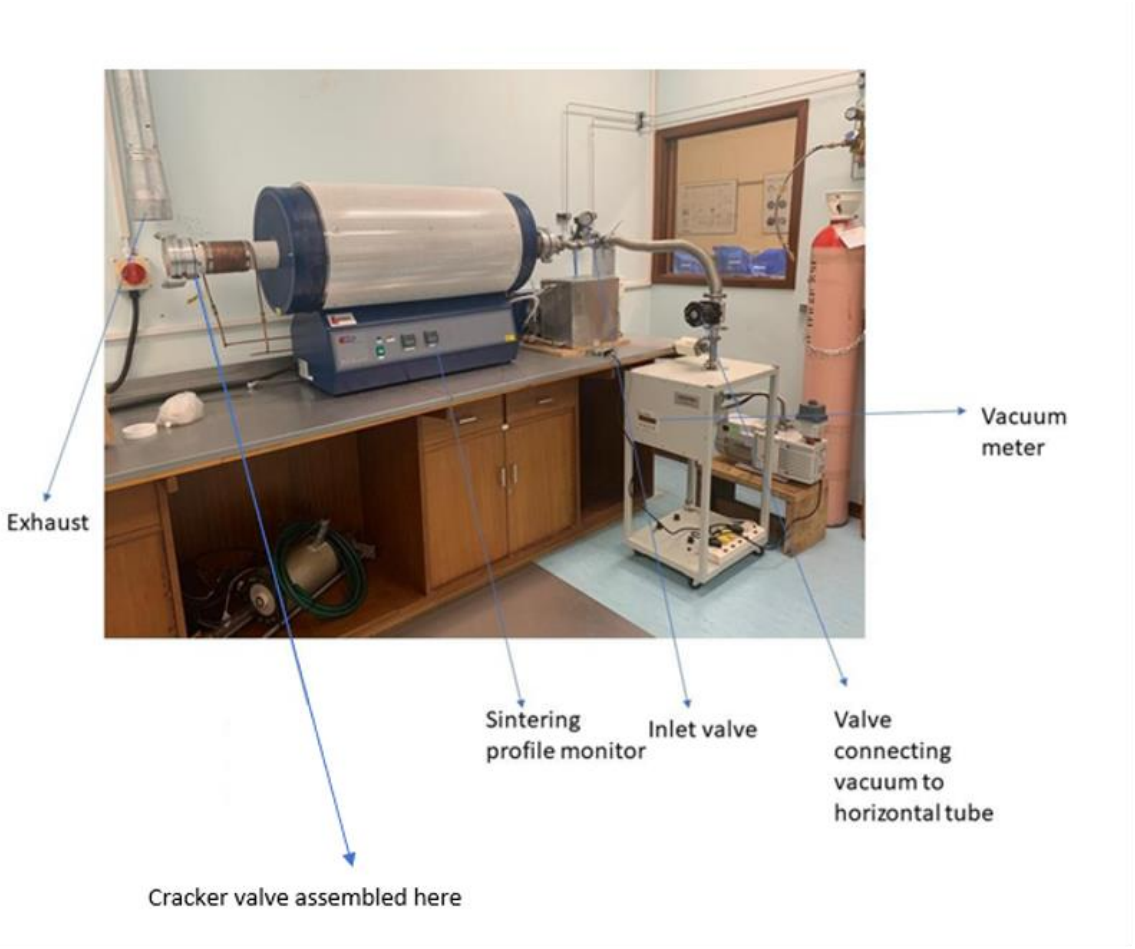

Figure 17: Vacuum Furnace set up

Table 6: The sintering temperature and time protocol

Temperature (°C)	Dwell Time (Hours)				
	0.5	1	2	3	4
1000	✓	✓	✓	✓	✓
1150	✓	✓	✓	✓	✓
1250	✓	✓	✓	✓	✓
1350	✓	✓	✓	✓	✓

3.3 Density Measurement

The density of the green and sintered samples was determined using the method described by the ASTM B962-13: Standard Test Methods for Density of Compacted or Sintered Powder Metallurgy (PM) Products Using Archimedes' Principle. Four samples of each specimen had their density measured using this method and the average is shown in the results section graphically.

The standard is used to determine the density of samples that contain less than 2% porosity. A test specimen support, as shown in Figure 18, was used for the measurements.

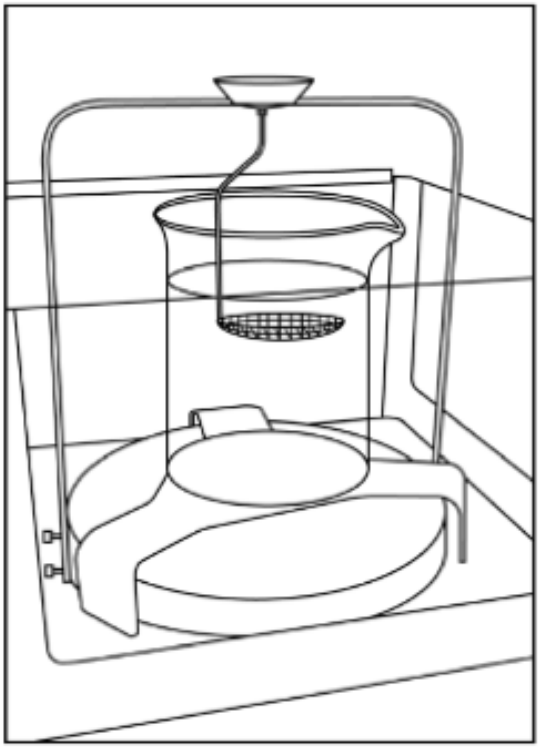

Figure 18*: Density Measurement set up*

Measurement and calculation of the density involve five steps: the mass of the sample in air (A); the mass of the oil-impregnated sample in air (B); the mass of the oil-impregnated sample and sample support structure immersed in water (C); the mass of the oil-impregnated sample support immersed in water (E); the density of the water at its specific temperature (ρ*w*). With these measurements it is possible to calculate the relative density (Ds) using the formula:

$$D_s = A\rho w / B - (C - E)$$

Equation 2

Relative density is calculated as a percentage of the theoretical full density of Ti-6Al-4V and a 4.43g/cm^3 is used for the density.

3.4 Metallographic Analysis

After sintering, the microstructures and densities of the various samples were observed and measured respectively. To perform these analyses the samples had to be prepared.

3.4.1 Hot Mounting

A Struers Labopress-3 was used to mount the samples. The samples were mounted in a thermoplastic acrylic resin for handling and polishing purposes. A 20 kN force and a temperature of 180 ˚C for seven minutes, followed by a seven-minute cooling period was used to melt, compress, and set the resin around the specimen.

3.4.2 Grinding and Polishing

Specimens were ground and polished using the technique outlined in Table 7. This method is based on the protocol recommended by Struers for the preparation of Ti-6Al-4V samples.

Table 7: The grinding and polishing protocol

Step	Grit/Pad	Speed (rpm)	Force (KN)	Time (min)	Lubricant
1	800 SIC	150	30	2:00	Water
2	1200 SIC	150	30	2:00	Water
3	MD DAC	150	30	10:00	9µm Diamond Paste
4	MD NAP	150	30	10:00	OP-S Attack Solution
5	MD NAP	150	30	5:00	Water

The attack solution used in step five of the polishing procedure was prepared as shown in Table 8.

Table 8: Attack solution constituents

Component	Volume (ml)
Hydrogen Peroxide	20
OP-S Colloidal Silica	100

3.4.3 Etching Procedure

Samples were etched for 30 seconds using Kroll's reagent and its composition is shown in Table 9. After etching, they were flushed with tap water to stop the corrosion reaction. The sample surface was cleaned with cotton wool and detergent. After cleaning, samples were rinsed with distilled water and ethanol and dried in hot air.

Table 9: Kroll's Solution

Component	Volume (ml)
50% Nitric Acid ($HN0_3$)	6
50% Hydrofluoric Acid (HF)	3
Distilled water	100

3.5 Phase Composition Analysis

3.5.1 Scanning Electron Microscopy

Phase composition analysis was carried out using scanning electron microscopy (SEM). The etched samples were analyzed using the Nova NanoSEM 230. The Nova NanoSEM 230 allows for high resolution imaging as well as energy dispersive X-ray spectroscopy (EDX) to be conducted on small samples. An accelerating voltage of 20 keV, a working distance of 5mm and multiple random selected 100 x 100µm areas were used to capture compositional information. EDX was used to measure composition in the selected are following the study that is to be discussed below by H. Naicker and R.D Knusten.[31]

The reason for not using spot analysis but using the above mentioned conditions when performing compositional analysis was based on a study by H. Naicker and R.D Knusten.[31] In the study they had 2 powder blends referred to as B1 (Blend 1) and B2 (Blend 2). B1 consisted of commercially pure titanium (CPTi) blended with commercially pure aluminium and commercially pure vanadium. B2 consisted of CPTi and a 60Al-40V master alloy (MA) powder.

SEM via EDX was used to determine the level of homogeneity achieved in the B1 and B2 sintered specimens. Their technique allowed for fast compositional analysis at different length scales depending on the size of the scanning raster selected. This provided good

opportunity to assess the degree of homogenization in sintered BE Ti-6Al-4V powder compacts. In their study, the approach to the EDX analysis was highlighted to illustrate the difference in homogenization progress for the respective powder blends.

They used accelerating beam voltage of 20 keV. Selecting the correct accelerating voltage was critical to ensure adequate intensities were obtained. The selection was dependent on the elements present in the specimen. The accelerating voltage could not be less than three times the highest excitation energy of one of the elements present.[31] In their blends the highest excitation energy belonged to vanadium (4.954 keV). A second reason for choosing this voltage was to minimize noise in the system. EDX makes use of exciting X-rays within the sample to generate a spectrum. X-ray intensities are measured by counting pulses generated in the detector by X-ray photons. There is however, a limit to the number of pulses that can be processed before the system becomes unresponsive to processing any more photons coming in (dead time). [31]It was therefore necessary to use a certain integrating time to minimize this noise. Throughput reaches a maximum, after which it begins to decrease as the input count rate increases. Energy resolution is also, however, a factor to consider, where the longer the integration time, the more smoothed out the noise is and higher the energy resolution. The study recommended that for maximum throughput rates, a count rate of >100 000 counts s^{-1} was necessary. Another way to adjust the system set-up to achieve this was to manipulate the accelerating voltage. For this investigation, 20 keV was found to satisfy the conditions mentioned above.[31]

Defining an appropriate length scale was another critical parameter that needed to be assessed. In the case of continuous solid solution alloys (single phase) the choice of length scale was quite straight-forward in that complete homogenization would ultimately be reflected when spot analyses (stationary beam) produced the same composition everywhere in the metal sample. However, the situation became more complicated when multi-phase alloys were investigated, since the inherent element partitioning between the phases influences the analysis. The challenge was to be able to measure the degree of diffusional mixing of the titanium, aluminium and vanadium powder particles whilst being able to account for the element partitioning that occurred between the α and β-phases that constitute the Ti-6Al-4V alloy. The appropriate length scale for EDX analysis is influenced by

initial powder size and the fine lamellar α/β micro-structure that evolved on cooling to room temperature.

Since spot analysis was not suitable given the two-phase nature of Ti-6Al-4V, it was first necessary to determine the minimum scan area that would exclude the effects of α/β element partitioning.

Figures 19 to 21 show the results obtained in their study[31]; they show the aluminium (Al) and vanadium (V) levels for several locations relating to each of the specific scan areas.

To investigate and refine the methodology to use in sintered specimens, a highly refined wrought Ti-6Al-4V sample was analysed under beam conditions ranging from stationary spot to dynamic area scans as large as 1.4x1.4 mm^2. The elemental indexing was limited to the element's titanium, aluminium, and vanadium.

Apart from some minor fluctuations throughout the length scale range, significant aluminium/vanadium partitioning became evident when the scan area was reduced to 10 x 10 μm^2. This length scale was consistent with the size and distribution of α/β lamellae which evolve during the Widmanstätten decomposition of the high temperature β-phase. Consequently, the minimum scan area for assessing homogenization had to be at least greater than 100 μm^2. However, they ensured that the area was not too large to average out possible inhomogeneities on a scale larger than the α/β phase partitioning. The same EDX scanning methodology was applied to B1 (Figure 20) and B2 (Figure 21) sintered specimens to observe variability in elemental composition across different length scales, extended to 3 × 3 mm^2. Figures 20 and 21 demonstrate α/β element partitioning at a scan area of 10×10 μm^2 for both B1 and B2 specimens due to the large scatter observed in this region for aluminium and vanadium compositions. An observation of note was the comparison between B1 and B2 at larger scan areas of 3×3 mm^2. Here, a higher degree of variability in aluminium and vanadium levels for B1 was evident at this large scan area.

Their methodology showed that when dealing with randomly distributed powder particles of discrete composition, one needs to be mindful of the limiting scan area size above which the EDX analysis would always yield the same composition. Consequently, it was important that homogenization was compared across a range of length scales. For all three cases

investigated, α/β element partitioning was evident for the 10 x 10 μm^2 scan area. However, when they compared Figures 20 and 21, they indicated significantly more variation in aluminium/vanadium levels for B1 even at scan areas up to 3 x 3 mm^2. The systematic approach to EDX analysis demonstrated the greater difficulty in homogenizing the elemental powder (B1) versus the blended master alloy (B2). It is possible that this behaviour may have been due to local melting of aluminium powder.

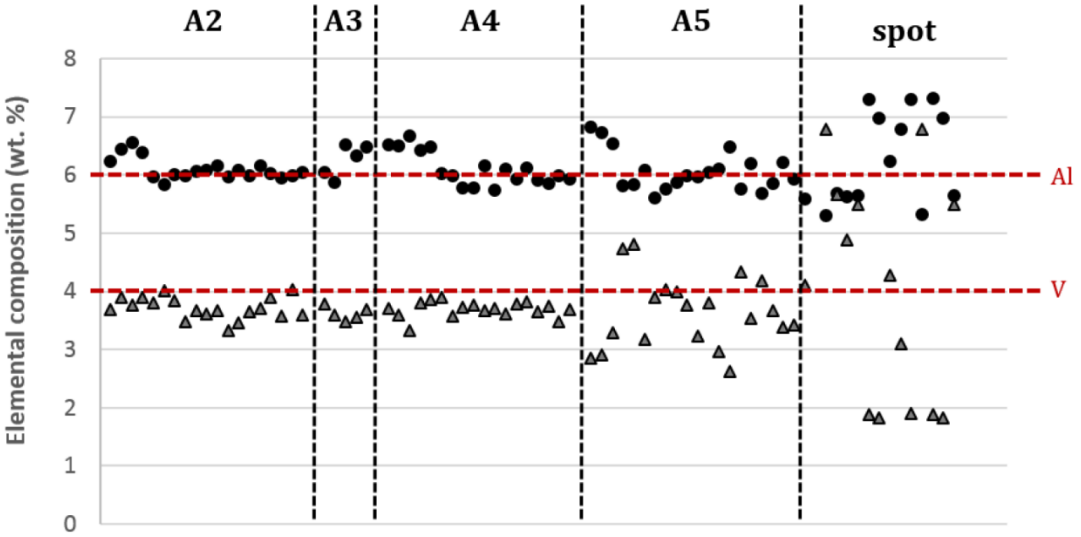

Figure 19: EDX analyses of wrought Ti-6Al-4V specimen at various length scales A2- spot. (A2=1.4x1.4mm^2; A3=350x350μm^2; A4=100x100μm^2 and A5=10x10μm^2). [31]

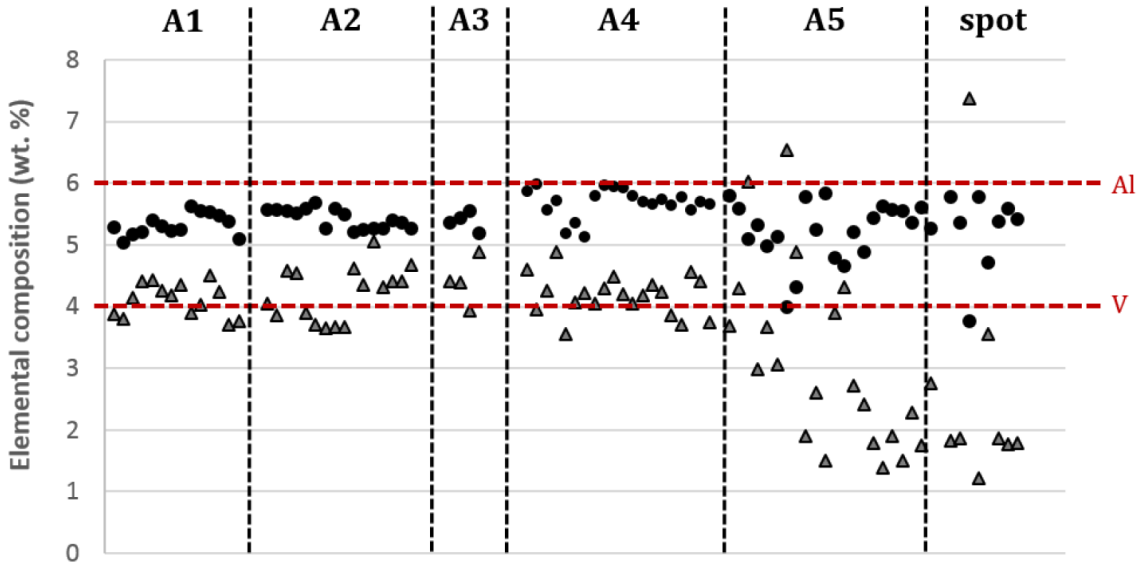

Figure 20: EDX analyses of B1 specimens at various length scales A1- spot. (A1 =3×3 mm^2; A2=1.4x1.4mm^2; A3=350x350μm^2; A4=100x100μm^2 and A5=10x10μm^2) [31]

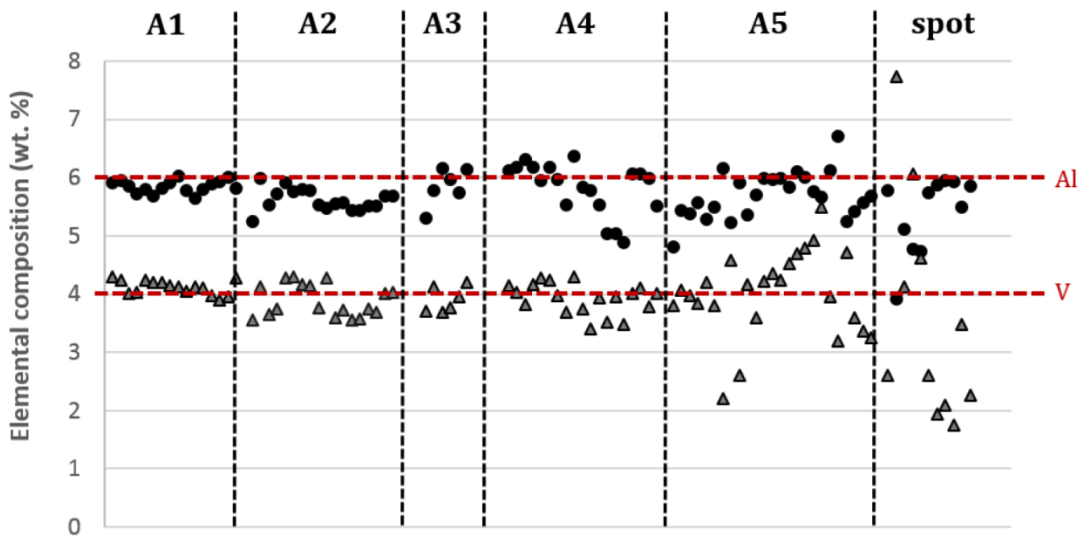

Figure 21: EDX analyses of B2 specimens at various length scales A1- spot. (A1 =3×3 mm^2; A2=1.4x1.4mm^2; A3=350x350μm^2; A4=100x100μm^2 and A5=10x10μm^2) [31]

3.5.2 X ray Diffraction

X- Ray Diffraction was used as another method to trace the path of homogenization. A wrought Ti6Al4V sample was used as a benchmark to measure the progression. XRD diffraction patterns representing relative X-ray intensity versus 2 theta angle (20°-100°) for this study were obtained when XRD diffraction was carried out in a Bruker D8 Advance X-ray diffractometer equipped with a cobalt source (λ = 1.78897 Å) and a Bruker Vantec position sensitive detector on the sintered samples. The optics were set to parallel beam geometry to prevent possible peak shifts that may be caused by sample height differences. The scan range was at 2 theta 20°-100° to cover enough alpha and beta peaks. The step size and the time per step were kept at 0.001° and 0.5s, respectively.

X–rays were discovered in 1895 by the German physicist Wilhelm Röntgen and named after him. These rays were invisible, unlike ordinary light, but they travelled in straight lines and affected photographic film in the same way as ordinary light. They were shown to be able to penetrate much more than light, and could easily pass through the human body, wood, thick

pieces of metal, and other opaque objects. Today we know that X-rays are electromagnetic radiation of the same nature as light, but with a much shorter wavelength. X-rays are measured in angstrom (Å), equal to 10^{-10} m, and X-rays used in diffraction have wavelengths usually lying in the range of 0.5-2.5Å, as compared to the wavelength of visible light lying in the order of 6000Å.[36]

X-ray diffraction has provided a wealth of important information to science and industry. For example, much that is known about the arrangement and the spacing of atoms in crystalline materials have been determined directly from diffraction studies. In addition, such studies have led to a much clearer understanding of the physical properties of metals, polymeric materials, and other solids. X-ray diffraction also provides a convenient and practical means for qualitative identification of crystalline compounds. The X-ray powder diffraction method can provide quantitative crystallographic information about the compounds present in a solid sample as well as indicating their amount.[36,37]

For analytical diffraction studies, the crystalline sample is either ground to a fine homogeneous powder (powder diffraction), or for solid samples (for example a piece of solid metal) the average grain size should be kept at a minimum. In this way large number of small crystallites/grains are oriented in every possible direction; thus, when an X-ray beam transverse the material, a significant number of the particles/grains can be expected to be oriented in such ways that the Bragg condition for reflection is fulfilled from every possible interplanar spacing.[37] For solid samples, such as pieces of metals, that are to be examined by X-ray diffraction, the prior thermomechanical treatment is of importance, since this may have induced texture into the material.[1,38,39] Texture means that there is a pronounced orientation of certain crystallographic planes in certain directions relative to the processing direction.[40] This texture means that the measured intensity from certain favourable oriented crystallographic planes, relative to the examined sample surface, will be higher than in a texture free specimen where some less favourably oriented crystallographic planes will diffract the incoming X-ray beam less or even not at all, thus leading to a decrease or lack of measured intensity for these.[40]

The identification of species/phases from their diffraction patterns is based upon the position of diffracted lines/peaks (in terms of θ, the angle of the crystal plane with respect to the direction of the X-ray beam) and their relative intensities. The diffraction angle 2θ is determined by the spacing, d, between a set of planes, in accordance with the Bragg equation, $n\lambda = 2d \sin\theta$, where λ is the known wavelength of the X-ray source; n is the order of reflection; which may take on any integral value, and d is the path difference, in terms of number of wavelengths, between waves scattered by adjacent planes of atoms.

The identification of phases from diffraction patterns is shown in Figure 22. In a study by Gökelma et al,[41] Ti6Al4V powder was hydrogenated and then dehydrogenated. XRD was performed to see if the hydrogenation introduced hydrogen to make the Titanium peaks TiH_2 and if the dehydrogenation resulted in the material going back to its original state. XRD patterns of the raw material (Ti6Al4V powder), and powders (in hydrogenised and dehydrogenised states) are shown in Figure 22. The XRD patterns of the powders indicate peaks of titanium hydrides (in the form of TiH_2 and $TiH_{1.5}$). As compared to the hydrogenised state, dehydrogenation caused domination of α and β-Ti phase peaks along with peaks of titanium hydrides by considering the intensity ratios of the Ti peaks with those of $TiH_{1.5}$ and TiH_2. However, the applied dehydrogenation process did not completely remove titanium hydrides from the powders.[41]

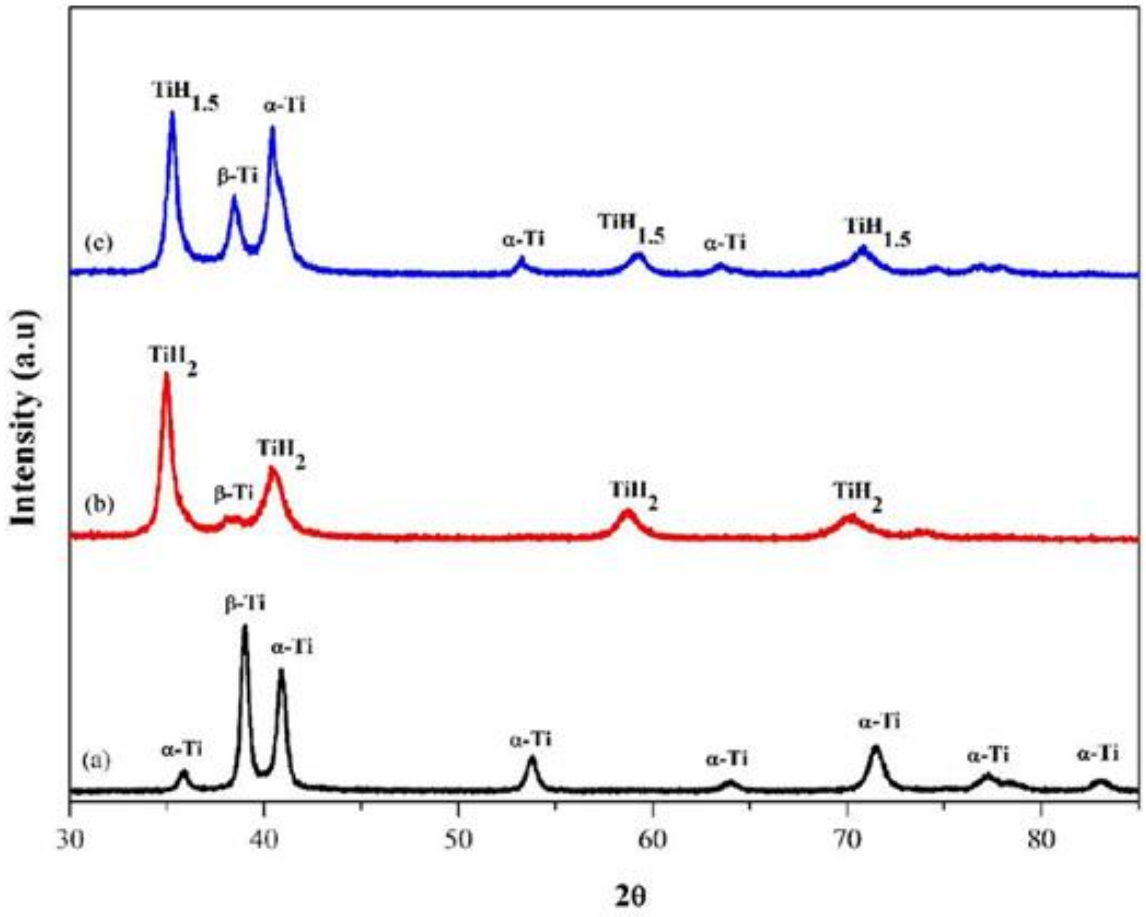

Figure 22: X-ray diffraction analysis of the (a) raw material (b) after hydrogenation and (c) after dehydrogenation.[41]

A study by Changzhou et al,[42] showed that the homogenization progress of titanium powder blends could be followed using XRD. Figure 23 shows the XRD patterns of Ti-6Al-4V sintered under different sintering temperatures. The XRD patterns of specimens sintered at 1150 °C show that the samples consisted of α-, β-Ti with some Ti_3Al peaks. The presence of the Ti_3Al phase when sintered at lower temperatures was indicative of the alloying process being incomplete at that temperature. The Ti_3Al phase has disappeared after completion of sintering at 1350°C.

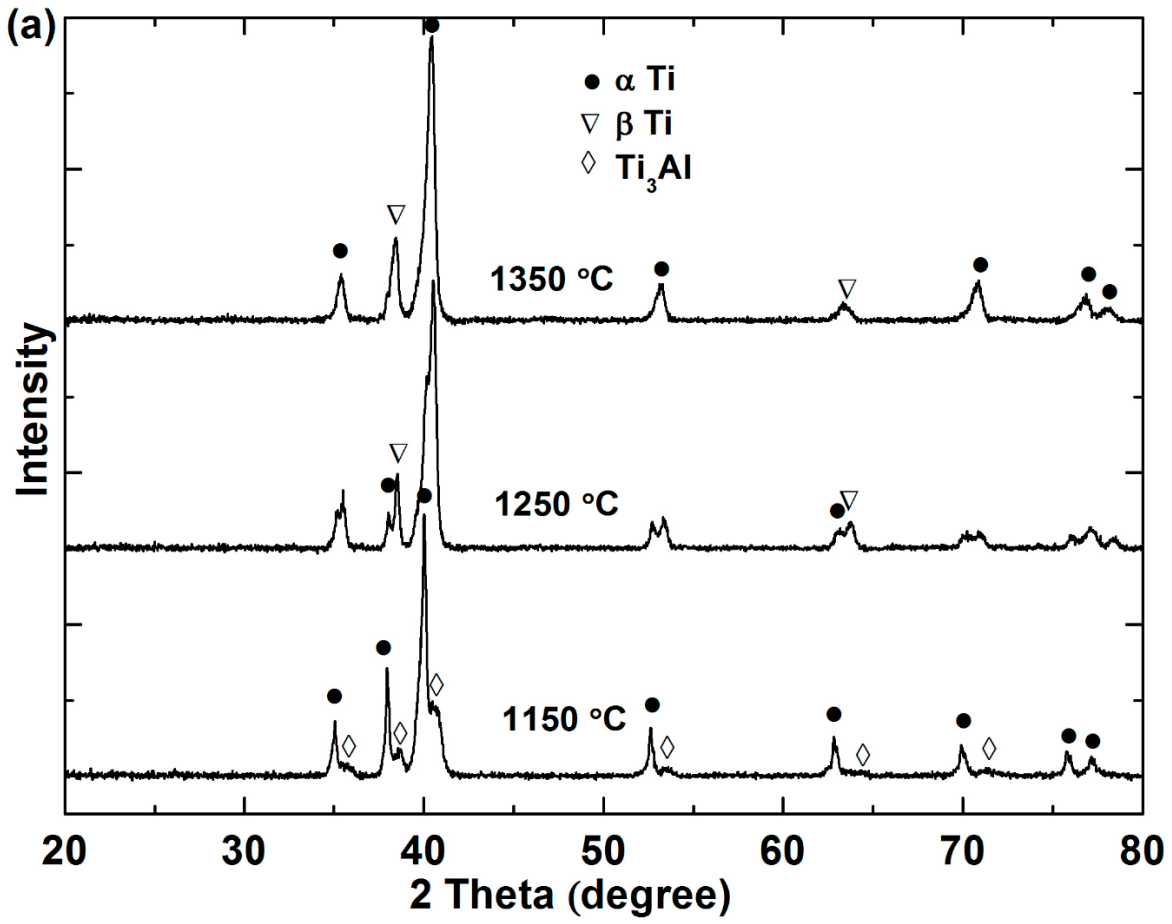

Figure 23: XRD patterns of Ti-6Al-4V sintered at various temperatures.[42]

4. RESULTS AND DISCUSSION

4.1 Powders, Compaction and Density

The results obtained by characterization of the blended starting powders and materials obtained from experimental work are presented and analysed concisely in this chapter. The particle size and shape characteristics are presented in the beginning of the chapter. The densities and compositional features of the blended material produced by the cold press and sinter techniques are then presented and compared.

4.1.1 As-received powder characterization

SEM images were taken using a FEI Nova NanoSEM 230 ETD detector. The CpTi and MA particles were highly angular with the vanadium particles less so, whereas the aluminium particles were somewhat elongated and nodular. Figure 24 shows representative SEM images of the CpTi, Aluminium, Vanadium, MA and TiH_2 powders, respectively.

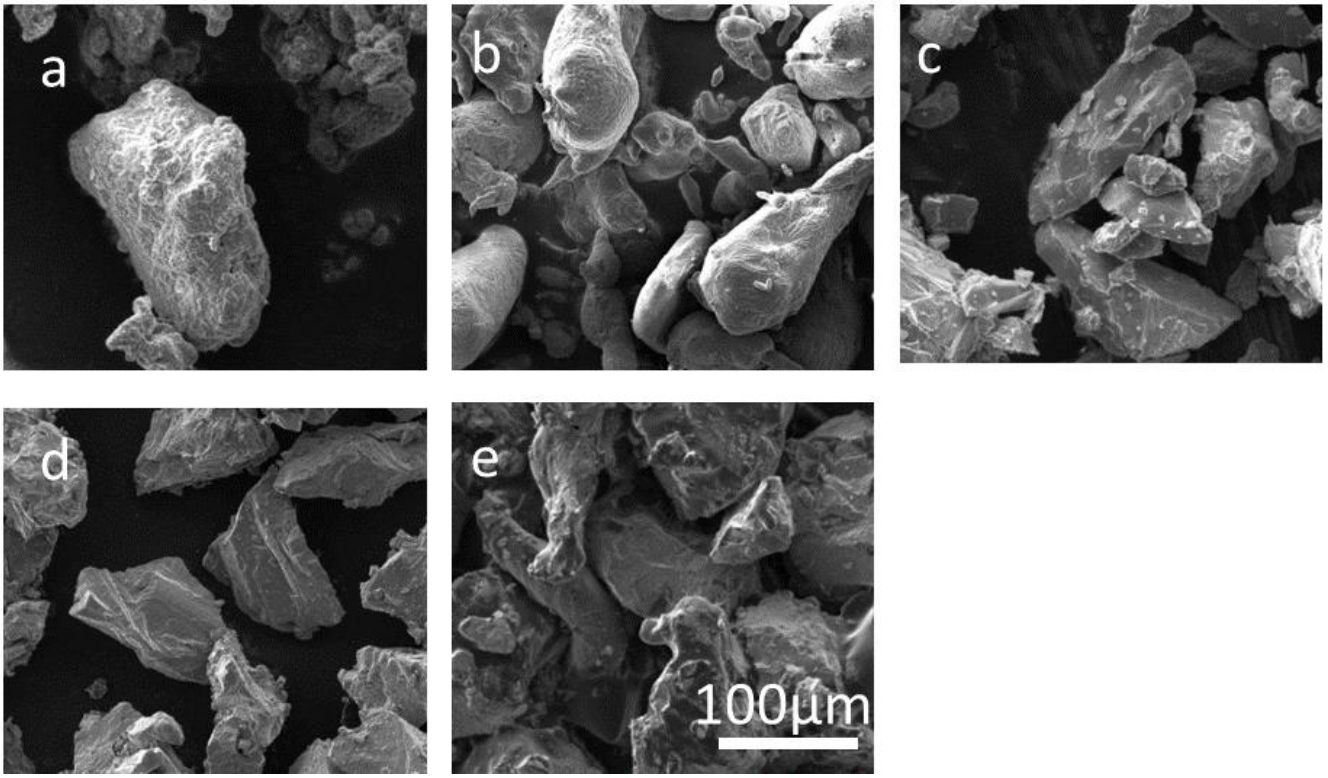

Figure 24: SEM image of the as-received (a) Commercially pure Titanium (CpTi) (b) Aluminium (c) Vanadium (d) 60Al:40V master alloy (MA) (e) TiH_2 powders

Table 10 gives powder specifications for all powders used in this study. Powder production method, mesh sizes and expected powder particle size range information was supplied by the manufacturer. Oxygen and nitrogen contents were analysed by the Advanced Materials Engineering Impact Area at CSIR.

It can be noted from Table 10 that there is a significant difference in particle size for the base powders TiH_2 and CpTi. Table 11 shows the shapes of the powders as analysed using a FEI Nova NanoSEM 230 ETD detector. The shape and size of the powders have vital roles to play in terms of the density and strength of the green compact. Flowability of the powder affects the density of their resulting green compacts. According to a study by Chikosha et al,[54] irregular powders, as compared to spherical or regular shaped powders, can interlock and undergo further cold welding, which assists in improving the density of the final product.

Thus, good green densities are expected from the compacts made from the three powders used for this dissertation due to their irregular shape. Cantin et al.[26] suggests that the bigger the size of the powder particles, the higher the green density. The reason being that while larger particles will result in bigger voids compared to compacts made from finer powder particles, the frequency of the smaller voids is so high that the overall final green densities of compacts with finer particles are lower than that of the compacts made from larger powder particles.

Since CpTi has a larger particle size, compared to TiH_2 as well as the MA powder, the green compacts with higher level of CpTi are expected to have higher green densities solely based on their particle size.[15] However, the mechanical properties of the powders also affect the green density and strength of the compacts pressed from the various powder blends.

Table 10: Powder specifications

Metal Powder	Powder Production	Mesh Size	Size Range	Oxygen	Nitrogen
Titanium	HDH	-100+200	74<Ti≤149	0.17±0.01	0.01±0.001
Titanium Hydride	HDH	-100+200	64<TiH_2≤113	0.17±0.01	0.01±0.001
Aluminium	Nitrogen Atomised	-100+325	44<Al≤149	0.98± 0.04	0.01±0.001
Vanadium	HDH	-325	V≤44	0.98± 0.04	0.03±0.001
60Al:40V master alloy	HDH	-230	MA≤63	0.21±001	0.003±0.0001

Table 11: Powder shapes

Powder Type	Particle Shape
CpTi	Angular and facetted
TiH_2	Angular and facetted
Al	Spherical
V	Angular and facetted
60Al:40V master alloy	Angular and facetted

4.1.2 Compaction and Density

4.1.2.1 Green Density

All the powder blends were blended and compacted at 350MPa.

Table 12 shows the green density average values of the compacted powder blends.

Table 12: Green density of the powder blends

Green Density of blended powders	g/cm^3
TiH_2 + MA	62.5 ± 1
TiH_2 + Al + V	62.5 ± 1
CpTi + MA	68.1 ± 1

As discussed in the literature section, when basing only on the chemical composition and mechanical properties of the powder blends, it was expected that TiH_2 powder blends would have a lower green density.[15] This is because the brittle and low-strength hydrogenated

titanium particles are crushed by compacting force forming fine fragments with a network of fine voids between them, whereas, CpTi forms relative coarse voids between particles, which size and amount are defined by particle size.[15]

This decrease in density is dominated by the difference in particle size between CpTi and TiH_2. The particle size of the TiH_2 used is smaller prior to compaction and thus when particles break (during compaction) there is a substantial difference in particle size compared to CpTi. This results in the size of the voids in TiH_2 compacts being smaller in size compared to compacts with CpTi. However, the frequency of the small voids is so high that it results in a lower overall density as compared to CpTi compacts. The results are supported by various research papers discussed in Chapter 2, [4,22] where larger particle size of CpTi had better relative green densities as compared to smaller CpTi as well as smaller TiH_2 powders. While it could be argued that bigger particles should be used, the use of smaller particles improves sintered density and is therefore more advantageous to use, to ensure sintered compacts have good end mechanical properties.

Therefore, the difference in particle size is significant and, in this case, outweighs the chemical composition and mechanical properties of the powders. To evaluate the difference in green density solely based on the chemical composition and nature, the powders used should have the same particle size and shape. The reducing ability of TiH_2 (due to the presence of hydrogen) is also expected to reduce the formation of surface oxides which in turn promotes sintering and densification.

4.2 Sintered Density

All the compacted powder blend green specimens were sintered at high vacuum at temperatures in the range of 1000−1350°C and time at a range of 0.5 to 4 hours and then densities obtained where compared relative to the density of wrought titanium of 100%.

4.2.1 CpTi + MA powder blend

The CpTi + MA compacts produced by the compaction method were characterized for density, and the resultant relative density results are illustrated in Figure 25. It is shown that the

density increases with increase in sintering temperature and time. An increase in time results in an increase in relative density; this can be observed at 1000°C, where the density increased by 11% ± 1 from when the blended samples were sintered for 0.5 hours to when the samples were sintered for 4 hours.

Diffusivity increases rapidly with temperature, since it follows an Arrhenius temperature dependence, and this is shown in Figure 25 when comparing the powder blend relative densities after sintering for 1 hour at 1000°C and 1350°C. There is an increase in relative density by 15% ± 1 when the samples were sintered at 1350°C. A combination of increase in temperature and time results in high increases in relative density as diffusion is promoted regardless of chemical composition; this is noted when we compare a sample sintered at 1000°C for 0.5 hours to a sample sintered at 1350°C for 4 hours. The relative density increased by 28% ± 1, resulting in a relative density of 97% ± 1.

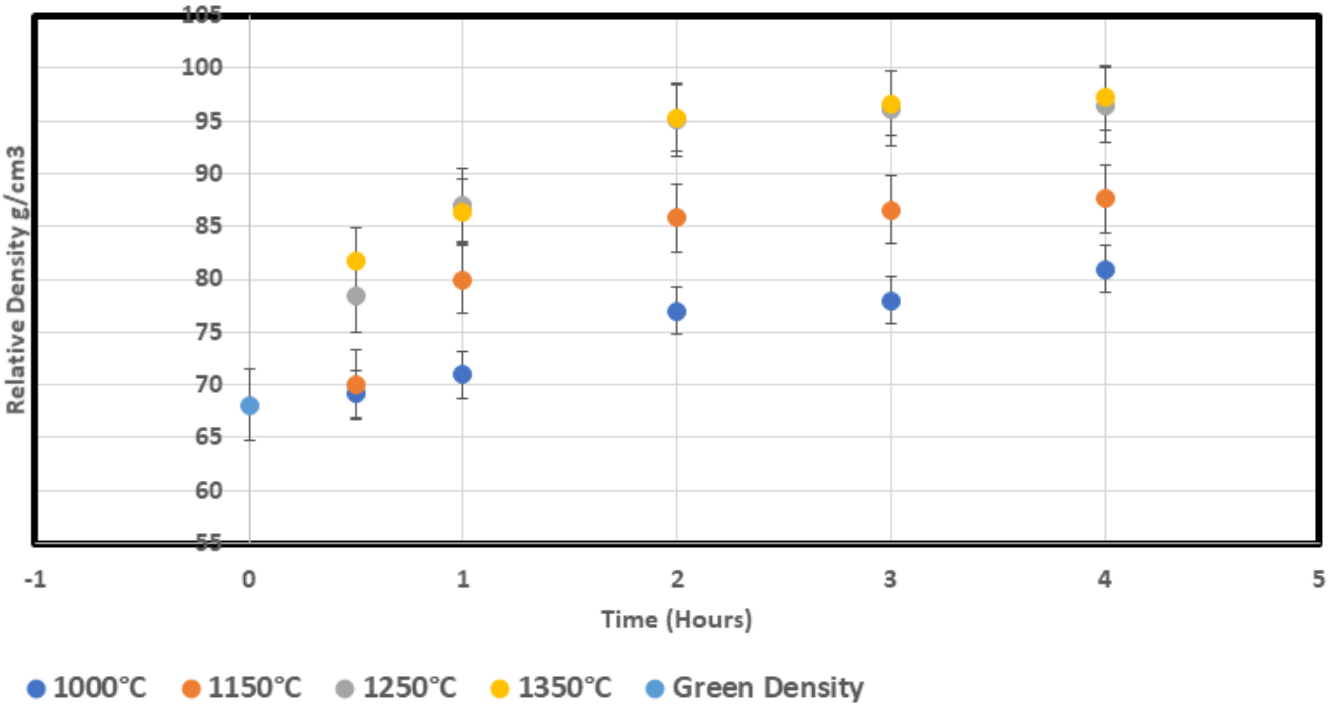

Figure 25: Relative density profiles of CpTi + MA compacts sintered under different conditions.

4.2.2 TiH_2 + MA powder blend

Figure 26 shows the relative density profile of TiH_2 + MA compacts sintered under different conditions. The TiH_2 + MA compacts produced by the compaction method were characterized for density, and the resultant density results are illustrated in Figure 26. It is shown that with

an increase in time and temperature there is an increase in relative density. There is a 35% increase in relative density when we compare the densities of the samples sintered at 1000°C for 0.5 hours to the samples sintered at 1350°C for 4 hours. It is observed that from a sintering time of 2 hours the relative density of the samples at a temperature of 1250°C and 1350°C are the same. After sintering for 2 hours at 1250°C the relative density was 98% ± 1 which is similar to the relative density obtained under the same conditions (sintering time) at a temperature of 1350°C. An increase in sintering time to 4 hours did not result in an increase in relative density for the samples at both sintering temperatures.

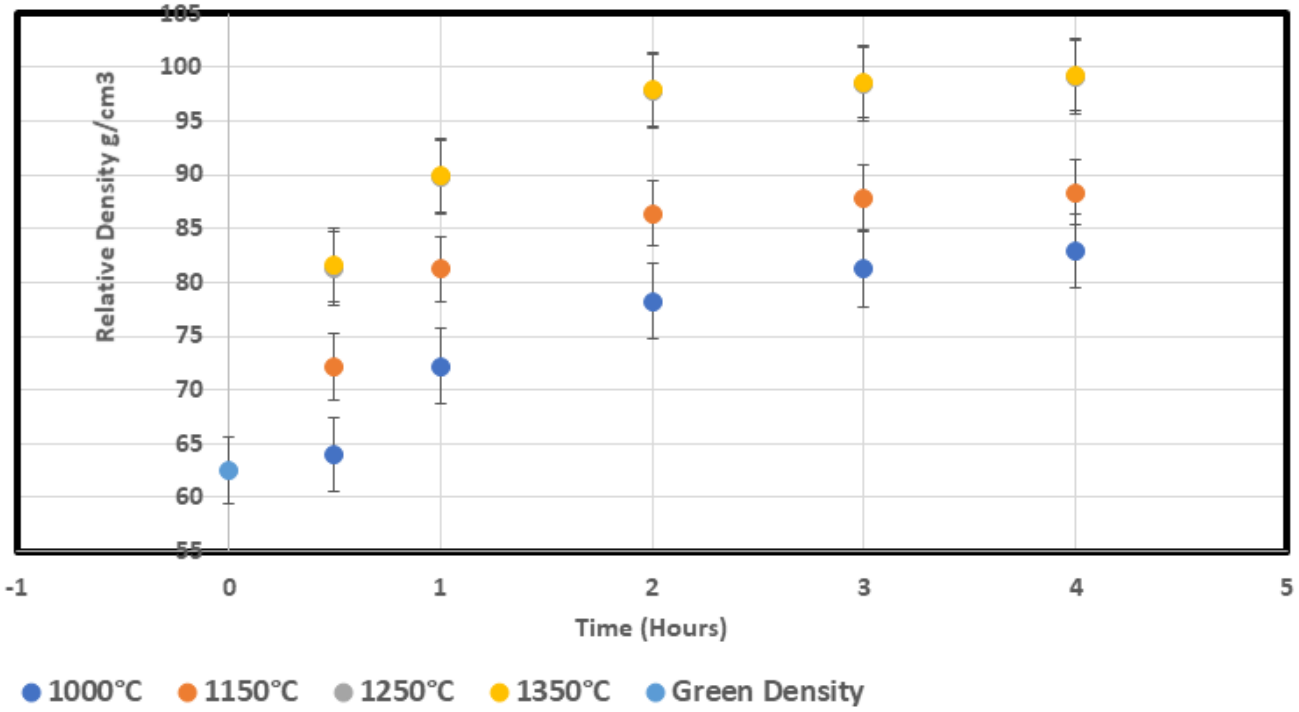

Figure 26: Relative density profiles of TiH_2 + MA compacts sintered under different conditions.

4.2.3 TiH_2 + Al + V powder blend

Figure 27 shows the relative density profile of TiH_2 + Al + V compacts sintered under different conditions. The TiH_2 + Al + V compacts produced by the compaction method were characterized for density, and the resultant density results are illustrated in Figure 27. It is shown that the density increases with increase in sintering temperature and time. There was a ±2% increase in relative density when the sample were sintered for 2 hours or more at temperatures 1250°C and 1350°C. After sintering at 1350°C and for 4 hours the relative density obtained was 96% ± 1. There was a 34% increase in relative density compared to that

of the green density.

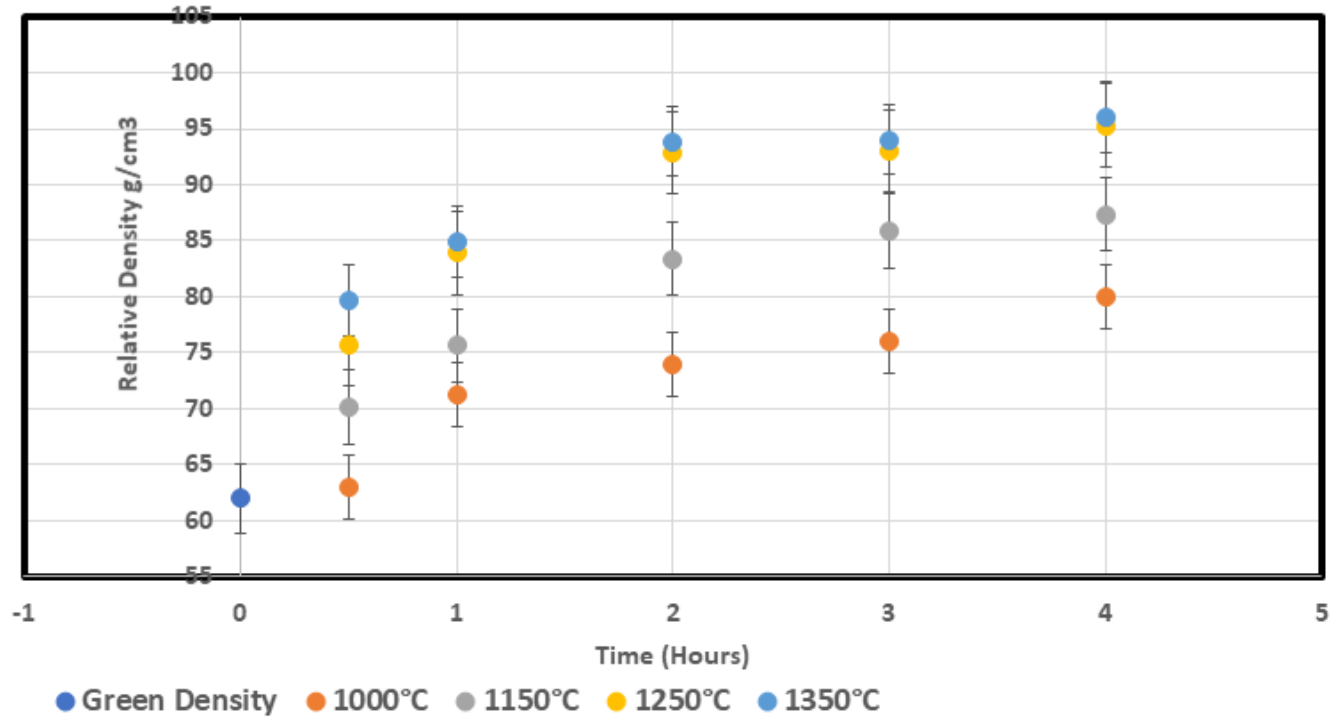

Figure 27: Relative density profiles of TiH_2 + Al + V compacts sintered under different conditions.

4.2.5 Discussion of Sintered Density

Table 10 above shows that CpTi had a larger particle size than TiH_2 which resulted in the green density of the CpTi to be higher at 68% as discussed in chapter 4.1.2.1 and that of TiH_2 to be lower at 62.5%.

In a study by Ivasishin et al.[15] , base powders that had a higher hydrogen content resulted in a high sintered density. There is a significant increase in diffusion and densification mainly because:

1. TiH_2 is brittle and during compaction as explained above, the titanium particles are crushed by the compacting force forming fine fragments with a network of fine voids between them. This results in a high sintered density as this increases flowability and promotes denisfication.[23]
2. On the contrary as explained above, ductile CpTi forms coarse particles and voids between particles which results in a high green density but not highly beneficial during sintering. Due to the large particle sizes the diffusion of powder particles are slower compared to the fine TiH_2 particles, therefore a decrease in density when sintered under the same conditions.

The vacuum atmosphere in which sintering is taking place is conducive for the $TiH_2 = Ti + H_2$, transformation that occurs when the furnace temperature goes above 320°C to take place. The low-pressure atmosphere enables hydrogen to be released which results in an increase in surface area and surface diffusion. As shown in Chapter 2, in Figure 10, this transformation also results in lattice defects forming which change the volume and enable volume diffusion to take place as well which increases diffusion as well.[6] Despite being a hydrogenated titanium blend, the TiH_2 + Al + V blend had the lowest densities at all temperatures and times, and this can be attributed to the difference in alloying powders.

Schaffer et al.[13] studied and found out that manipulating the particle size of alloying powders had a greater impact than manipulating the size of the titanium powder. As shown in table 11, Al has a particle size of 75 µm and V has a particle size of 25 µm whereas the master alloy had a particle size of 40 µm. In their study the use of the Al-V master alloy gave a lower green density and a higher sintered density compared to elemental Al and V when producing Ti-6Al-4V. The low green density that the master alloy gives is because the master alloy has a higher hardness compared to the elemental powders.[13]

A densification parameter (ΔD) was calculated using Equation 3[45] and the values in Table 13. The results are represented in figure 28 to show the effect of particle size on the sinter ability of the powder blends. ΔD is defined as the change in density from the green state divided by the maximum possible density change.[45] Figure 28 shows that the TiH_2 + MA powder blend, which had the lower particle size in terms of the base powder as well as alloying elements, had a higher density parameter, followed by CpTi + MA then TiH_2 + Al+ V. Reducing the particle size generally increased the sintered density by an amount greater than the decrease in the green density.

Equation 3:

$$\Delta D = \frac{\rho sintered - \rho green}{\rho theoretical - \rho green} \times 100$$

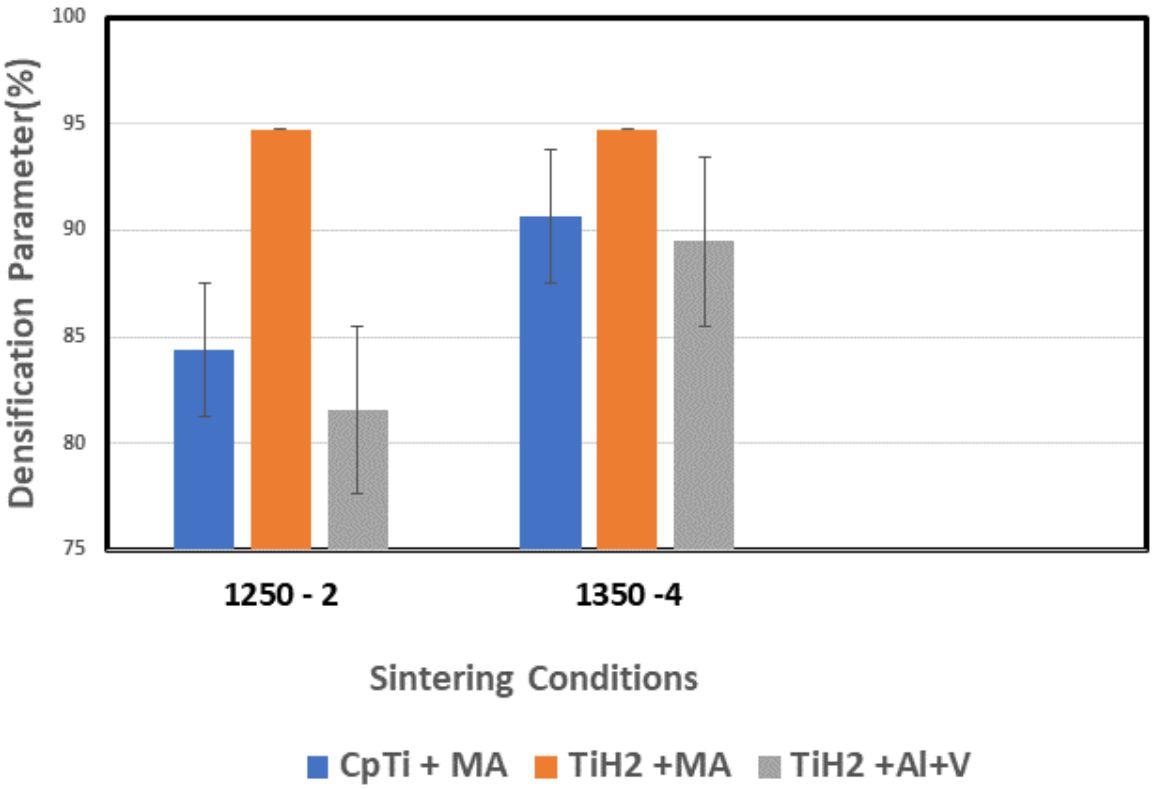

Figure 28: Densification parameter of the titanium powder blends at 1250°C after 2 hours sintering time and 1250°C after 4 hours sintering time.

Table 13: Green and sintered densities of the powder blends (values used to calculate densification parameters in Figure 28, above)

Powder Blend	CpTi + MA	TiH_2 + MA	TiH_2 + Al + V
Green Density (%)	68 ± 1	62 ± 1	62 ± 1
Sintered Density 1250 -2 (%)	95 ± 1	98 ± 1	93 ± 1
Sintered Density 1350 -4 (%)	97 ± 1	98 ± 1	96 ± 1

Chemical composition also plays a role in the densification of powder blends during sintering. Figure 29 shows comparative plots of the 3 blends at the different temperatures and times. If there is minimal chemical reaction during sintering, solvation leads to a homogeneous final product. Homogenization occurs by each species diffusing into the other. In cases where strong chemical reactions occur, the chemical gradients bias diffusion to induce pore formation and swelling. If diffusion rates for the two components are different, then pores form.[15] This is observed when the melting temperatures of the mixed powders are very

different. Melting points are indicators of diffusion rates (lower melting temperature materials have weaker atomic bonding which allows faster diffusion). The difference in diffusion rates between the high and low melting temperature powders leads to vacancy accumulation, pore growth, and compact swelling.

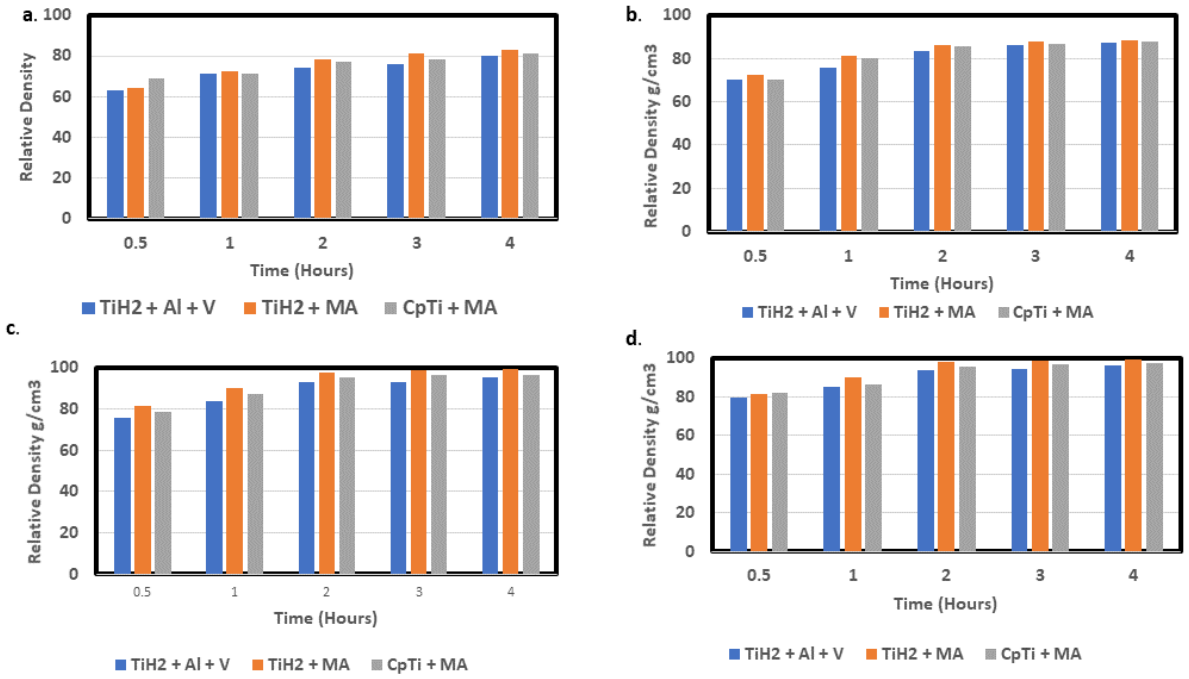

Figure 29: Comparative relative density profiles of all the powder blends sintered under temperatures of a. 1000°C, b.1150°C, c.1250°C, d.1350°C.

From Table 14 - 15 it can be noted the higher the diffusivity of an element the less solubility it would have in commercially pure titanium.

Table 14: Average solubility of alloying elements in β-Ti at sintering temperatures.[32]

Temperature	Al	V	Mo	Cr	Fe
1250°C	<27 wt. %	Not Limited	Not Limited	<44 wt. %	<24.7wt. %
1020°C	12 wt. %	Not Limited	Not Limited	<27 wt. %	<24wt. %
α- Ti	6 - 10 wt.%	<3 wt.%	<1 wt. %	<1 wt.%	<0.047 wt. %

Table 15: Average diffusivity of alloying elements in β-Ti at sintering temperatures.[33]

Temperature	Al ($x10^{-13}m^2s^{-1}$)	V ($x10^{-13}m^2s^{-1}$)	Mo ($x10^{-13}m^2s^{-1}$)	Cr ($x10^{-13}m^2s^{-1}$)	Fe ($x10^{-13}m^2s^{-1}$)
1250°C	12.5 ± 7.5	14 ± 1	3.25 ± 1.25	~ 40	~ 300
1020°C	1 ± 0.2	1.25 ± 0.25	0.33 ± 0.15	~ 4	~ 30

According to Ivasishin et.al,[15] titanium has two allotropic modifications, low-temperature α-phase and high-temperature β-phase with α→β transus temperature at 882,5°C. Generally, the temperature ranges in which the α and the β phases exist can be expanded by additions of α (Al, O, N, C) and β (V, Mo, Fe, Cr,) stabilizing elements. Solubility of alloying elements depends on the Titanium matrix phase composition: α-stabilizers are contained mainly in the α-phase and correspondingly, β- stabilizers mainly in the β-phase. Introducing the alloying powders separately in the TiH_2 +Al+ V powder blend resulted in the stabilisation of their respective phases; Al having a higher diffusivity would stabilise the alpha phase and Vanadium would stabilise the beta phase resulting in slow diffusion of the elements in the opposing phases causing a delay in homogenization. Aluminium also forms a eutectic at lower temperatures which melts and results in pores forming which would further decrease density in this blend.[22]

Introducing the alloying elements as a master alloy would result in better homogenization under the right conditions because the stabilization of the respective phases is not as prominent as when the alloying elements are introduced separately.[22] There will be a difference in diffusion mobility of Titanium atoms penetrating former MA particles and mobility of Al and V atoms moving in opposite direction resulted in appearance of vacancies and their coagulation with pore formation, but it would not be as pronounced as when added separately. This effect becomes more apparent when using coarse alloying powders due to more significant localization of Al and V atoms.[19]

4.3 Compositional analysis

4.3.1 SEM Analysis

The composition of the blends was analyzed via the use of SEM analysis. The aim of this analysis

was to measure the composition change of the alloying elements at the different times and temperatures and compare them to the wrought Ti6Al4V sample shown in Figure 30 as the base of homogeneity.

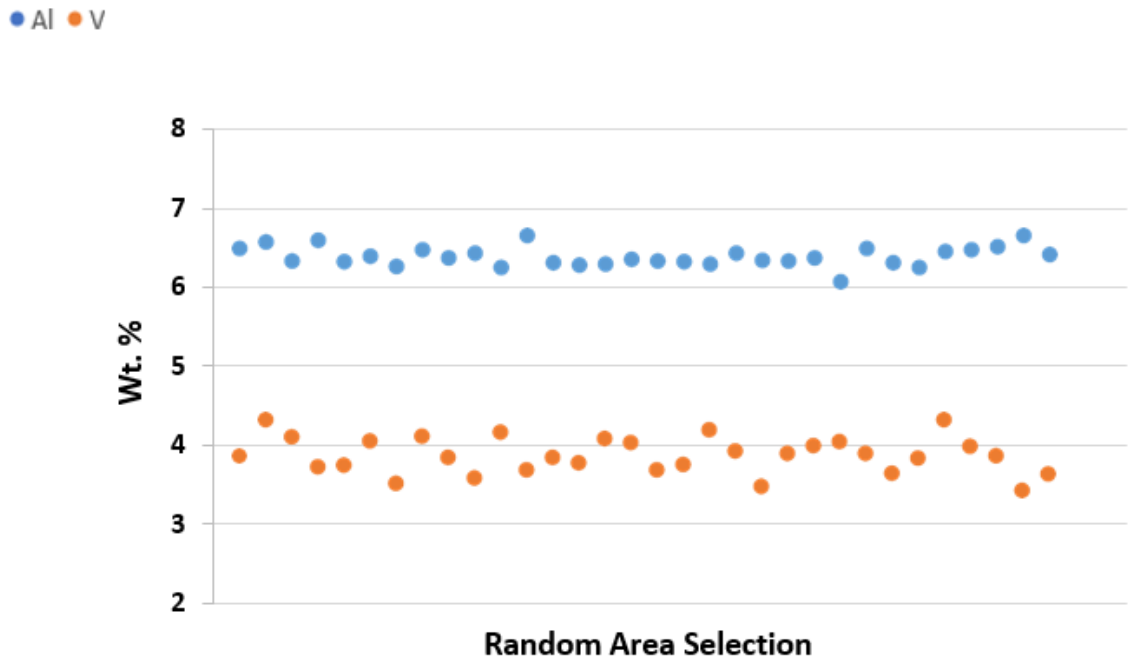

Figure 30: EDX analyses at a scan area of 100×100µm for a wrought Titanium sample

The results of the scans for the as sintered and wrought materials are shown graphically in the same way as in Figure 30. To show the results in this chapter, figures like Figure 30 will be used to depict the weight percentage of both Al and V. In each of the cases, titanium will make up the balance of the composition. The wrought Ti6Al4V sample analysed had a chemical composition of 6-6.7 wt.% of Al and 3.5-4.5 wt.% of V which goes along with the standard for Ti-6Al-4V by the Society of Automative Engineers (SAE) AMS4911 for the alloy in aerospace applications. When comparing the performance of each blend, the analysis for the wrought alloy (i.e., Figure 30) is included for graphical comparison. The values of the EDX ranges are extracted from the graphs by reading the lowest and highest value of the elements in the sample.

The acceptable level of scatter is that of wrought titanium as shown in Figure 30, any deviation from that scatter that will be shown in the findings below demonstrates in homogeneity.

4.3.2 TiH_2 + MA powder blend

Figures 31 – 34 show the results of the EDX scans of the as sintered samples of the TiH_2 + MA powder blend.

The sintered, TiH_2 + MA compacts were characterized for composition homogeneity at the different temperature and times using the EDX tool of the SEM at 20KV, deadtime less than 40% and a spot size of 5. The homogeneity path was followed for each temperature at each time stage.

As can be seen from Figure 31, sintering at 1000°C, does not result in a homogenous composition of the sintered Titanium powder blend. It does allow for improvement in diffusion of Al towards homogeneity, but vanadium distribution is slower and is not supported by the temperature.

Increase in time, as can be seen, results in diffusion of Al towards an average wt.% which is closer to 6, after starting off at a range of 1-8 wt.% at 0.5 hours, it gets to a maximum of range of 2.5 -6 at 4 hours. The vanadium wt.% distribution at this temperature changes slightly from a minimum of 1 to 2 wt.% as the sintering time increases.

Figure 32 shows that the higher sintering temperature of 1150°C resulted in an increase in diffusivity of both Al and V. Increase in time at the sintering temperature resulted in an improvement in distribution of Al which was within a range of 1.5 to 8 wt.% at 0.5 hours and after sintering for 4 hours the distributions improved to 3 to 6.5 wt.%. There was no significant change in the V distribution.

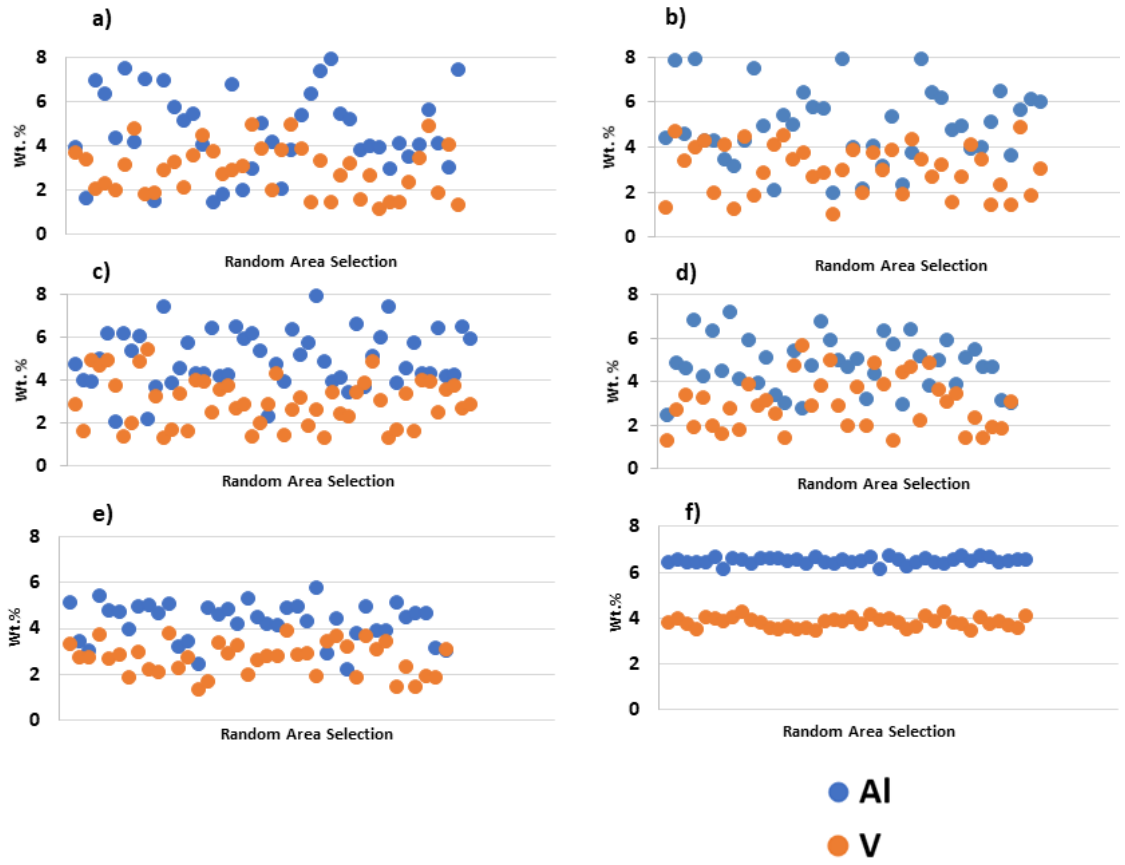

Figure 31: EDX analyses at a scan area of 100×100µm for TiH_2 + MA blend compacts sintered at 1000°C for (a) 0.5 hours (b) 1-hour (c) 2hours (d) 3 hours and (e) 4 hours compared to (f) wrought Ti6Al4V (W-Ti).

Figure 33 shows that an increase in temperature to 1250°C improves the diffusivity of the alloying elements to a high extent. The elemental composition improved in 2 hours as can be noted in Figure 33 (c) where the elemental compositions of aluminium and vanadium demonstrate much less scatter. An increase in time to 4 hours resulted in the composition representing a more homogenized sample relative to the wrought Ti6Al4V (W-Ti) sample with a composition of 5.5 -6.5 wt.% of aluminium and 3.5 – 4.5wt.% of vanadium.

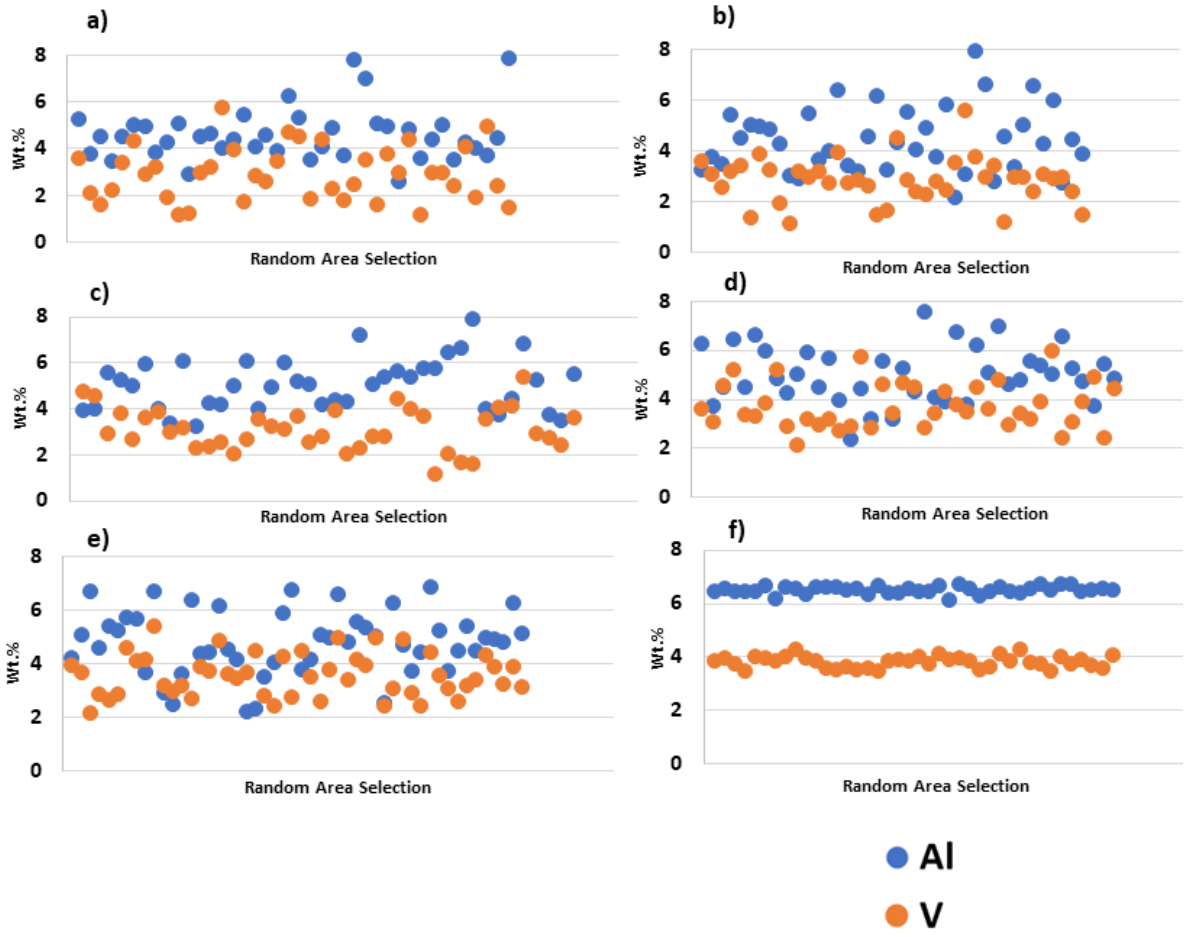

Figure 32: EDX analyses at a scan area of 100×100µm for TiH_2 + MA blend compacts sintered at 1150^{o}C for (a) 0.5 hours (b) 1-hour (c) 2hours (d) 3 hours and (e) 4 hours compared to (f) wrought Ti6Al4V (W-Ti).

Figure 34 shows that at 1350°C it can be noted that the diffusivity of the elements even at a lower time for example after an hour the composition of the elements had already greatly improved and were moving towards homogeneity. After 2 hours of sintering the samples were fully homogenized relative to the wrought Ti6Al4V (W-Ti) sample.

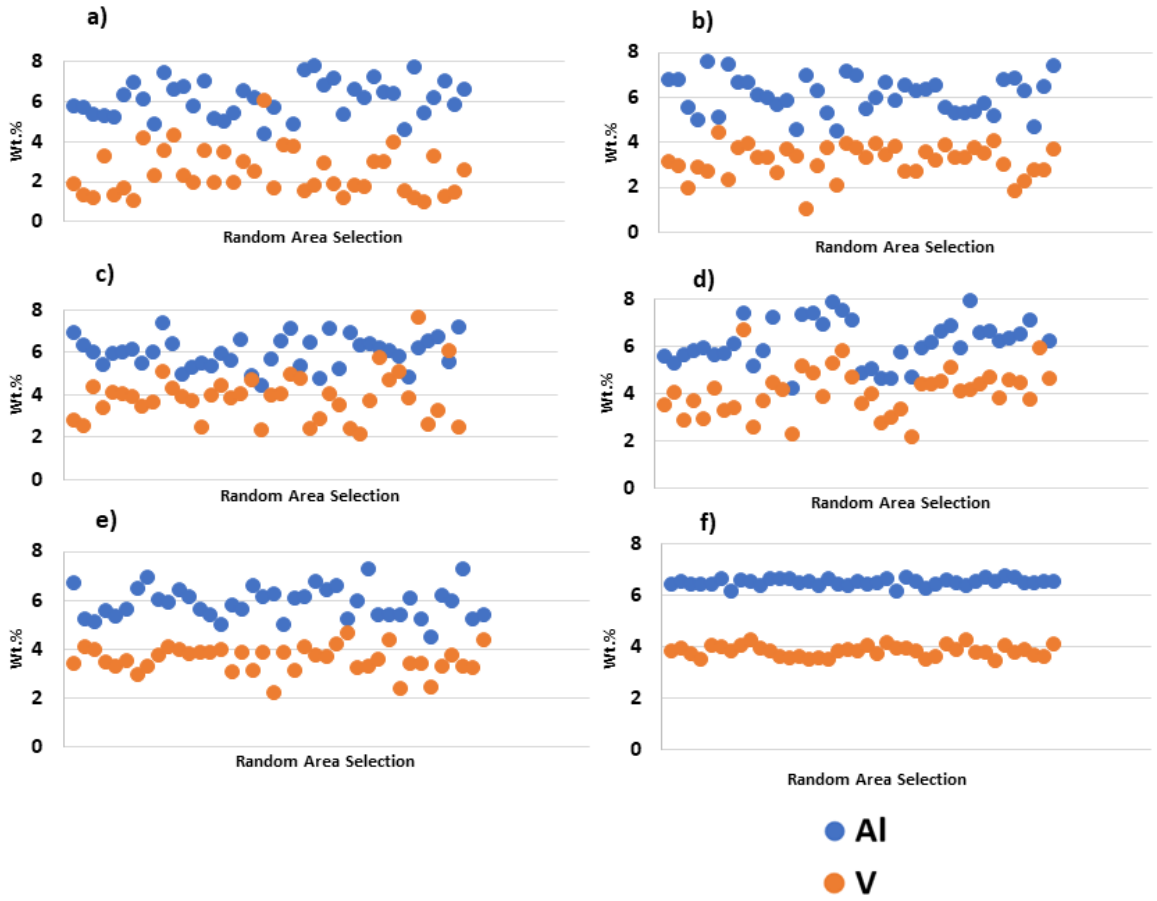

Figure 33: EDX analyses at a scan area of 100×100µm for TiH_2 + MA blend compacts sintered at 1250^{o}C for (a) 0.5 hours (b) 1-hour (c) 2hours (d) 3 hours and (e) 4 hours compared to (f) wrought Ti6Al4V (W-Ti).

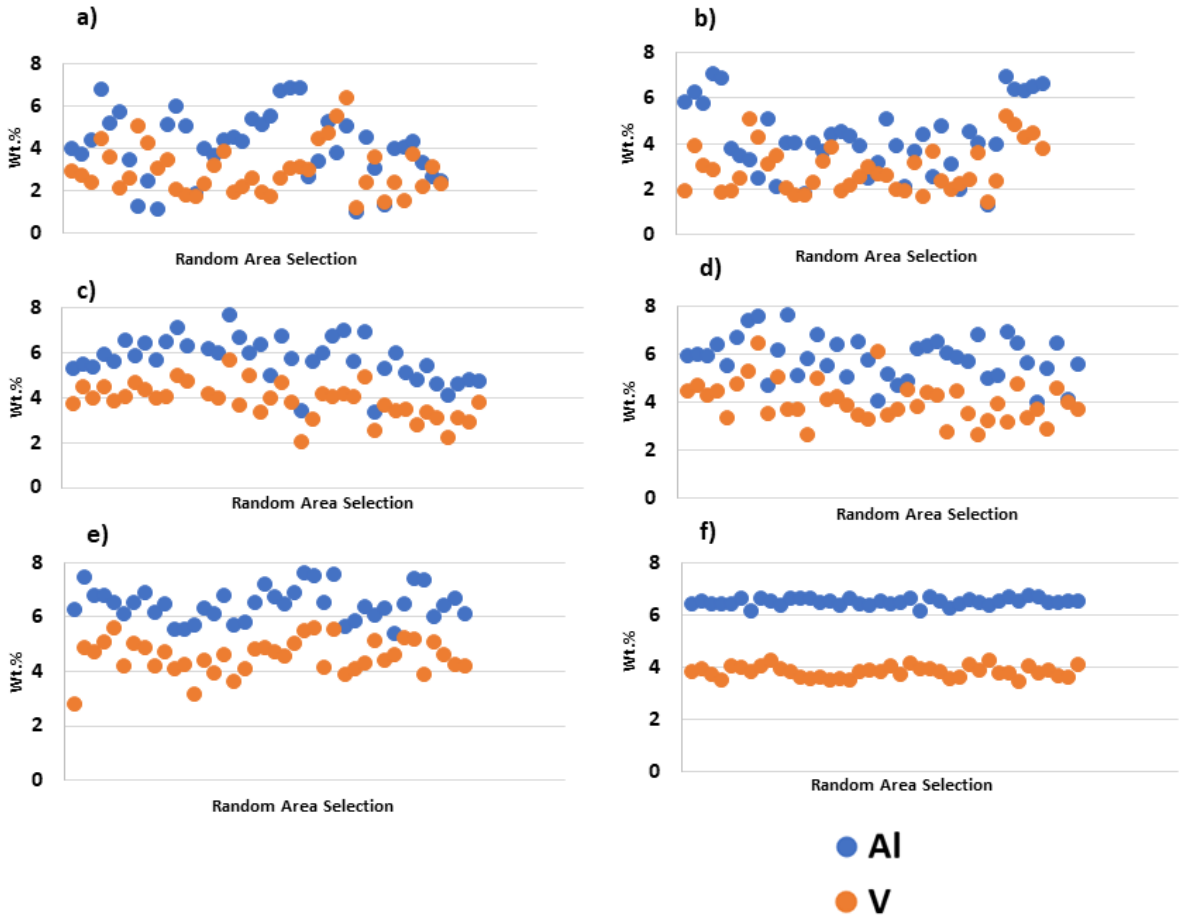

Figure 34: EDX analyses at a scan area of 100×100µm for TiH_2 + MA blend compacts sintered at 1350^{o}C for (a) 0.5 hours (b) 1-hour (c) 2hours (d) 3 hours and (e) 4 hours compared to (f) wrought Ti6Al4V (W-Ti).

4.3.3 CpTi + MA powder blend

Figures 35 - 38 show the results of the EDX scans of the as sintered samples of the CpTi + MA powder blend.

Increase in time, results in diffusion of Al towards a wt.% of 6.5 after starting off at a range of 1 to 8 wt.% at 0.5 hours. It gets to a range of 2.5 to 6.5 wt.% after 4 hours sintering time. The vanadium wt.% distribution at this temperature starts at 0.5 to 6 wt.% at 0.5 hours which is a wide range compared to the same conditions with the TiH_2 + MA blend seen on Figure 31 above. After 4 hours of sintering the range moves to 2 – 5 wt.% at 4 hours where there is a slight increase of 0.5wt.% in the lower part of the range.

Figure 35 confirms that a sintering temperature of 1000°C at any time within the range of 0.5 to 4 hours does not result in a homogenous composition of the sintered titanium powder blend. It does allow for some diffusion of aluminium and vanadium towards homogeneity, but the distribution is slower and is not supported by the temperature.

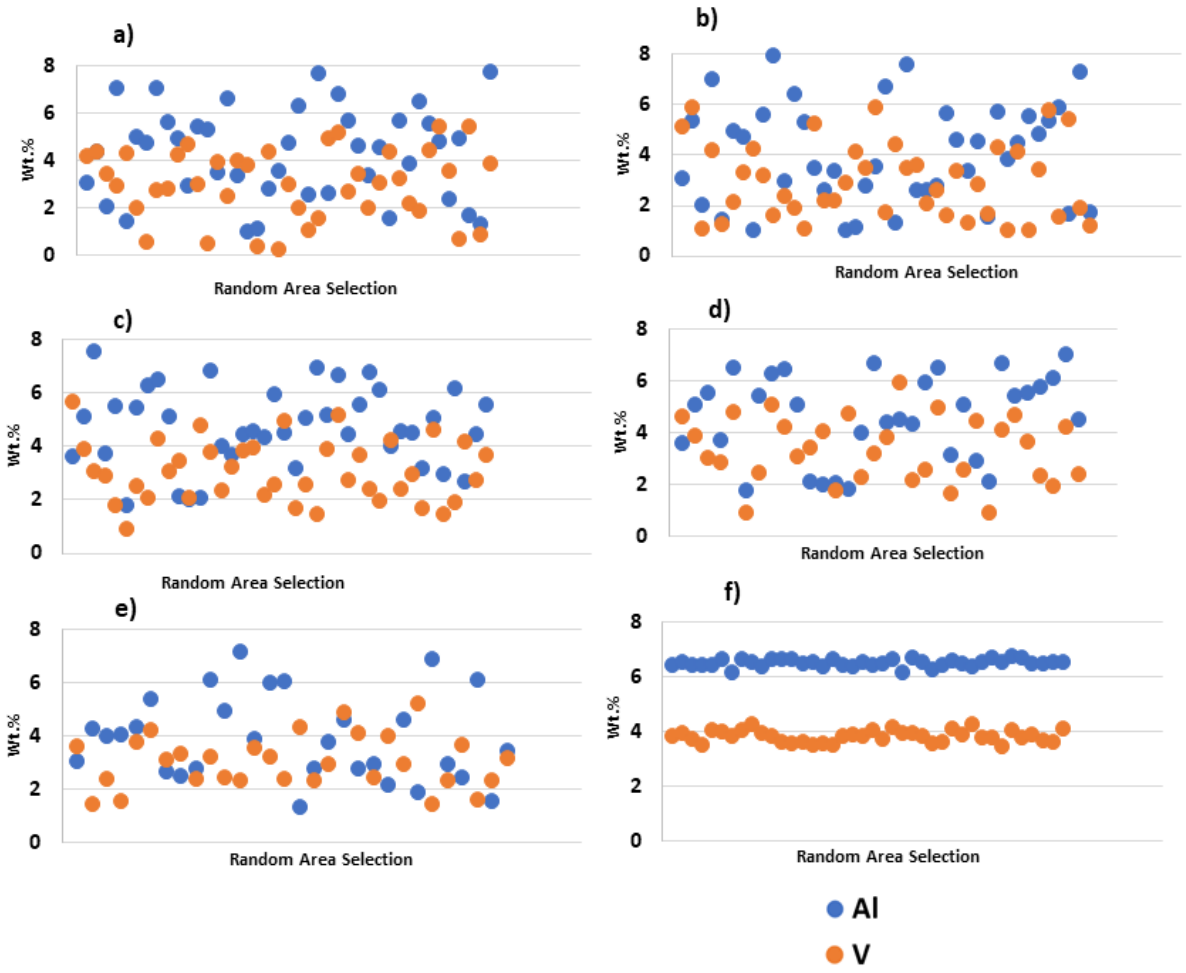

Figure 35: EDX analyses at a scan area of 100×100µm for CpTi + MA blend compacts sintered at 1000°C for (a) 0.5 hours (b) 1-hour (c) 2hours (d) 3 hours and (e) 4 hours compared to (f) wrought Ti6Al4V (W-Ti).

Figure 36 shows that the higher sintering temperature of 1150°C resulted in an increase in diffusivity of vanadium. The range of vanadium improved from 1 – 7 wt.% to 2.5 – 6.5 wt.% after 2 hours of sintering. Increase in time at the sintering temperature resulted in an improvement in distribution of vanadium which was distributed between 0.5 – 4 wt.% at 0.5 hours and after sintering for 4 hours the distribution improved to 2 – 4.5 wt.%.

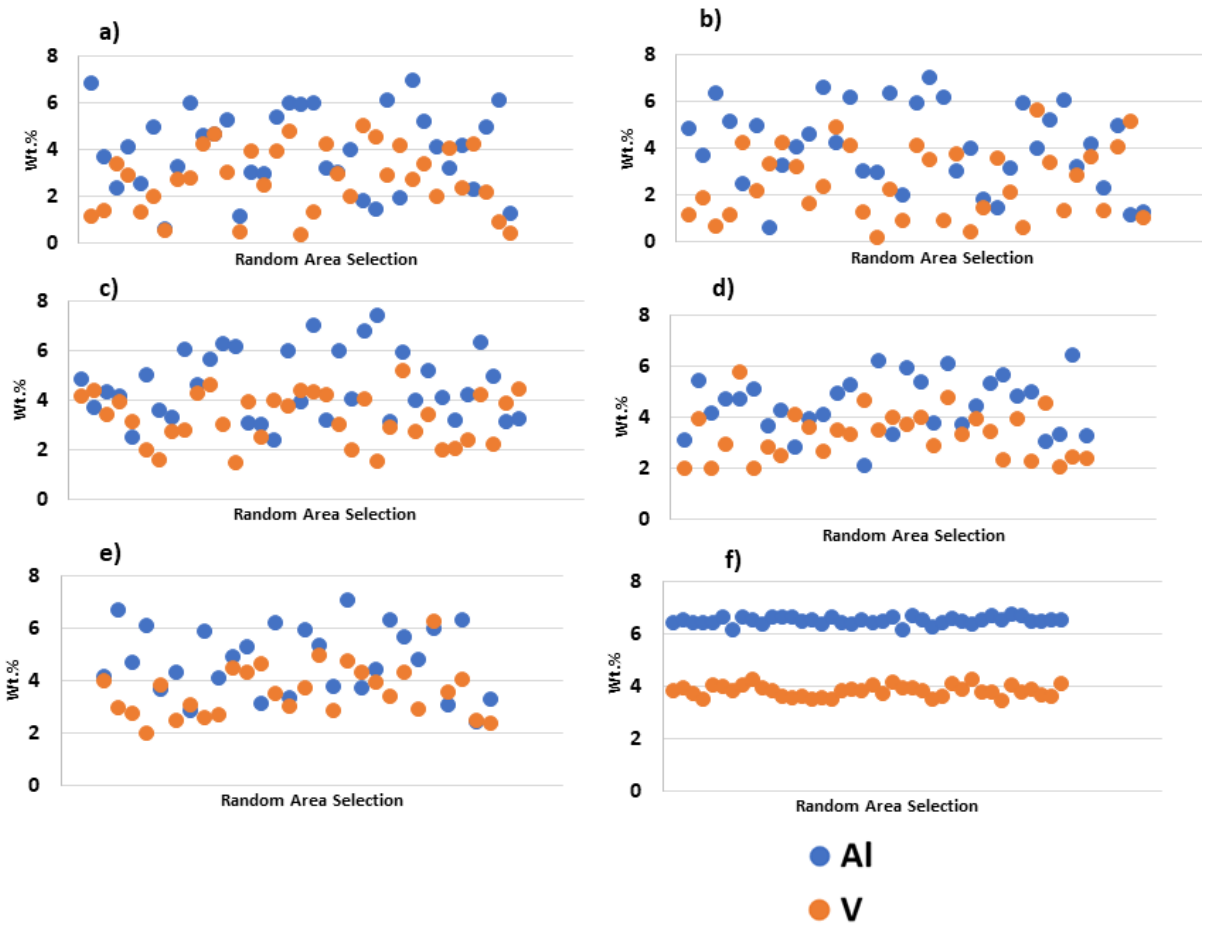

Figure 36: EDX analyses at a scan area of 100×100µm for CpTi + MA blend compacts sintered at 1150°C for (a) 0.5 hours (b) 1-hour (c) 2hours (d) 3 hours and (e) 4 hours compared to f) wrought Titanium (W-Ti).

Figure 37 shows that an increase in temperature to 1250°C improves the diffusivity of the alloying elements to a higher extent. It can be noted that CpTi + MA blend took longer than the TiH_2 + MA blend to reach this composition range of a composition of 4 -6.5 wt.% of aluminium and 1 – 4.5wt.% of vanadium as it took 4 hours compared to the 2 hours that the latter blend took to reach the same state. It can also be noted that the diffusivity of vanadium was slower as the range for the TiH_2 + MA blend at 2 hours was 3 – 4.5 wt.%, whereas for the CpTi +MA blend it was 1 – 4.5 wt.%.

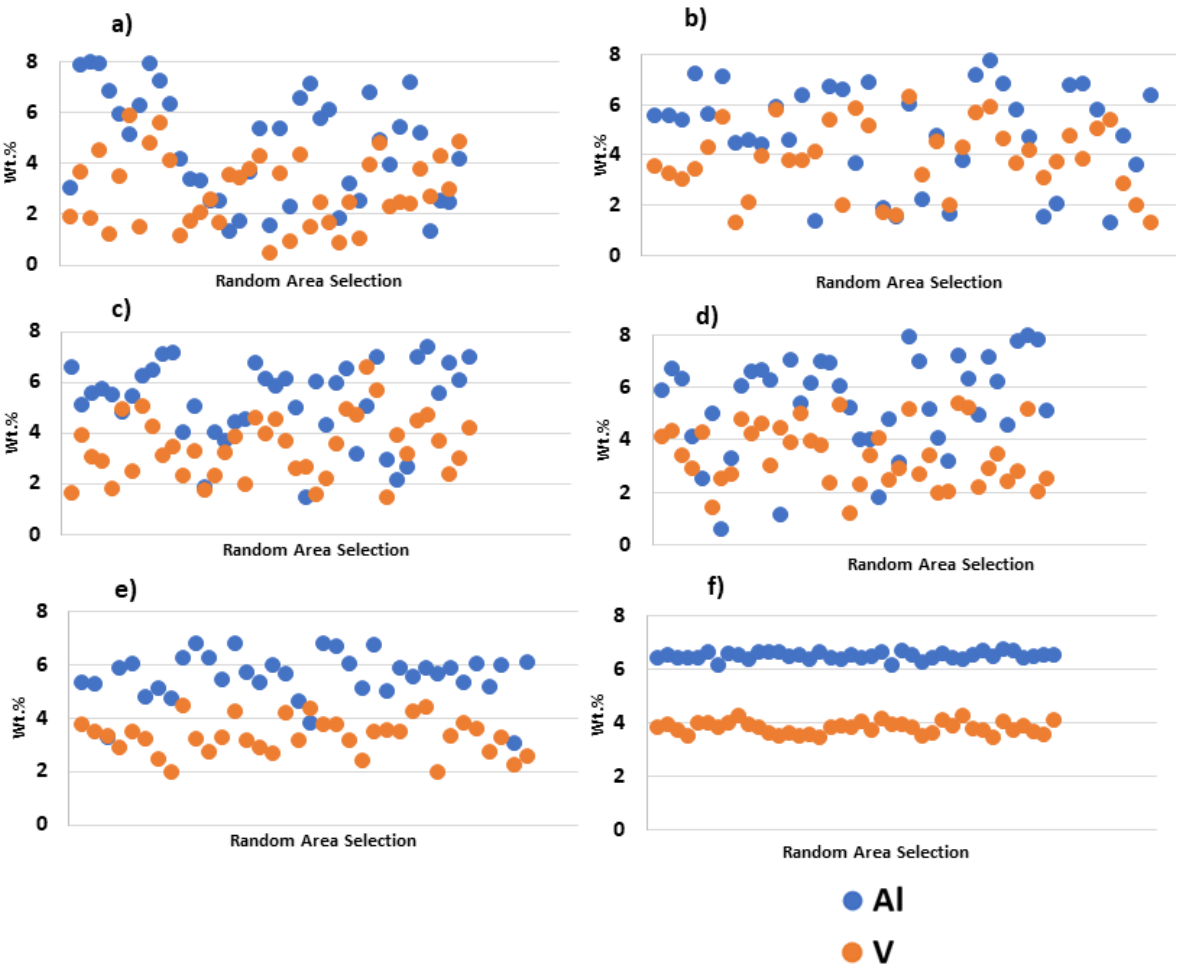

Figure 37: EDX analyses at a scan area of 100×100µm for CpTi + MA blend compacts sintered at 1250^{o}C for (a) 0.5 hours (b) 1-hour (c) 2hours (d) 3 hours and (e) 4 hours compared to (f) wrought Ti6Al4V (W-Ti).

Figure 38 shows that at 1350°C it can be noted that the diffusivity of the elements greatly improved. It is observed that even at a lower time for example after an hour the composition of the elements had already greatly improved and moved towards homogeneity. After 4 hours of sintering the samples demonstrated reasonable homogeneity, although still significantly less homogeneous than the wrought alloy with a composition range of 4.5 -6.5 wt.% of aluminium and 2 – 4.5wt.% of vanadium

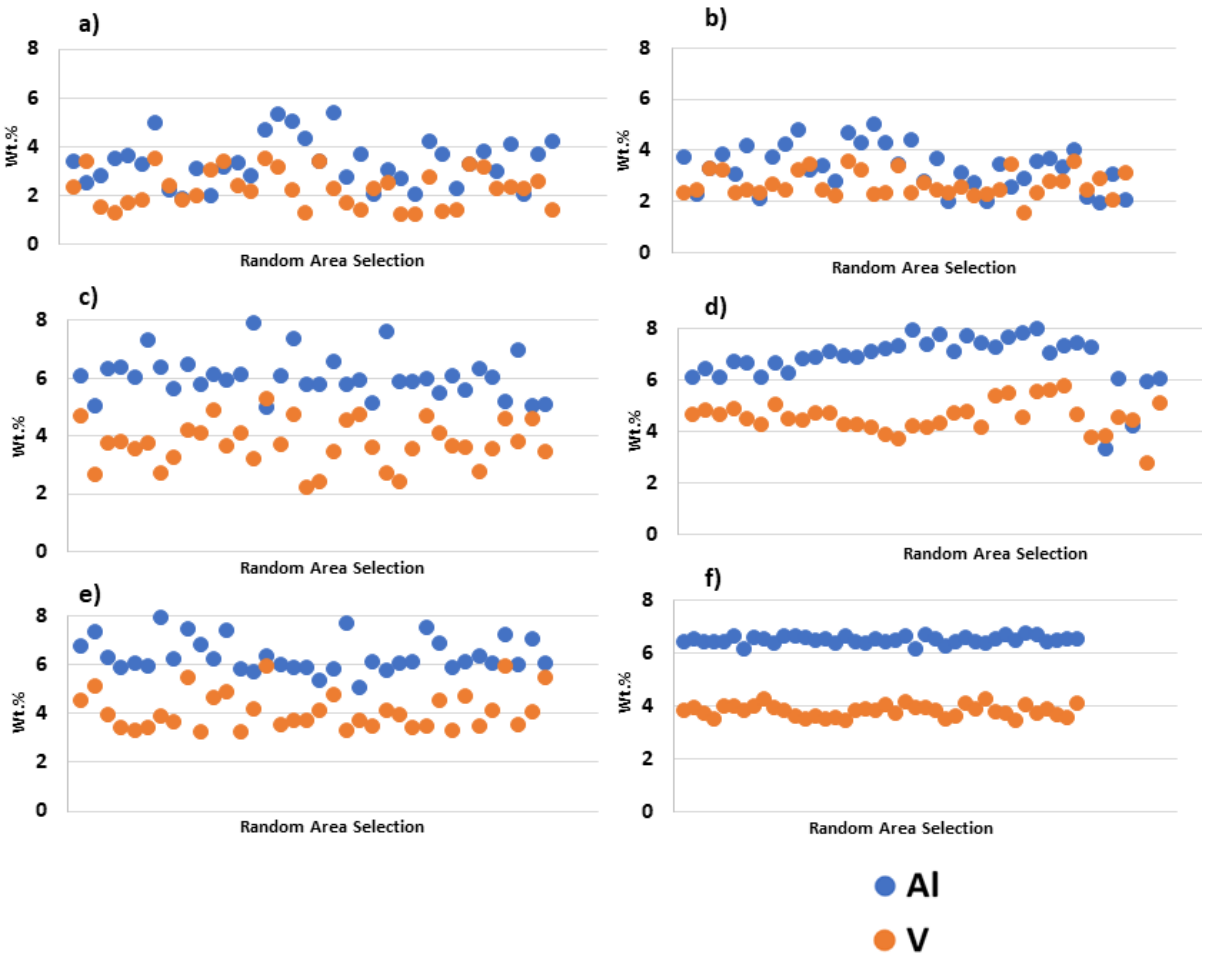

Figure 38: EDX analyses at a scan area of 100×100µm for CpTi + MA blend compacts sintered at 1350^{o}C for (a) 0.5 hours (b) 1-hour (c) 2hours (d) 3 hours and (e) 4 hours compared to (f) wrought Ti6Al4V (W-Ti).

4.3.4 TiH_2 + Al + V powder blend

Figures 39 – 42 show the results of the EDX scans of the as sintered samples of the TiH_2 + Al + V powder blend.

Compared to the first two blends, the TiH_2 + Al + V powder blend had the least diffusivity with increase in sintering time for both Aluminium and Vanadium. At times 0.5 hours to 2 hours at a sintering temperature of 1000°C in figure 39, there was extremely low diffusivity, and in some cases neither of the elements were detected. This is attributed to the low diffusivity of these elements as well as the small area scans that were analysed. With such a low diffusivity of the elements some areas would not have the elements diffused into them.

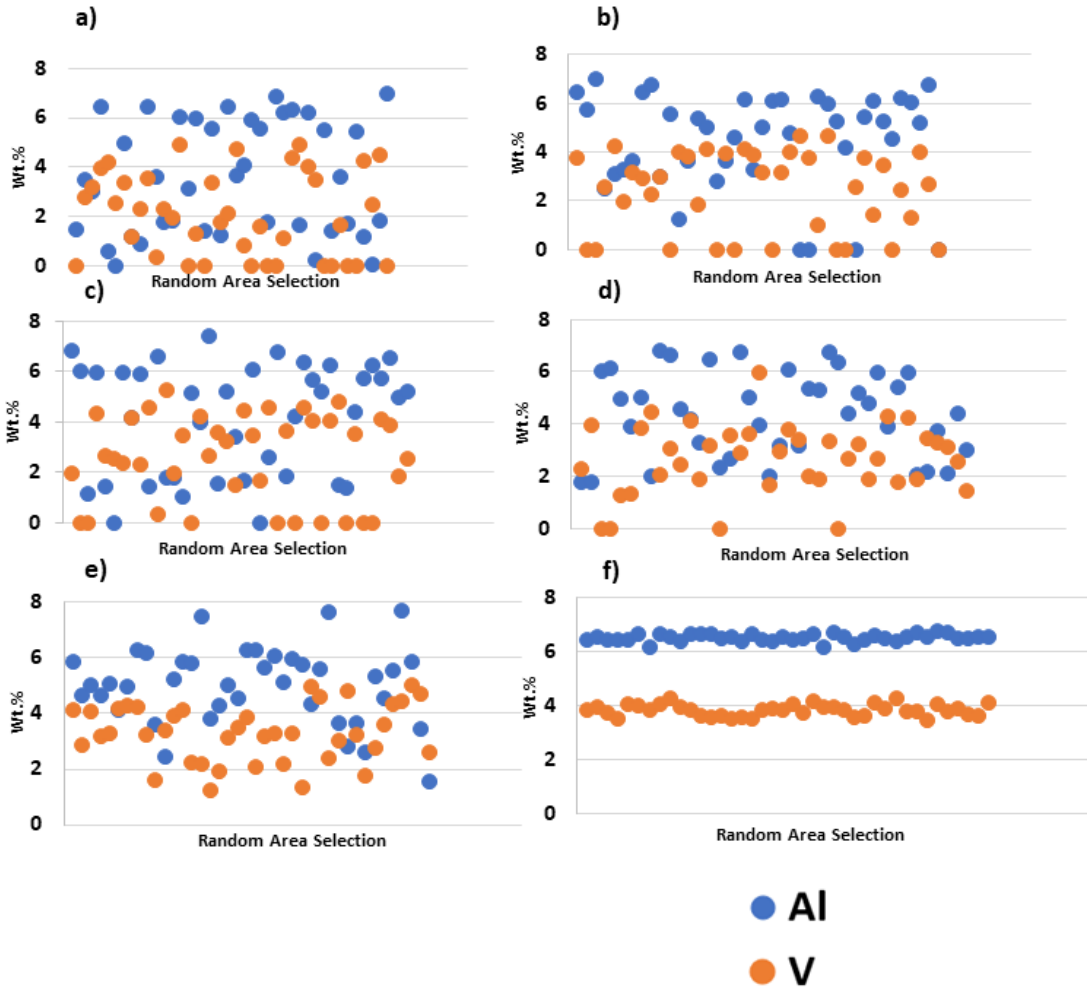

Figure 39: EDX analyses at a scan area of 100×100µm for TiH_2 + Al + V blend compacts sintered at 1000°C for (a) 0.5 hours (b) 1-hour (c) 2hours (d) 3 hours and (e) 4 hours compared to (f) wrought Ti6Al4V (W-Ti).

An increase in temperature to 1150°C, Figure 40, resulted in an improvement of the diffusivity of aluminium. After sintering for 3 hours the lower wt.% composition range had moved from 0 to 1 wt.%, whereas the upper limit remained the same at 7.5 wt.%. The increase in temperature to 4 hours of sintering improved the range to 2 to 6.5wt.%.

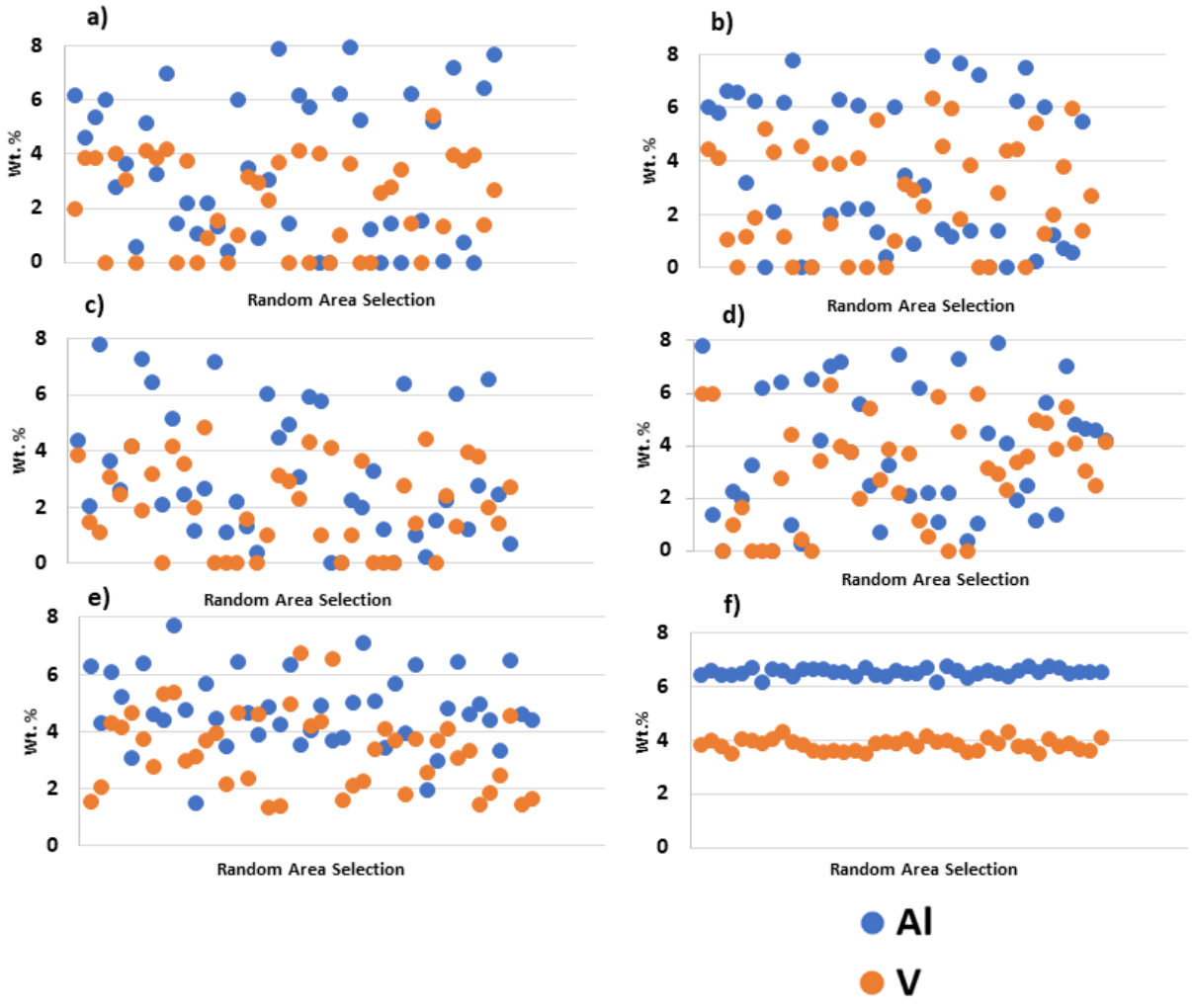

Figure 40: EDX analyses at a scan area of 100×100µm for TiH_2 + Al + V blend compacts sintered at 1150°C for (a) 0.5 hours (b) 1-hour (c) 2hours (d) 3 hours and (e) 4 hours compared to (f) wrought Ti6Al4V (W-Ti).

The diffusivity of aluminium increased at 1250°C, Figure 41, with the wt.% range starting from 1.5 after sintering for 2 hours. The diffusivity of vanadium also increased with most areas showing vanadium after 3 hours of sintering.

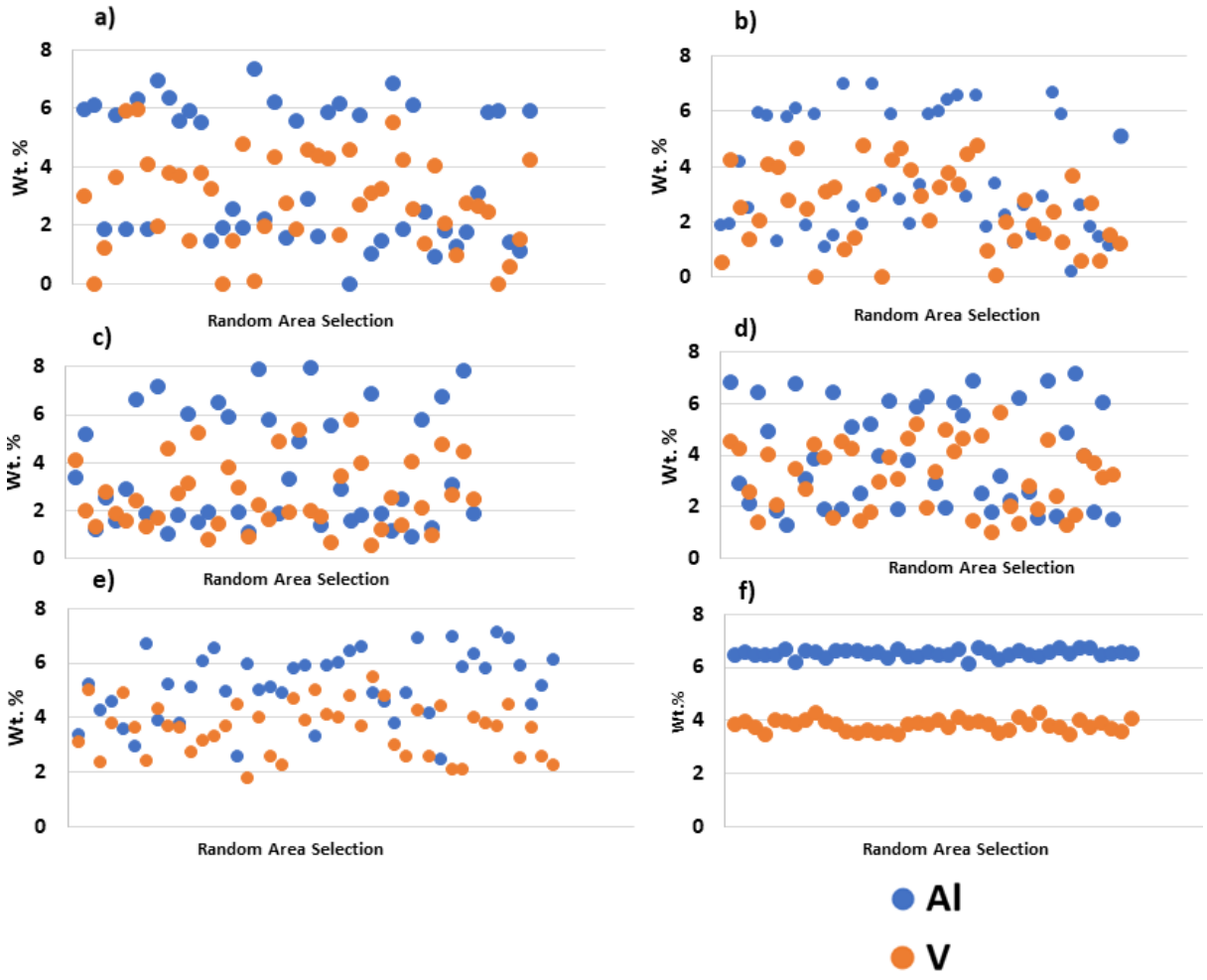

Figure 41: EDX analyses at a scan area of 100×100µm for TiH_2 + Al + V blend compacts sintered at 1250°C for (a) 0.5 hours (b) 1-hour (c) 2hours (d) 3 hours and (e) 4 hours compared to (f) wrought Ti6Al4V (W-Ti).

An increase in temperature to 1350°C, Figure 42, resulted in an increase in the diffusivity of both aluminium and vanadium. After 4 hours of sintering the samples demonstrated substantial improvement in homogenization with much closer tolerances around the Al=6.0 and V=4.0 set values.

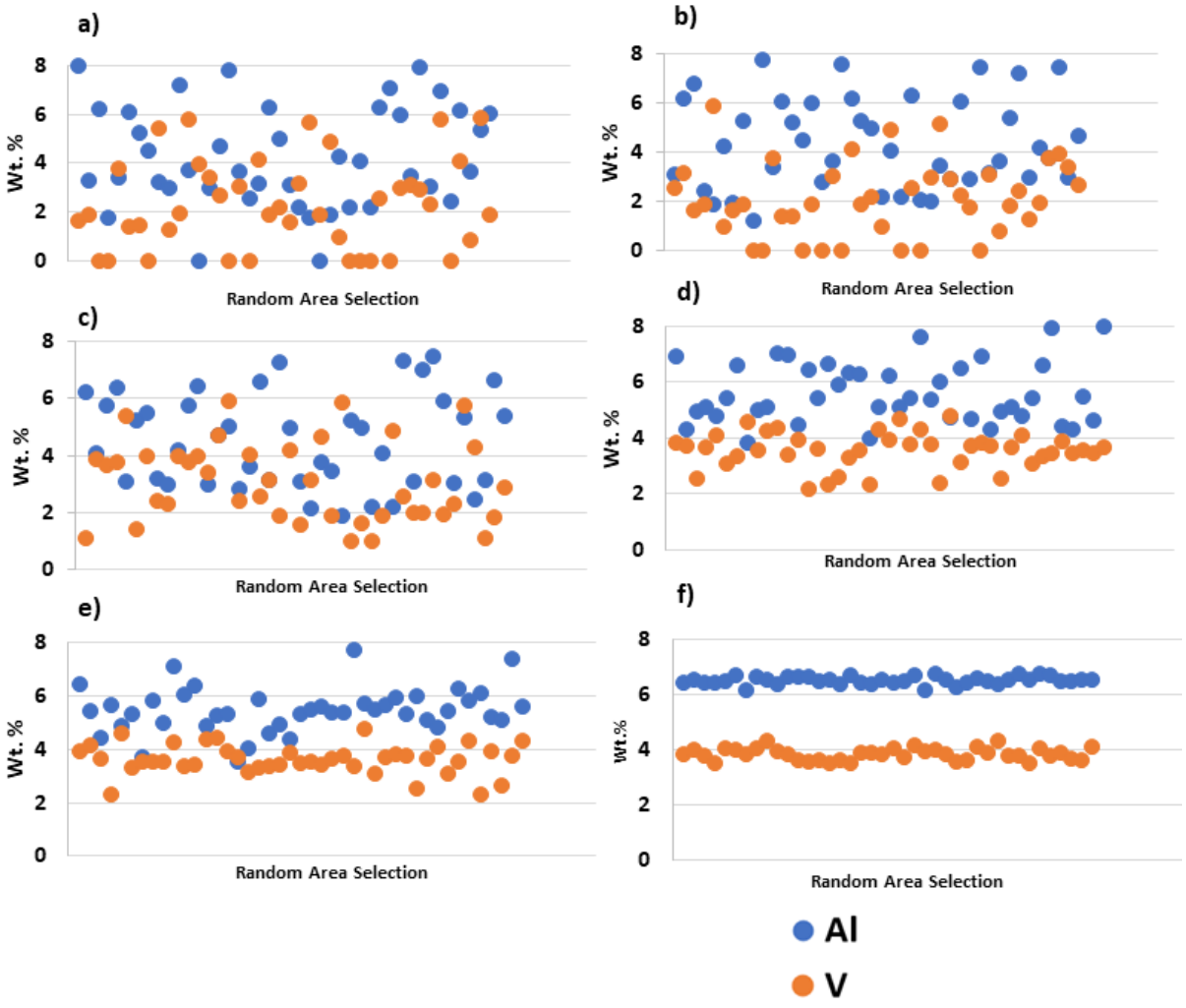

Figure 42: EDX analyses at a scan area of 100×100µm for TiH_2 + Al + V blend compacts sintered at 1350^{o}C for (a) 0.5 hours (b) 1-hour (c) 2hours (d) 3 hours and (e) 4 hours compared to the (f) wrought Ti6Al4V (W-Ti).

4.3.5 Discussion of composition analysis

It can be noted that the progress in homogenization as function of time and sintering temperature varied for the different powder blends. The reason behind this is because of the different diffusivities of the base powders and alloying powders used to create the powder blends.

As discussed above in the density section, it can be noted that the TiH_2 + MA powder blend sinters better followed by the CpTi + MA and then lastly the TiH_2 + Al + V powder blends. This was also seen in this section where the TiH_2 + MA powder reached a level of homogeneity at a temperature of 1350°C and sintering time of 2 hours, whereas CpTi + MA reached a reasonable level of homogeneity at a temperature of 1350°C and sintering time of 4 hours. TiH_2 + Al + V had an improvement in the diffusivity of alumimium and vanadium but did not reach homogeneity after sintering at 1350°C for 4 hours. This aligns with literature which states homogeneity in titanium powder blends starts to show after a sintering temperature of 1200°C.[22]

4.3.5.1 Effect of the Base powders on the chemical homogenization of the powder blends

The time and temperature needed for the chemical composition of powder blends to reach homogeneity is mainly a result of the base powder. In this project we had two base powders namely, TiH_2 and CpTi and the type of the alloying elements was elemental aluminium and vanadium and as well as the 60%Al-40%V master alloy.

TiH_2 has a better sinter ability than CpTi. When TiH_2 is sintered in vacuum, hydrogen is released. The release of hydrogen results in the reduction of surface oxides which improves mass transfer and increases diffusivity of Al and V into the titanium matrix.[6] The release of hydrogen, as shown in Figure 43, causes a phase transformation which also results in the formation of crystal defects. These lattice defects cause atoms to move via vacancy movement. The crystal defects result in the reaction of titanium and aluminium happening at low temperatures of 570 – 630°C which are lower than the melting temperature of aluminium which is 665°C.[34] This results in a reduction of pores and an increased diffusivity of aluminium in the solid state. This increased diffusivity also decreases the formation of $TiAl_3$ intermetallic forming which is the initial phase formed when titanium reacts with liquid aluminium.

Whereas when CpTi is used as a base powder, diffusion of aluminium in the solid state is decreased, and aluminium melting occurs and an exothermic reaction forming $TiAl_3$ takes place. $TiAl_3$ intermetallic decreases the ductility of the titanium alloy and reduces homogeneity by tying up aluminium, reducing aluminium diffusion during sintering. Having intermetallics in the structure results in less resistance to oxidation at higher temperatures which is an undesirable property for Ti-6Al-4V.

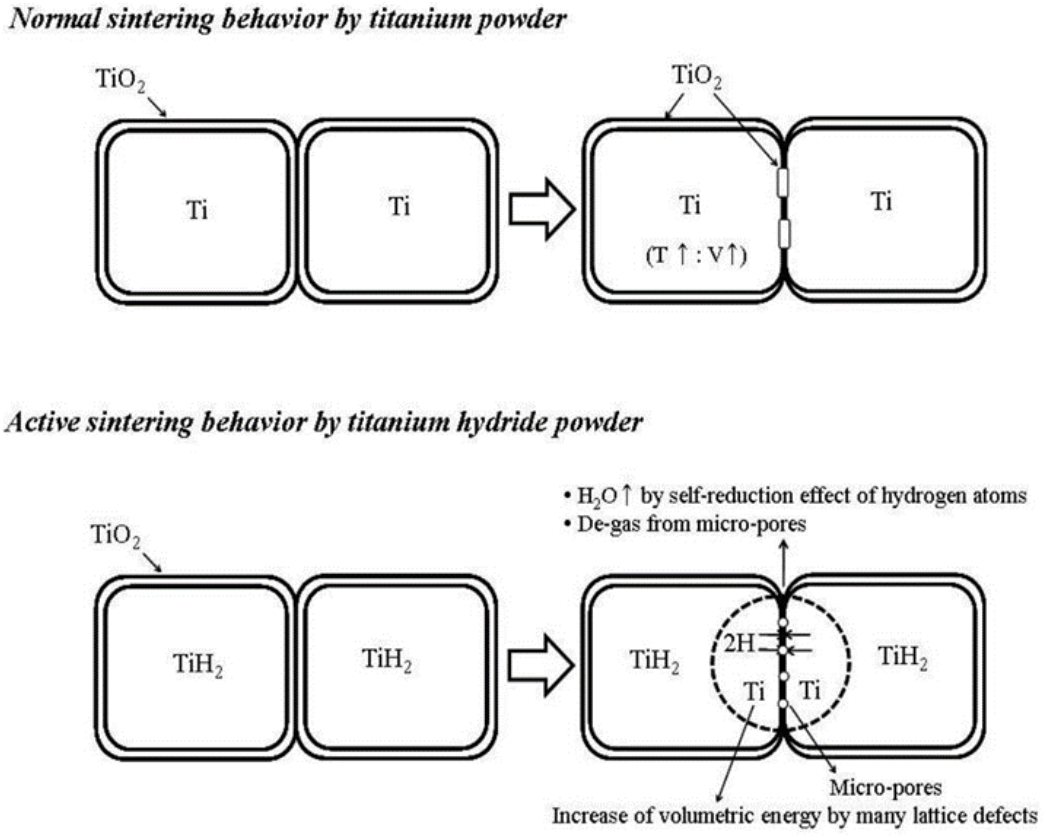

Figure 43: Comparison of the sinter ability of CpTi and TiH_2 [6] .

4.3.5.2 Effect of alloying elements on the chemical homogenization of the powder blends

Diffusivity is primarily temperature dependent and an increase in temperature increases diffusivity. Therefore, the higher the processing temperatures the faster it is for elemental diffusion to occur in the titanium matrix. Sintering and chemical homogenization of the titanium matrix is mainly assisted by alloys containing faster diffusing elements such as Al and Fe, while slower diffusing elements such as Mo and V delay elemental homogenization. [22] The diffusion of alloying elements with different diffusivities, in this case Al and V, can impact on

the diffusion of each other. Aluminium is an alpha stabilizer whilst vanadium is a beta stabilizer which would mutually hinder diffusion due to the stabilization of corresponding phase barriers. So, at lower temperatures, the diffusion of V is slowed down by Al. As the Al diffuses the degree of saturation of Al in such areas is reduced, so that when the temperature increases, V can diffuse faster. It is better to introduce Al and V as a master alloy than as elemental powders.[14]The results in this project show that powder blends that had the Al-V master alloy as the alloying element had an increased homogeneity compared to the blend made from elemental Al and V regardless of the base powder. As mentioned above the combination of different alloying elements has a synergistic effect that can affect chemical homogenization of powder blends.

Introduction of α or β alloying elements separately as two powders, each containing only one type of element results in stabilization of the corresponding phases in areas enriched with α or β elements due to diffusion from alloying powder into the matrix. Penetration of α-stabilizers in the β-phase and vice versa, β-stabilizers in α-phase is difficult thus hindering overall homogenization. This is shown in the results where it took a high temperature of 1350°C after 4 hours for the TiH_2 + Al+ V blend to produce reasonable diffusivity of Al and V. Adding elemental aluminium separate from elemental vanadium results in aluminium melting and pores being formed in the original elemental aluminium regions. The diffusion of aluminium in the liquid state causes pore formation resulting in a decrease in density as well as chemical composition in homogeneity. As can be seen from the results above at lower temperatures of the TiH_2 + Al+ V blend there were scanned areas that did not have aluminium present or very low composition of aluminium present.

Aluminium is an alpha stabilizer and therefore diffuses into the titanium matrix at lower temperatures. This results in an aluminium enriched alpha phase of titanium. Penetration of the aluminium stabilised titanium matrix by vanadium becomes very difficult as vanadium is blocked from penetrating the alpha areas. This hinders homogenization.

Therefore, in the figures 39 - 42 vanadium took a long time to reach a chemical composition close to homogeneity and would have some areas with 0 wt.% at all sintering temperatures. A reasonable level of homogenization of the powder blend containing elemental Al and V can

be reached by increasing the temperature as demonstrated where temperature was increased to 1350°C. The increase in temperature would then allow alpha to beta transformation to occur in the aluminium rich areas or very long exposure time like above 4 hours would be enough for aluminium to penetrate the beta phase. In this project a combination of a high temperature plus a long exposure time of 4 hours encouraged a more homogeneous structure to form. However, high temperatures and high exposure times are not ideal as it is expensive. To avoid more expensive sintering conditions Ti-6Al-4V, a master alloy is used instead. The master alloy contains both Al and V, with a composition of 60%Al-40%V. To ensure homogeneity in the powder blends that were alloyed with the master alloy a combination of time and temperature was considered. In the case of the TiH_2 + MA powder blends, improved homogenization occurred at 1250°C after sintering for 2 hours. This is because aluminium possesses a higher solubility in the alpha phase at lower temperatures than vanadium. Therefore, aluminium saturates the titanium matrix as observed and aluminium generally reaches closer to homogenization prior to homogenization of the vanadium content.

Aluminium saturates the matrix around the initial master alloy particles and preserves areas of alpha phase titanium up to temperatures higher than the beta transus temperature. These alpha areas would then act as barriers to vanadium resulting in aluminium being at a higher concentration as shown in the Figures above. Increase in aluminium concentration results in an increase in mutual diffusivity. Increase in temperature increases vanadium diffusivity but it will still be lower than aluminium diffusivity because of the high vanadium content in the beta phase that remains in the area where the master alloy was when aluminium diffuses out first. Formation of a homogenous alloy is determined by slow vanadium redistribution and again needs long time exposure or increased temperature to attain chemical homogeneity.

4.4 XRD Analysis

XRD Analysis was also used to measure homogenization progress by identifying how the structure of the sintered powdered blends was moving towards the wrought Ti6Al4V structure. The analysis was done by overlaying peaks of possible transition compounds and intermetallics obtained from literature that would form as the powder blends were moving

towards homogeneity. $TiH_{1.5}$, was one of the compounds that were chosen; this was because of a study by Gökelma et al,[41] discussed earlier, that showed that dehydrogenation of TiH_2 powders did not result in the powders going to their original state of CpTi and powder peaks in the form of TiH_2 and $TiH_{1.5}$ appeared on the XRD spectra as shown by Figure 22. The intermetallics that were chosen were $TiAl_3$ and Ti_3Al; $TiAl_3$ was chosen because a study by Skolakova[50], it showed that when sintering TiAl powder blends, solid titanium reacted with liquid aluminium to form $TiAl_3$. Ti_3Al phase was also formed around unreacted particles of titanium, and its formation was probably enabled by the reaction between titanium and an already present phase, probably the $TiAl_3$ phase, or when the presence of Ti_3Al was detected on the XRD spectra indicative of the alloying process being incomplete at lower temperatures as shown in Figure 23[42].

The 2 Theta peak positions of the intermetallics, other compounds, starting powders (shown in appendix A) and W-Ti were added to the XRD spectra as markers to determine how the structure of the sintered powders were moving towards homogeneity and the extent to which the compounds and intermetallics formed during the process. Three important aspects to note as the blends move towards homogeneity are peak shift, peak widening, and peak splitting and will be discussed further and taken note of as the results are relayed. To make peak shift and peak splitting clearer the XRD spectra of relative X-ray intensity versus 2 Theta° was split according to 40°-51°, 58°-64°, 74°- 80°,82°-88° and 89°- 95° respectively. Figure 44 below shows the XRD spectra of W-Ti and will be referred to throughout this section.

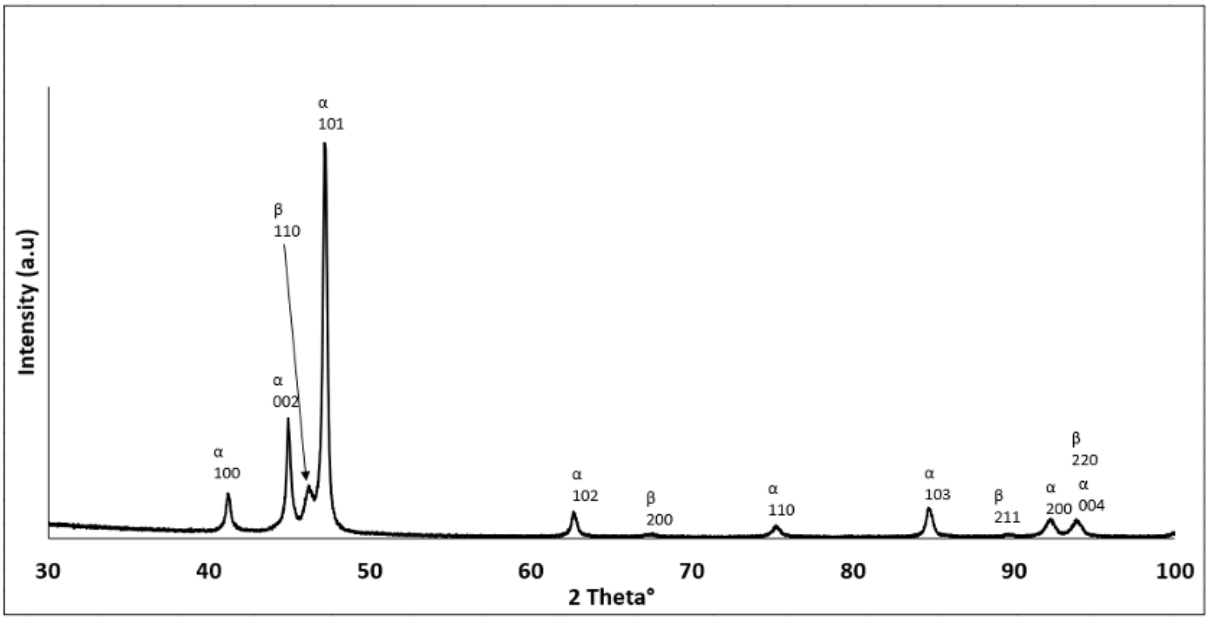

Figure 44 : XRD Spectra of Wrought Ti6Al4V sample.

4.4.1 TiH_2 + MA powder blend

Figures 45 – 48 and Figures A1-A4 show the XRD patterns for the specimens sintered at 1000°C, 1150°C ,1250°C and 1350°C for Titanium hydride and the master alloy powder blend.

As shown in Figure 45 and 46, at 1000°C and 1150°C, none of the expected intermediary compounds or intermetallic match the peaks. Figure A1 – A4 also shows that the sintered powder blends had moved away from its original powder elements as well as none of the peaks coincided with the starting powders; therefore, unidentified intermediate phases are present. However, as the sintering time increases there is a peak shift towards the W-Ti peaks shown, the peak widening intensity decreases and the peak height intensity increases showing diffusion is taking place and new phases are forming.

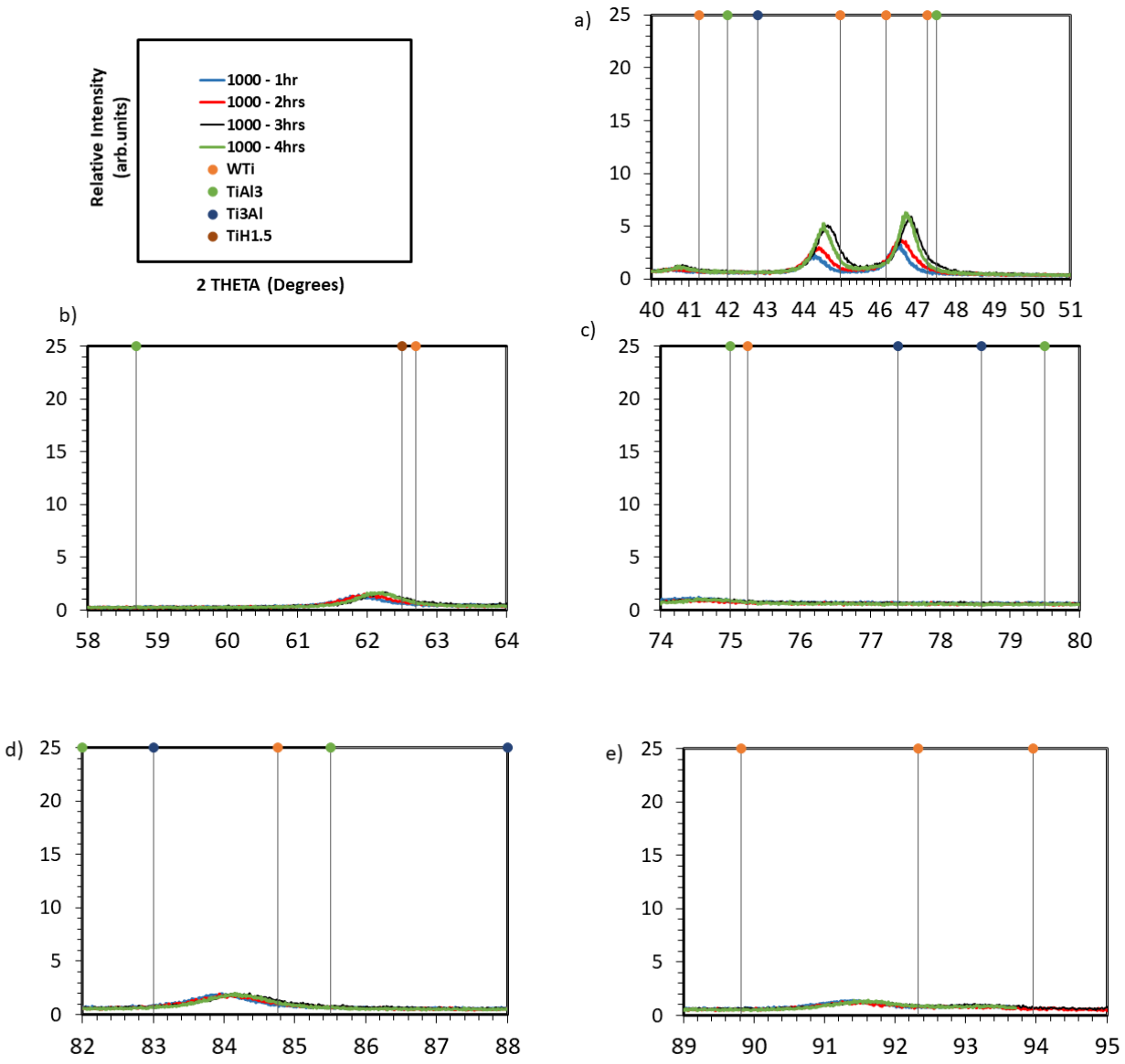

Figure 45: XRD spectrum for; TiH_2 + MA blend compacts sintered at 1000°C for 1hour, 2 hours, 3hours and 4 hours respectively and W-Ti, $TiAl_3$, Ti_3Al and $TiH_{1.5}$ peaks represented by lines on a split 2 Theta of a) 40-51° b) 58-64° c) 74-80° d) 82-88 ° e) 89-95°.

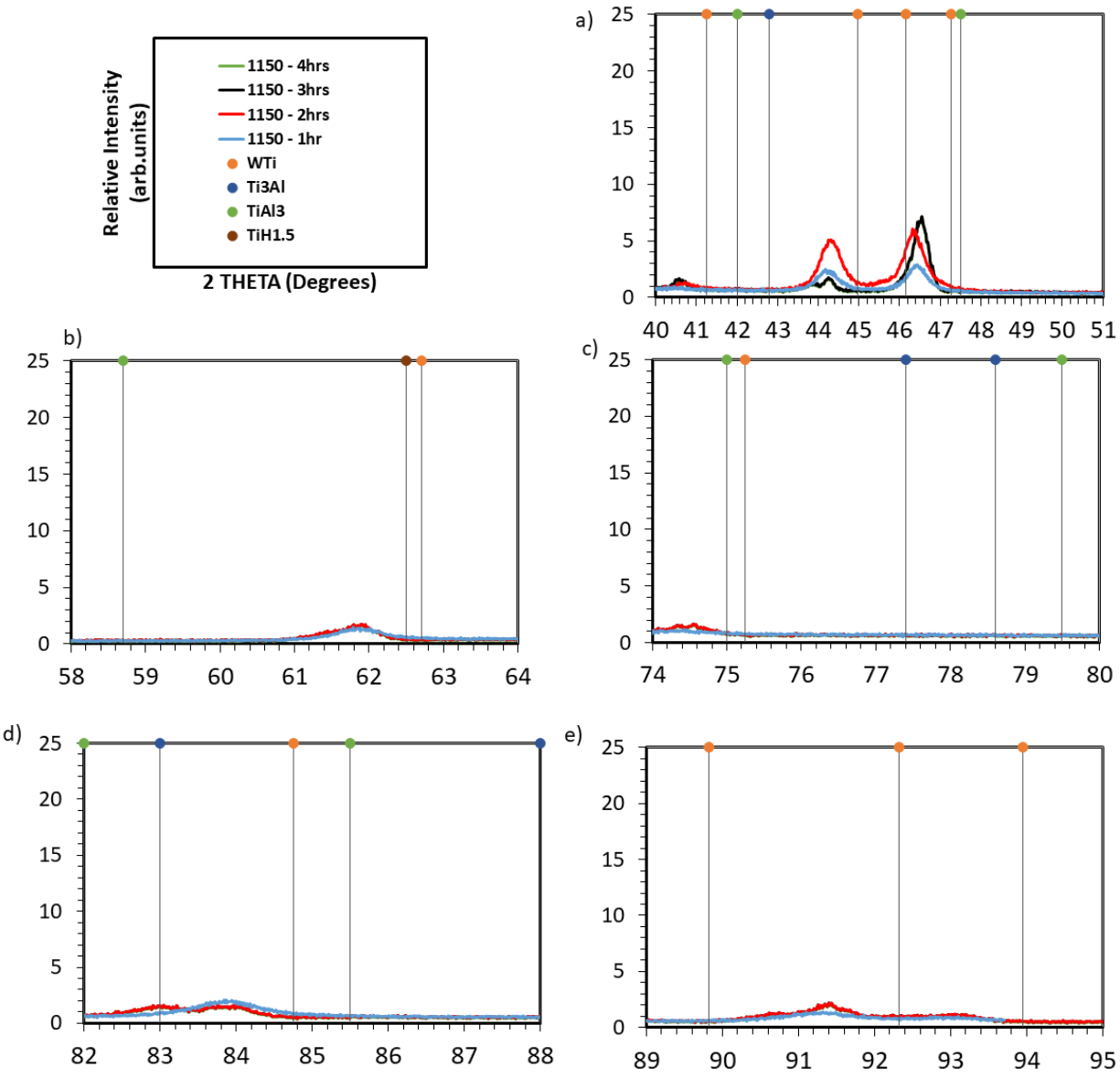

Figure 46: XRD spectrum for; TiH_2 + MA blend compacts sintered at 1150°C for 1hour, 2 hours, 3hours and 4 hours respectively and W-Ti, $TiAl_3$, Ti_3Al and $TiH_{1.5}$ peaks represented by lines on a split 2 Theta of a) 40-51° b) 58-64° c) 74-80° d) 82-88 ° e) 89-95°.

Figure 47 shows that at 1250°C there is an increase in the peak height intensity as the sintering time increases from 1hr to 4 hrs. Increasing the sintering temperature, results in the dissolution of the master alloy particles and a new peak indicating a new phase not shown in the spectra at 1000°C and 1150°C is shown to form between 46.2 and 46.7 after sintering for 2 hours at 46.37° which corresponds with the beta phase forming which is not completely stable. This observation coincides with the literature that homogenization of titanium powder blends starts occurring at temperatures above 1200°C.[22]

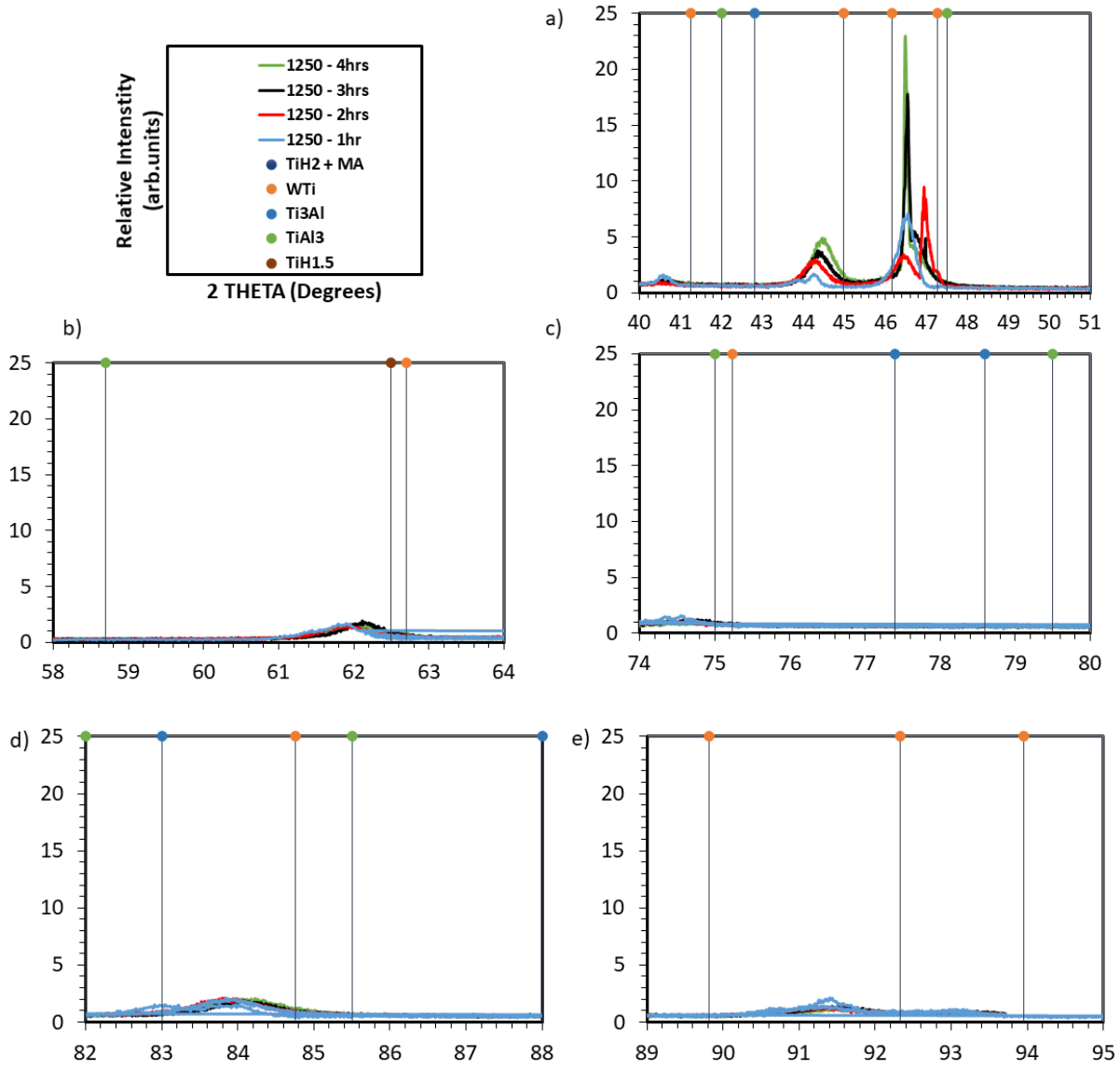

Figure 47: XRD spectrum for; TiH_2 + MA blend compacts sintered at 1250^{o}C for 1hour, 2 hours, 3hours and 4 hours respectively and W-Ti, $TiAl_3$, Ti_3Al and $TiH_{1.5}$ peaks represented by lines on a split 2 Theta of a) 40-51° b) 58-64° c) 74-80° d) 82-88 ° e) 89-95°.

Figure 48 shows the beta phase that was seen after sintering for 2 hours at 1350°C at 46.3° to be stabilized and coinciding with the W-Ti beta peak at that 2 theta. It shows the beta peak at 89.4°and the beta peak at 94.2° coinciding with the W-Ti beta peak markers and the remaining peak not mentioned more closely correlates with W-Ti meaning homogenization had taken place at this temperature after sintering for more than 2 hours.

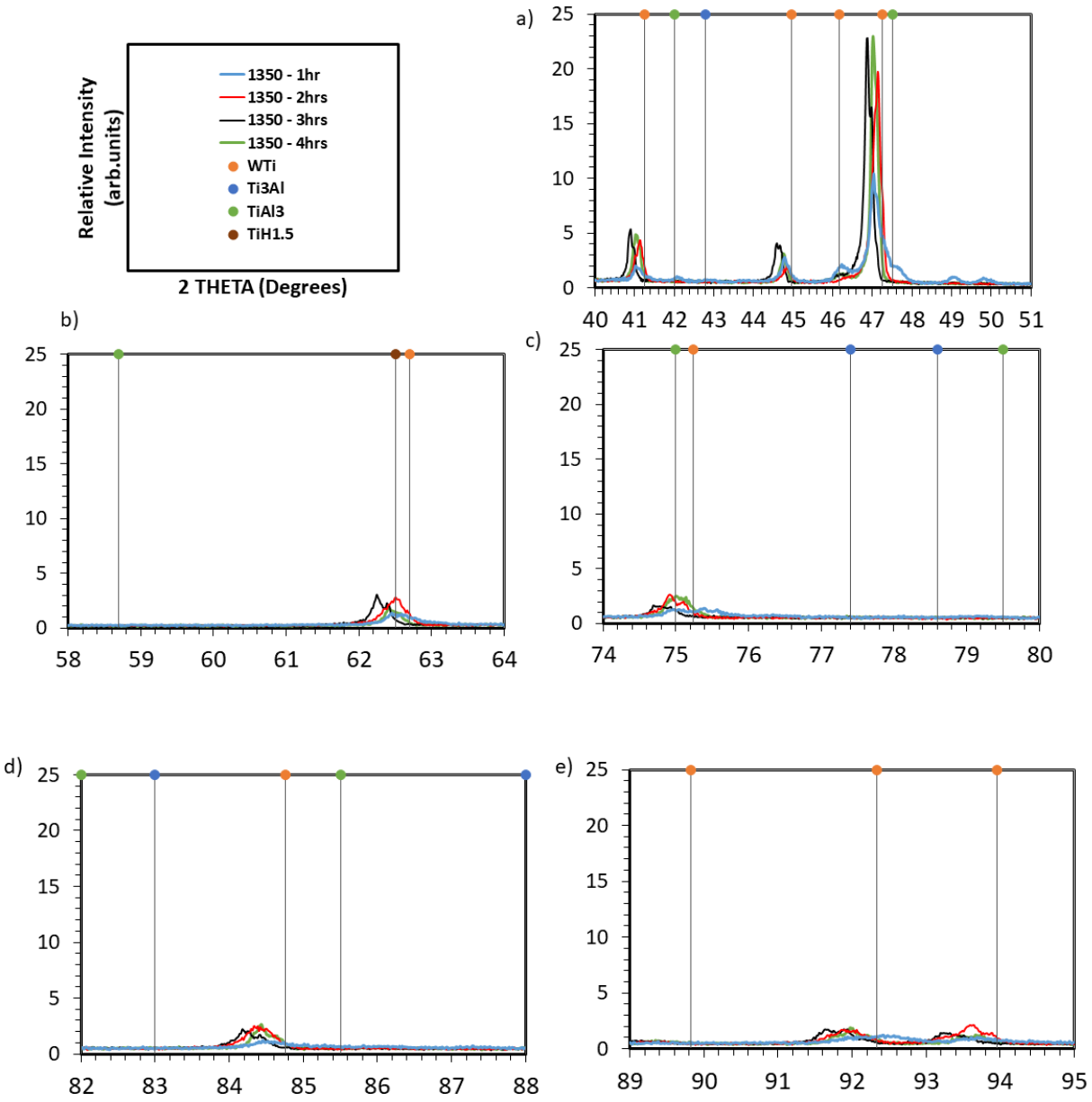

Figure 48: XRD spectrum for; TiH_2 + MA blend compacts sintered at 1350°C for 1hour, 2 hours, 3hours and 4 hours respectively and W-Ti, $TiAl_3$, Ti_3Al and $TiH_{1.5}$ peaks represented by lines on a split 2 Theta of a) 40-51° b) 58-64° c) 74-80° d) 82-88 ° e) 89-95°.

4.4.2 CpTi + MA powder blend

Figures 49 – 52 show the XRD patterns for the specimens sintered at 1000°C, 1150°C ,1250°C and 1350°C for the CpTi + MA powder blend.

At 1000°C and 1150°C there is a match for $TiAl_3$ after sintering for 2 hours. Diffusion is taking place as the peaks did not match with any of the starting powders as shown in Figures A5 –

A8 and there is right peak shift shown moving towards the W-Ti peak markers.

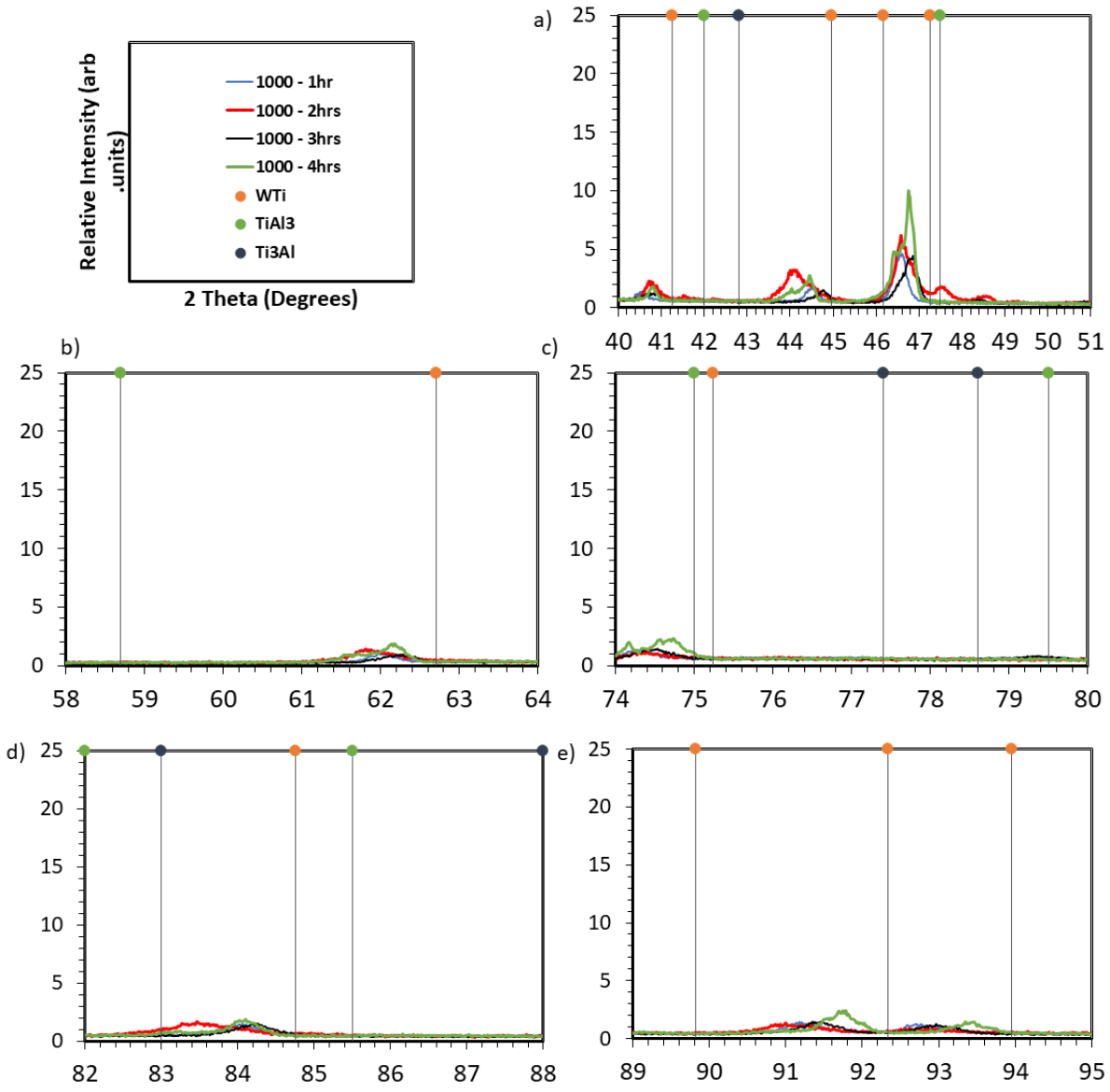

Figure 49: XRD spectrum for; CpTi + MA blend compacts sintered at 1000^{o}C for 1hour, 2 hours, 3hours and 4 hours respectively and W-Ti, $TiAl_3$, and Ti_3Al peaks represented by lines on a split 2 Theta of a) 40-51° b) 58-64° c) 74-80° d) 82-88 ° e) 89-95°.

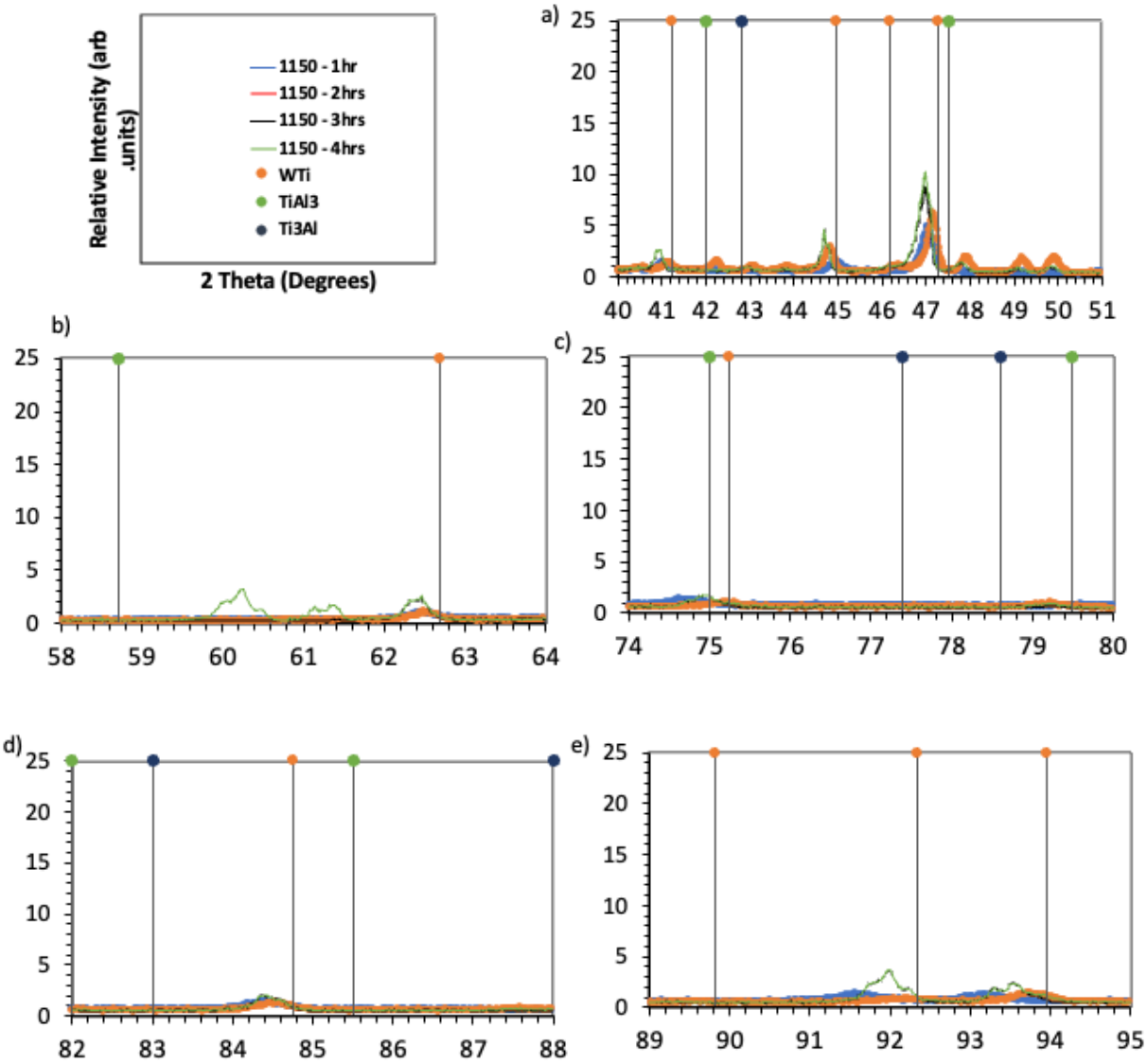

Figure 50: XRD spectrum for; CpTi + MA blend compacts sintered at 1150°C for 1hour, 2 hours, 3hours and 4 hours respectively and W-Ti, $TiAl_3$, and Ti_3Al peaks represented by lines on a split 2 Theta of a) 40-51° b) 58-64° c) 74-80° d) 82-88 ° e) 89-95°.

When increasing the sintering temperature, the dissolution of the master alloy particles continues, and at 1250°C, shown in Figure 51, the beta phase was not detected after sintering for 2 hours unlike in the TiH_2 + MA blend. This means that diffusion had not fully occurred to stabilize the beta phase in titanium. Peak splits at 2 theta values 42°-45° and 47°-50° are observed which are not observed in the TiH_2 + MA sample. This means that diffusion had not fully occurred, and the peak splits were caused by the presence of unknown intermediate phases being formed. After sintering for 4 hours the beta phase had still not been stabilized but there were no peak splits observed.

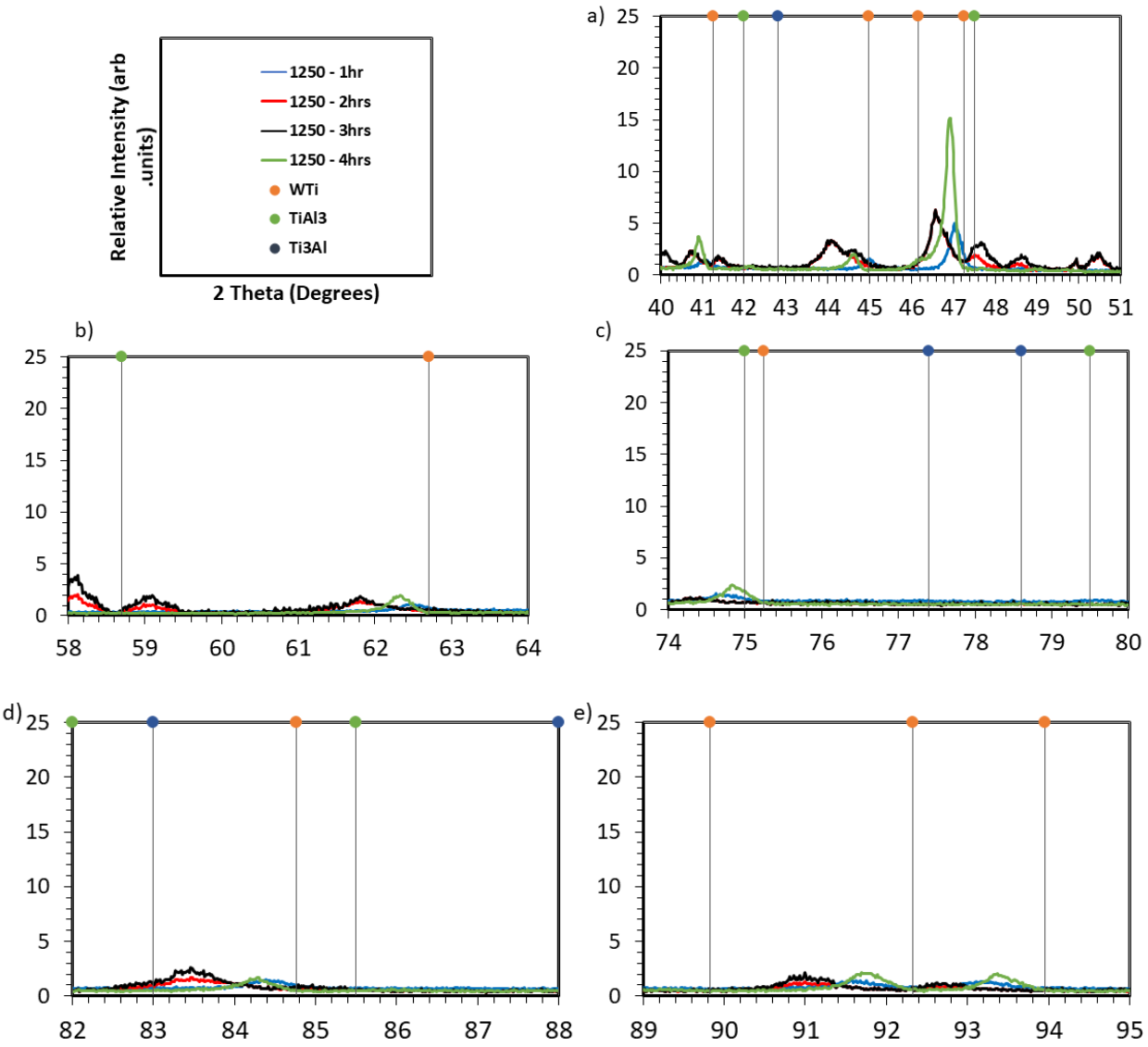

Figure 51: XRD spectrum for; CpTi + MA blend compacts sintered at 1250°C for 1hour, 2 hours, 3hours and 4 hours respectively and W-Ti, $TiAl_3$, and Ti_3Al peaks represented by lines on a split 2 Theta of a) 40-51° b) 58-64° c) 74-80° d) 82-88 ° e) 89-95°.

A further increase of the sintering temperature to 1350°C, as shown in Figure 52, indicate that after sintering for 2 hours a new phase was observed at 47.03°; this phase maybe a partially stabilized Beta phase overlapping with $TiAl_3$ which could cause a peak shift to the left. After 4 hours the beta phase became more stabilized (but still not fully stable) showing the phase at 46.43°.

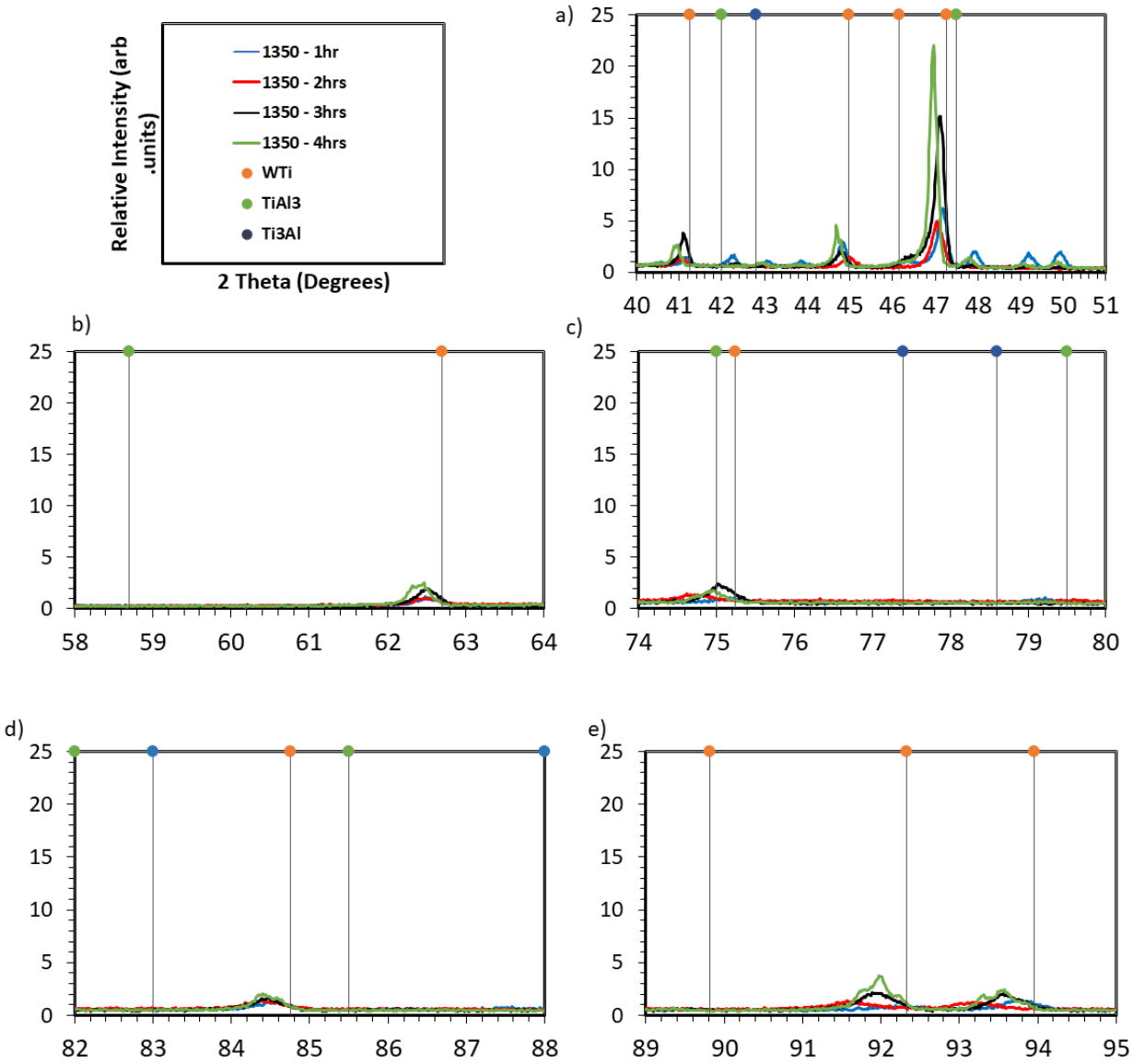

Figure 52: XRD spectrum for; CpTi + MA blend compacts sintered at 1350°C for 1hour, 2 hours, 3hours and 4 hours respectively and W-Ti, $TiAl_3$, and Ti_3Al peaks represented by lines on a split 2 Theta of a) 40-51° b) 58-64° c) 74-80° d) 82-88 ° e) 89-95°.

4.4.3 TiH_2 + Al + V powder blend

Figures 53 – 56 shows the XRD patterns for the specimens sintered at 1000°C, 1150°C ,1250°C and 1350°C for TiH_2 + Al + V powder blend.

At low temperatures of 1000°C, 1150°C and 1250°C, figures 53 – 55, diffusion is noted as none of the peaks match with their starting powders as shown in Figures A9 – A12. There is increase

in peak intensity as sintering time increases.

Peak broadening is also shown, as mentioned in the TiH_2 + MA section, sintering does not result in the expulsion of all the hydrogen and therefore dissolved hydrogen in the lattice results in peak broadening.

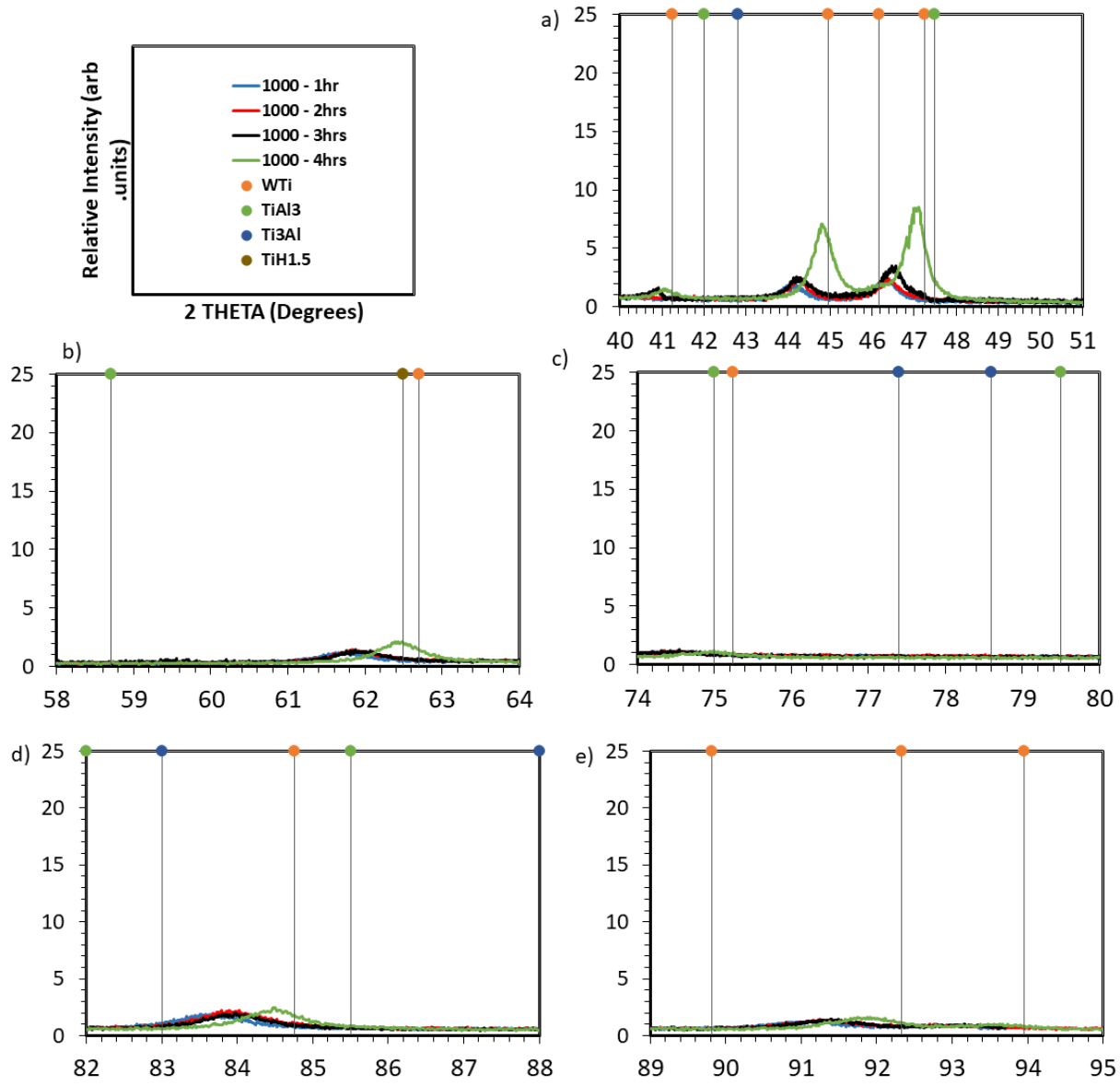

Figure 53: XRD spectrum for; TiH_2 + Al + V blend compacts sintered at 1000^{o}C for 1hour, 2 hours, 3hours and 4 hours respectively and W-Ti, $TiAl_3$, Ti_3Al and $TiH_{1.5}$ peaks represented by lines on a split 2 Theta of a) 40-51° b) 58-64° c) 74-80° d) 82-88 ° e) 89-95°.

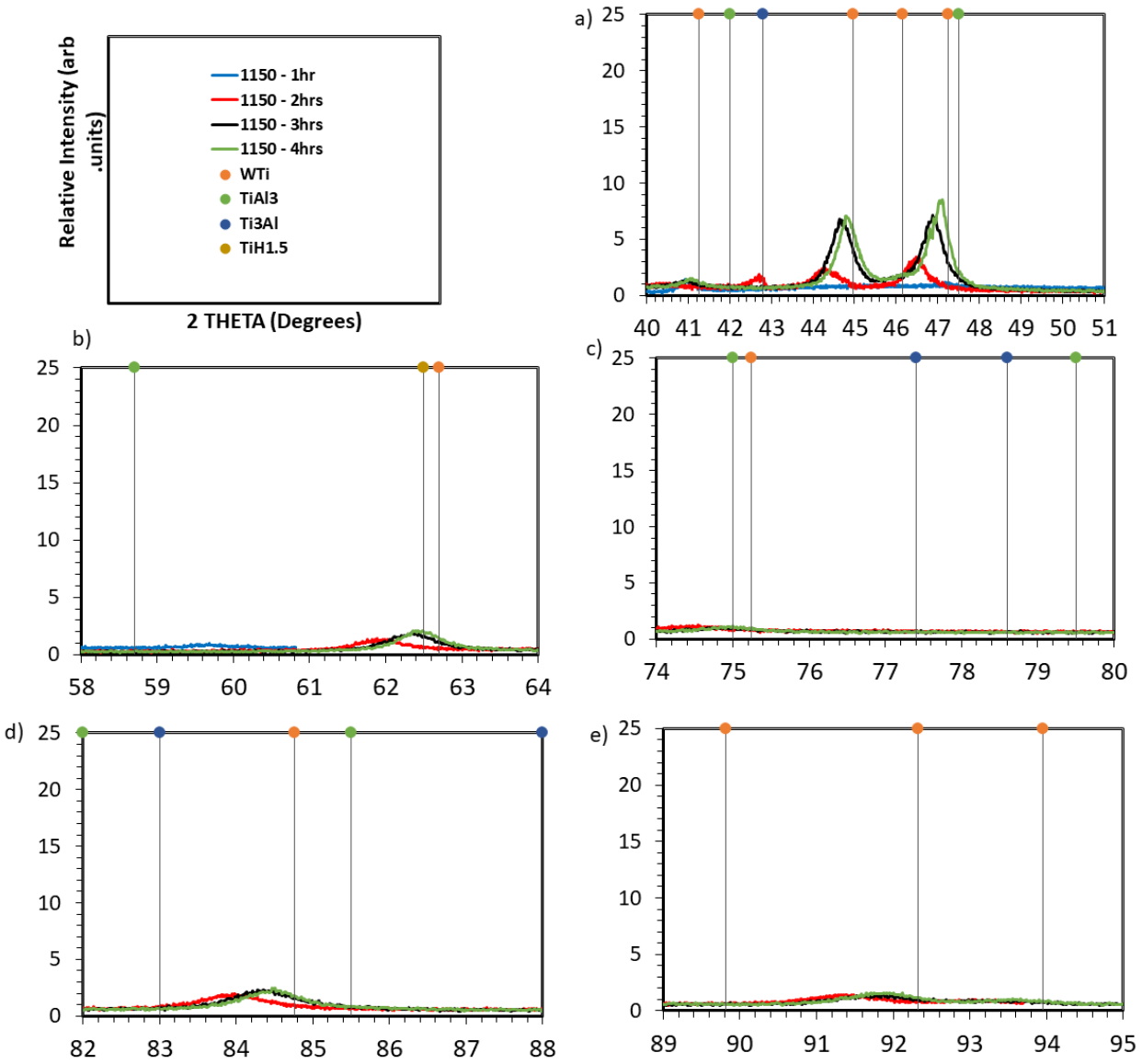

Figure 54: XRD spectrum for; TiH_2 + Al + V blend compacts sintered at 1150°C for 1hour, 2 hours, 3hours and 4 hours respectively and W-Ti, $TiAl_3$, Ti_3Al and $TiH_{1.5}$ peaks represented by lines on a split 2 Theta of a) 40-51° b) 58-64° c) 74-80° d) 82-88 ° e) 89-95°.

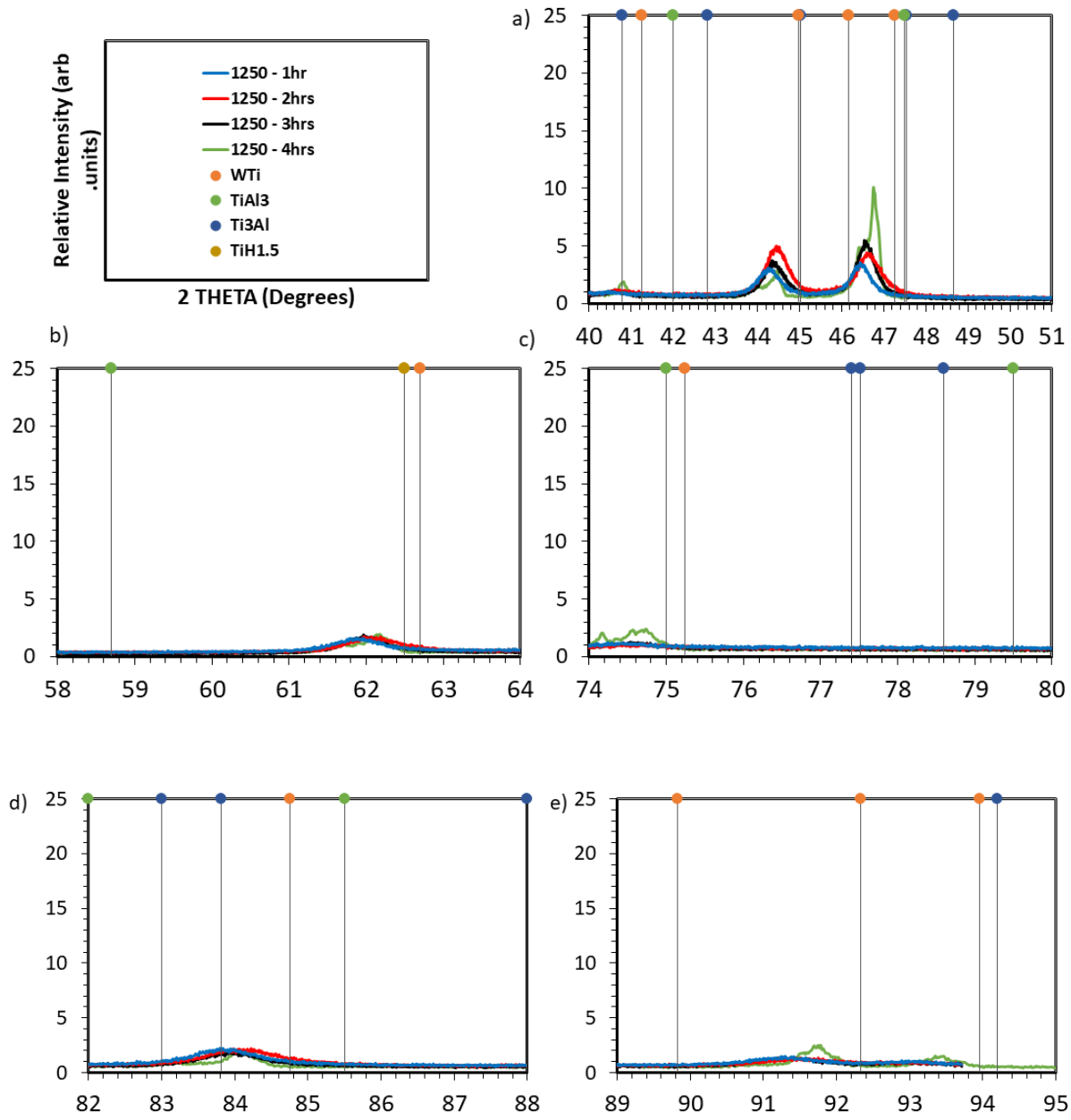

Figure 55: XRD spectrum for; TiH_2 + Al + V blend compacts sintered at 1250^{o}C for 1hour, 2 hours, 3hours and 4 hours respectively and W-Ti, $TiAl_3$, Ti_3Al and $TiH_{1.5}$ peaks represented by lines on a split 2 Theta of a) 40-51° b) 58-64° c) 74-80° d) 82-88 ° e) 89-95°.

When the sintering temperature was increased to 1350°C, peak splits at 2 theta values, 40°-44° and 46°- 47 are observed after a sintering time of 2 hours. Peak splits at 2 theta, 41- 44° values are observed after sintering for 4 hours. This means that diffusion had not fully occurred. After 4 hours there was still no beta phase, this means that diffusion had not fully occurred to stabilize the beta phase in titanium in this powder blend. The observed peak splits are caused by the presence of alpha Ti_3Al precipitates near 2 theta 42° and 45°.[48] This temporary phase may be generated by occurrence of the Beta Hydride phase when hydrogen

is added, or by a disproportionation effect when the hydride is formed.[49]

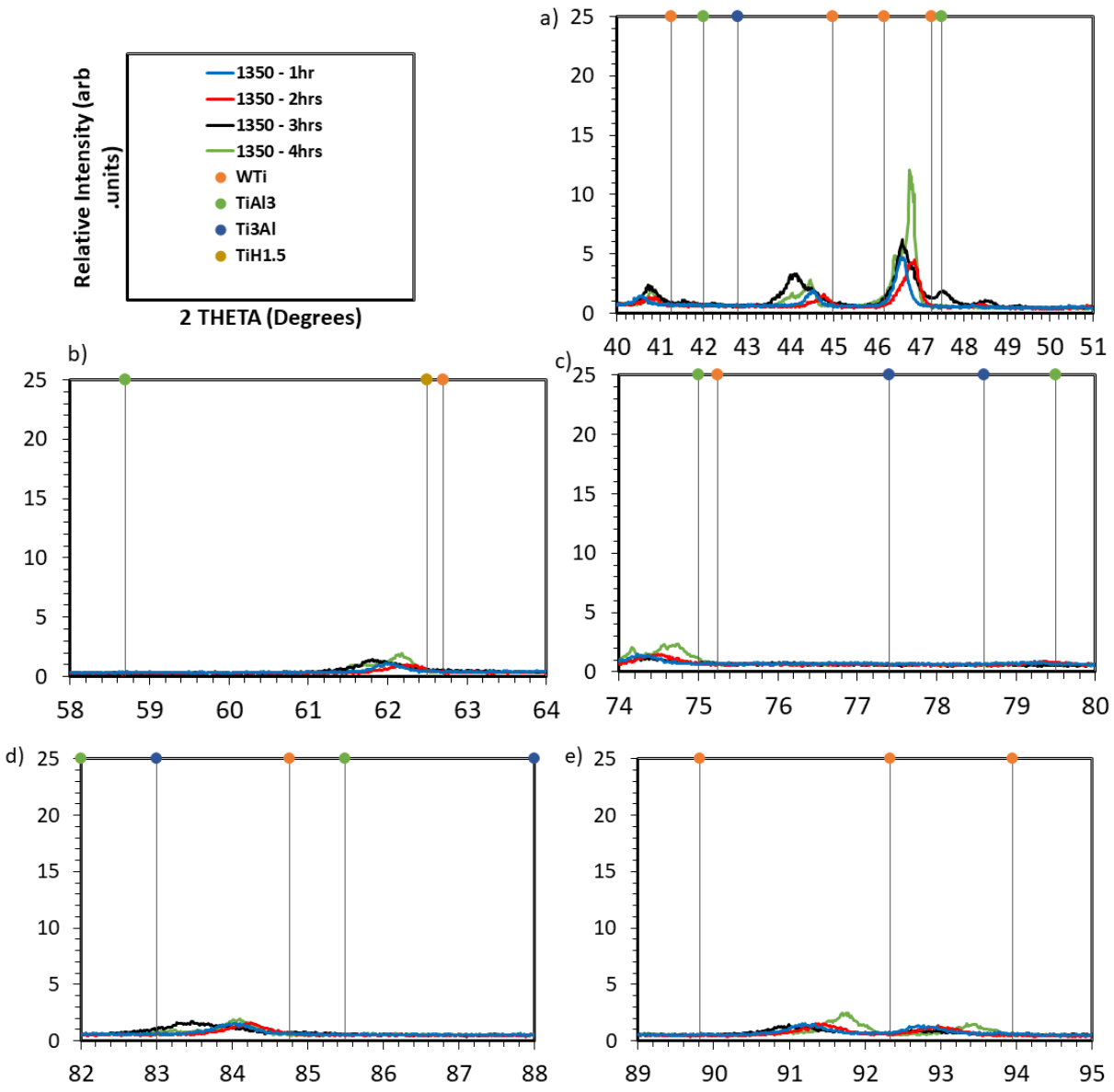

Figure 56: XRD spectrum for; TiH_2 + Al + V blend compacts sintered at 1350°C for 1hour, 2 hours, 3hours and 4 hours respectively and W-Ti, $TiAl_3$, Ti_3Al and $TiH_{1.5}$ peaks represented by lines on a split 2 Theta of a) 40-51° b) 58-64° c) 74-80° d) 82-88 ° e) 89-95°.

4.4.4 Discussion of XRD Results

The XRD analysis of the sintered TiH_2 + MA is shown by the corresponding XRD traces in Figures 45 – 48.

Figures 45 - 46 at 1000°C and 1150°C shows dominant peaks for all sintering times at 2 Theta of, 40- 41°,46° and 47°, 62°, and 74.3°, 84° and 91.3°. The peaks did not coincide with any of the expected intermediary compounds and intermetallic as well as the starting powders but there is suggestion of diffusion taking place as sintering time increases as none of the peaks match with the starting powders. With increase in sintering time right peak shift towards the W-Ti peak markers is noted after 3 and 4 hours of sintering. Compared to the W-Ti spectra in Figure 44 there is relative peak widening and the peak intensity is lower.

Peak broadening and reduction in intensity can be influenced by the presence of hydrogen in the alloy. Figure 22,[41] showed that Titanium hydride does not fully dehydrogenate during sintering. The presence of hydrogen causes the broadening of all alpha Ti diffraction peaks.[47] The peak broadening is caused by the lattice strain of alpha phase and the overlap of reflections belonging to the alpha phase and intermetallic Ti_3Al phase with an hcp lattice, which also results in peak shifts occuring. It should be noted that the overlap of the Ti_3Al, and α-Ti phases in hydrogenated samples causes broadening of the peaks compared to the Wrought Ti6Al4V sample. Another thing to note is hydrogen is a beta stabilizer and therefore the presence of hydrogen in the sample results in the stabilization of the beta phase quicker than in samples without hydrogen. The dissolved hydrogen then results in lattice volume expansion which is shown in all the XRD spectra of the TiH_2 + MA powder blend as peak broadening and peak shift.

After sintering at 1250°C the same peaks in 1000°C and 1150°C are present with more definition, right peak shift and less intensity of peak broadening and increase in peak intensity. An additional peak is shown at 46.3° after 2 hours of sintering which closely correlates with the W-Ti Beta phase forming although it doesn't match with the beta phase marker of W-Ti which could be due to peak shifts.

At 1350°C the peaks are more defined and there is a significant increase in peak intensity.

Alpha peaks at 40-41° are more defined with less peak broadening and higher intensity. The beta phase marker of W-Ti coincides with the additional peak that was a beta peak at 46.37° that first appeared after sintering at 1250°C for 2hours; the peak appears to be more defined and stable, whilst the other beta peaks of the powder blends still show relative peak shifts. These results coincide with the density results discussed earlier where the relative density of the TiH_2 + MA powder blend was 98%±1 after 1350°C 4 hours showing that enough diffusion had taken place to reduce any pores that might have formed during sintering and producing a near homogenized compact. It also coincides with the EDX results where the composition of the alloying elements had greatly improved and were moving towards homogeneity relative to the wrought Ti6Al4V (W-Ti) sample.

Figures 49 to 52 show the XRD spectra of CpTi + MA. Figures 49 – 50 at 1000°C and 1150°C show dominant peaks for all sintering times at 2 Theta of 40.8°, 44° and 45°, 46° and 47°, 62°,74.3°, 84° and 91.3°. The peaks did not coincide with any of the expected intermediary compounds and intermetallics as well as the starting powders, hence suggesting that diffusion was taking place as sintering time increases. With increase in sintering time right peak shift towards the W-Ti peak marker is noted for the powders after 3 and 4 hours of sintering. Compared to the W-Ti spectra in figure 44 the peak broadening intensity is lower compared to the TiH_2 + MA spectra and the peak intensity is higher which supports that the presence of hydrogen in TiH_2 + MA causes the effects.

At 1250°C there is no formation of an additional peak at 46.3° that was shown in the TiH_2 + MA XRD spectra. Peak splitting is recognized as there are more peaks than were at the lower temperatures, with extra peaks between 47° and 51°, 58°,59° and 91°. There is still presence of peak splitting after sintering at 1350°C. After sintering at 1350°C, an additional peak is shown at 46.3° that coincides with the beta peak of W-Ti. Peak splitting may be caused by CpTi not having enough surface area to diffuse the Al and V and therefore many unknown intermediary phases are formed as temperature increases and the reaction continues. This coincides with the density results discussed where the relative density was 96% ±1, therefore showing the compact was not fully homogenized and there was some presence of pores. The EDS results also coincide with these results, the diffusivity of the elements was greatly improved but the powder blend was significantly less homogeneous than W-Ti.

Figures 53 to 56 show the XRD spectra for the TiH_2 + Al + V powder compacts. The XRD results coincide with the density and EDS results and show no homogenization occurred over the full temperature and time sintering parameters. There is peak splitting and peak broadening caused by hydrogen discussed above and there was no additional peak that coincides with the beta peak at any of the sintering temperatures and times.

The above results show us that XRD can be used to measure the homogenization progress of titanium powder blends. In most cases the XRD spectra indicate X-Ray peaks that do not match known reflections for W-Ti, there is formation of unidentified intermetallics and compounds. The results show that with increase in sintering time and temperature the definition of the X-ray peaks, particularly in terms of peak width and peak height intensity move progressively towards what is expected for W-Ti for all the powder blends.
The XRD results of all the spectra show consistency with the EDS and some contradict the density results for all the powder blends. For the TiH_2 + MA powder blend, after sintering at 1250°C for 2 hours the elemental compositions of aluminium and vanadium demonstrate much less scatter and after 4 hours represent a more homogenized composition relative to the wrought Ti6Al4V (W-Ti) sample. This coincided with the XRD results that showed that there was formation of a peak at 46.37° that correlated to a beta peak, but it was not stable at 1250°C. The density results contradict here as the relative density achieved after sintering for 2 hours was 98%±1 suggesting a homogenized sample. After sintering at 1350°C for 4 hours the XRD spectra showed 3 stabilised beta phases that coincided with the W-Ti peaks and one peak which correlated to the beta phase but with a peak shift. This reconciled with the composition distribution shown at the same temperature in EDS where the homogenization was nearly complete relative to the W-Ti and a density of 98%.

For the CpTi + MA powder blend, after sintering at 1250°C, the XRD spectra did not show any peaks that would correlate to beta peaks which reconciles with the EDS results where the homogeneity of the blend was slower compared to TiH_2 + MA and took 4 hours to reach level the of homogeneity shown at 2 hours. After sintering at 1350°C for 4 hours, the XRD spectra did not show any peaks that correlated to stabilised beta peaks, however a partially stabilized beta phase was seen after sintering at 1350°C for 2 hours and a more stabilized (not fully

stabilized) after sintering at 1350°C for 4 hours, this was also demonstrated in the EDS results were the composition of the elements showed reasonable homogeneity, although still significantly less homogeneous relative to the wrought alloy. The density value coincided with results having a 97% ± 1 relative density.

The TiH_2 + Al+ V did not reach homogeneity at any sintering temperature and time, and this was shown by all three methods that were used.
The best method to measure progress of homogenization would be a combination of EDS and density.

This is because EDS may be a more laborious and expensive method than XRD but it gives us relative composition distribution which is a preferred way as it is quantifiable, whereas, in our case the powder blends were inhomogeneous and no single phase. Therefore, when the samples were not fully homogenized, we could not identify phases that were intermediate.

5. CONCLUSIONS

Based on the research conducted and presented in this dissertation, the following conclusions were drawn:

- CpTi based powder blend compacts have a higher green density than TiH_2 powder blend compacts because of the coarse powder particles and the softer CpTi particle plastically deforms during pressing and fill voids.
- TiH_2 has a better sinter ability as compared to CpTi.
- As sintered densities and chemical homogenization for the three powder blends evolved differently, with TiH_2 + MA blend reflecting a higher density and higher chemical homogeneity at a lower temperature and shorter time. It can thus be concluded that the other two blends required additional energy for densification and chemical homogenization.
- A combination of SEM/EDS analysis and XRD was successfully used to measure homogenization progress of the powder blends.

5.1 TiH_2 and MA powder blend

The blending of TiH_2 powder with the Al - V Master powder followed by pressing this powder into a green compact at a pressure of 375MPa resulted in this blend performing better than the other blends.

The combination of having TiH_2 and Al-V master alloy gave it an advantage over the other blends due to the advantage that the release of hydrogen had in sintering.

Hydrogen release resulted in lattice defects and vacancy movement resulting in a higher rate of diffusion and reduction of pores forming attributing to the 98% relative density that was found after sintering at 1250°C for 2 hours.

Sintering at a temperature of 1350°C for 2 hours created a material that had a relatively high homogenization, this was supported by EDS showing a composition of a fully homogenized sample and stable beta peaks were also shown in the XRD spectra at that sintering temperature and time.

5.2 CpTi and MA powder blend

The blending of CpTi powder with the Al - V Master powder followed by pressing this powder into a green compact at a pressure of 375MPa resulted in this powder blend performing better than the TiH_2 + Al + V powder blend.

The main reason it did not perform as well as the TiH_2 + MA powder blend was because of the base powder CpTi, it resulted in a reduced surface area compared to that given by TiH_2 when sintering. Resulting in less surface diffusion and a lower relative density of 97%±1 after sintering for 4 hours at 1250°C

The powder blend did not reach full homogeneity after sintering at 1250°C for 4hours which was demonstrated by XRD and EDS. After sintering at 1250°C for 4hours, there were no stable beta peaks shown in the XRD trace and the EDS showed the composition was not fully homogeneous relative to the wrought alloy.

After sintering at 1350°C for 4 hours the relative density was still at 97%±1, EDS composition showed full homogenization had not occurred and XRD beta peaks that were not fully stabilised.

5.3 TiH_2 and elemental Al and V powder blend

The blending of TiH_2 powder with elemental Al and V followed by pressing this powder into a green compact at a pressure of 375MPa and sintering at a temperature of 1350°C for 4 hours created a material that had a low homogeneity.

The relative density of the powder blend at 1350°C for 4 hours was 96%±1. Density is lowest in this blend due to Al melting which would result in the material having a high porosity.

XRD and EDS analysis showed the powder blend did not reach complete homogeneity as the other blends over the full temperatures and time selected for the experiments.

After sintering at 1350°C for 4 hours EDS showed that the composition of the powder blend had not reached full homogeneity relative to the wrought alloy

After sintering at 1350°C for 4 hours, there were no beta peaks showing on the XRD spectra showing beta stabilisation had not occurred.

6. FUTURE WORK AND RECOMMENDATIONS

As a result of the current research and findings, the author suggests the following:

- Any further research conducted on Blended Elemental (BE) Ti-6A-l-4V should be produced using an Al-V master alloy and TiH_2 powder rather than separate elemental powders. This will reduce processing costs and improve the compositional control.
- Mechanical tests, for example hardness and tensile tests, should be performed on the sintered samples to see if the mechanical properties match the homogeneity level.
- The microstructure of the sintered samples should be analyzed to assess phase transformations at different sintering times and temperature.
- Analysis of the unknown phases that were detected in the XRD spectra should be performed to determine what they are.
- Use of “Pressure assisted rapid Solid-State Sintering”, the current work focused on time and temperature parameters of sintering. However, a third critical parameter in sintering in Pressure. Thus, by considering solid state sintering techniques like Spark Plasma Sintering, one can use pressure to significantly reduce the sintering temperature and time, which will have impact on improving the mechanical properties.

7. REFERENCES

1. Lütjering, G. (1998). "Influence of processing on microstructure and mechanical properties of (α+ β) titanium alloys." Materials Science and Engineering 243(1-2): 32-45.

2. Peters, C. L. a. M. (2003). "Titanium and titanium alloys: fundamentals and applications." John Wiley & Sons.

3. Y. N. Podrezov, V. N., A. Vdovichenko, V. Danilenko, O. Koryak, and Y. I. Evich (2009). "Mechanical properties of powder titanium at different production stages. III. Contact formation in powder titanium based on examination of mechanical properties in sintering." Powder Metallurgy and Metal Ceramics 3(48): 201-210.

4. Eylon, F. F. a. D. (1990). "Powder metallurgy of titanium alloys." International Materials Reviews 35(1): 162-184.

5. S. Malinov, Z. G., W. Sha, and A. Wilson: (2001). "Differential scanning calorimetry study and computer modeling of β⇒ α phase transformation in a Ti-6Al-4V alloy." Metallurgical and materials transactions A, 32(4): 879-887.

6. D.-W. Lee, H.-S. L., J.-H. Park, S.-M. Shin, and J.-P. Wang: (2015). "Sintering of titanium hydride powder compaction." Procedia Manufacturing 2: 550-557.

7. Barter, R. W. a. S. (2011). "Fatigue of beta processed and beta heat-treated titanium alloys." Springer Science & Business Media.

8. Morinaga, M. (2018). "A Quantum Approach to Alloy Design: An Exploration of Material Design and Development Based Upon Alloy Design Theory and Atomization Energy Method." Elsevier.

9. S. S. Naboychenko, I. B. M., and O. D. Neikov (2009). "Production of refractory metal powders in Handbook of Non-ferrous Metal Powders." Elsevier.: 436-484.

10. Randal, M. (2005). "Powder metallurgy & particulate materials processing." Princeton: Metal Powder Industry.

11. Subramanian, P. A. a. R. (2008). "Powder metallurgy: science, technology and applications." PHI Learning Pvt. Ltd.

12. B. Panigrahi, M. G., K. Das, P. Mukunda, and P. Ramakrishnan (2005). "Sintering kinetics of micrometric titanium powder." Materials Science and Engineering:A 396(1-2): 255-262.

13. Schaffer, I. R. a. G. (2010). "Review of densification of titanium-based powder systems in press and sinter processing." Powder metallurgy 53(2): 146-162.

14. Manufacturing.com, T. l. o. "Pressing and sintering." Retrieved 2022/07/03, 2022, from thelibraryofmanufacturing.com/pressing_sintering.html.

15. O. M. Ivasishin, D. E., V. Bondarchuk, and D. G. Savvakin (2008). "Diffusion during powder metallurgy synthesis of titanium alloys." Defect and Diffusion Forum, 2008, Trans Tech Publ: 177-185.

16. M. Gasik, A. K.-H., and Y. Bilotsky (2009). "Sintering kinetics of titanium and titanium alloy powders."

17. J.-M. Oh, K.-H. H., W.-B. Kim, G.-S. Choi, and J.-W. Lim (2013). "Sintering Properties of Ti–6Al–4V Alloys Prepared Using Ti/TiH2 Powders." Materials Transactions 54(1): 119-121.

18. Qian, M. (2010). "Cold compaction and sintering of titanium and its alloys for near-net shape or preform fabrication." International journal of powder metallurgy 46(5).

19. O. M. Ivasishin, D. G. S., F. H. S. Froes, and K. A. Bondareva (2002). "Synthesis of Alloy Ti—6Al—4V with Low Residual Porosity by a Powder Metallurgy Method." Powder Metallurgy and Metal Ceramics 41(7-8): 382-390.

20. V. Duz, M. M., A. Klevtsov, and V. Moxson (2017). "Industrial application of titanium hydride powder." Met Powder Rep 72(1): 30-38.

21. Froes, M. Q. a. F. H. (2015). "Titanium powder metallurgy: science, technology and applications." Butterworth-Heinemann.

22. L. Bolzoni, P. E., E. M. Ruiz-Navas, and E. Gordo (2012). "Mechanical behaviour of pressed and sintered titanium alloys obtained from master alloy addition powders." Journal of the mechanical behavior of biomedical materials 15: 33-45.

23. C. Yu, P. C., and M. I. Jones (2017). "Microstructural evolution during pressureless sintering of blended elemental Ti-Al-V-Fe titanium alloys from fine hydrogenated-dehydrogenated titanium powder." Metals 7(8): 285.

24. G. Cantin, N. A. S., D. Alexander, M. A. Gibson, D. Ritchie, R. Wilson, M. Yousuff, R. Rajakumar, and K. Rogers (2010). "Production of Ti-6Al-4V Strip by Direct Rolling of Blended Elemental Powder." Materials Science Forum, Trans Tech Publ: 807-810.

25. Samal, P. K. (1986). "Direct powder rolling of dispersion strengthened metals or metal alloys." Google Patents.

26. G. Cantin, P. K., N. Stone, R. Wilson, M. Gibson, M. Yousuff, D. Ritchie, and R. Rajakumar (2011). "Innovative consolidation of titanium and titanium alloy powders by direct rolling'." Powder metallurgy 2(2): 121-144.

27. Saito, T. (1995). "A cost-effective P/M titanium matrix composite for automobile use." Advanced Performance Materials 2(2): 121-144.

28. Newkirk, P. S. a. J. (2015). "Powder metallurgy methods and applications." ASM handbook of powder metallurgy 7.

29. Medlin, H. K. a. D. (2000). "Mechanical Testing and Evaluation (Vol. 8). ASM Handbook." International, Materials Park (OH) USA.

30. Knutsen, V. V. a. R. D. (2013). "Grain refinement in cast Ti-6Al-4V by hydrogenation, deformation and recrystallisation." Materials Science Forum, 2013, Trans Tech Publ: 271-274.

31. Knusten, H. N. a. R. (2019). "Assessment of homogenization progress in sintered direct powder rolled Ti-6Al-4V strip." University Of Cape Town.

32. D. Janeba, P. Č., Z. Weiss, and H. Schenk (1998). "Characterization of intercalated smectites using XRD profile analysis in the low-angle region." Clays and clay minerals 46(1): 63-68.

33. B. Zhang, F. G., J. Xue, L. Yang, Y. Zhao, M. Ge, Q. Cai, B. Liu, Z. Xie, and D. Chen (2017). "Photoluminescence Study of the Photoinduced Phase Separation in Mixed-Halide Hybrid Perovskite CH 3 NH 3 Pb (Br x I 1− x) 3 Crystals Synthesized via a Solvothermal Method." Scientific reports 7(1): 1-8.

34. Toyozawa, Y. (1962). "Further Contribution to the theory of the line-shape of the exciton absorption band." Progress of Theoretical Physics 27(1): 89-104.

35. Paul, M. V. a. S. (2012). "Correlation between full width at half maximum (FWHM) of XRD peak with residual stress on ground surfaces." Philosophical Magazine 92(33): 4194-4204.

36. Cullity, B. D. (1956). "Elements of X-Ray Diffraction." Addison-Wesley Publishing Company, Inc., USA.

37. D. A. Skoog, F. J. H., T. A. Nieman (1998). Principles of Instrumental Analysis. USA, Harcourt Brace & Company.

38. D. P. Garriga-Majo, B. A. S., M. G. Arkadani (1999). Micro-texture Study oF Ti-6Al-4V Using Electron Back Scattering Diffraction. UK, Imperial College.

39. H. Moustahfid, N. G., M. Humbert, and M. J. Philippe (1997). "Study of β-α PhasE Transformations of a Ti-64 Sheet Induced from High-Temperature β State and a High-Temperature α+β State". Metallurgical and Materials Transactions A 28A: 51-61.

40. Satyam Suwas, R. R. (2014). Crystallographic Texture of Materials.

41. Gökelma, M. ç., Dilara & Tazegul, Onur & Cimenoglu, Huseyin & Friedrich, Bernd (2018). "Characteristics of Ti6Al4V Powders Recycled from Turnings via the HDH Technique." Metals - Open Access Metallurgy Journal 8(5): 336.

42. Changzhou Yu, P. C. a. M. I. J. (2017). "Microstructural Evolution during Pressureless Sintering of Blended Elemental Ti-Al-V-Fe Titanium Alloys from Fine Hydrogenated-Dehydrogenated Titanium Powder." Metals 7(8): 285.

43. Friese, R. E. D. K. "MODERN XRD METHODS IN MINERALOGY." Max-Planck-Institute for Solid State Research.

44. German, R. M. (2014). Mixed Powders and Composites.

45. Schaffer, I. M. R. a. G. B. (2009). "Some effects of particle size on the sintering of titanium and a master sintering curve model." Metall. Mater. Trans. A 40(8): 1968.

46. S.L.R. da Silva, L. O. K., L. Amaral (1999). "X-ray diffraction measurements of plasma-nitrided Ti–6Al–4V." Elsevier, Surface, and coatings technology 116-119: 342-346.

47. C. C. Shen, C. Y. Y., and T. P. Perng (2009). "Variation of structure and mechanical properties of Ti-6Al-4V with isothermal hydrogenation treatment." Acta Mater. 57(3): 868-874.

48. Wang, C.-C. S. a. C.-M. (2014). "Effects of hydrogen loading and type of titanium hydride on grain refinement and mechanical properties of Ti–6Al–4V." Alloys Compd 601: 274-279.

49. C. Yu, C. S., and T. Perng (2006). "Microstructure of Ti–6Al–4V processed by hydrogenation." Scripta Mater., 55(11): 1023-1026.

50. Andrea Školáková, P. S., Jindˇrich Leitner, Tomáš Lovaši and Pavel Novák (2020). "Formation of Phases in Reactively Sintered TiAl3 Alloy." molecules.

51. F.H. (Sam) Froes, M. Ashraf Imam, and Derek Fray (2004). “Cost Affordable Titanium.” Warrendale, PA: TMS.

52. F. H Froes, D. E. (1985). “Titanium Technology: Present status and future trends.” Titanium Development Assn.

53. Daniel Eylon, J. N., John Thorne (1990). Titanium and Titanium alloy castings.

54. Chikosha, S., Shabalala, T. C. & Chikwanda, H. K. (2014) “Effect of particle morphology and size on roll compaction of Ti-based powders.” Powder Technol. 264, 310–319.

Appendix A

Figures A1 -A12 are XRD spectra of TiH_2 + MA, TiH_2 + Al +V and CpTi + MA, 2 Theta peak positions of the powder blend starting powders were added to the XRD spectra as markers to determine how the structure of the sintered powders were moving towards homogeneity during the sintering process. The XRD spectra of 2 Theta ° was split to 40°-51°, 58°-64°, 74°-80°,82°-88° and 89°- 95° respectively.

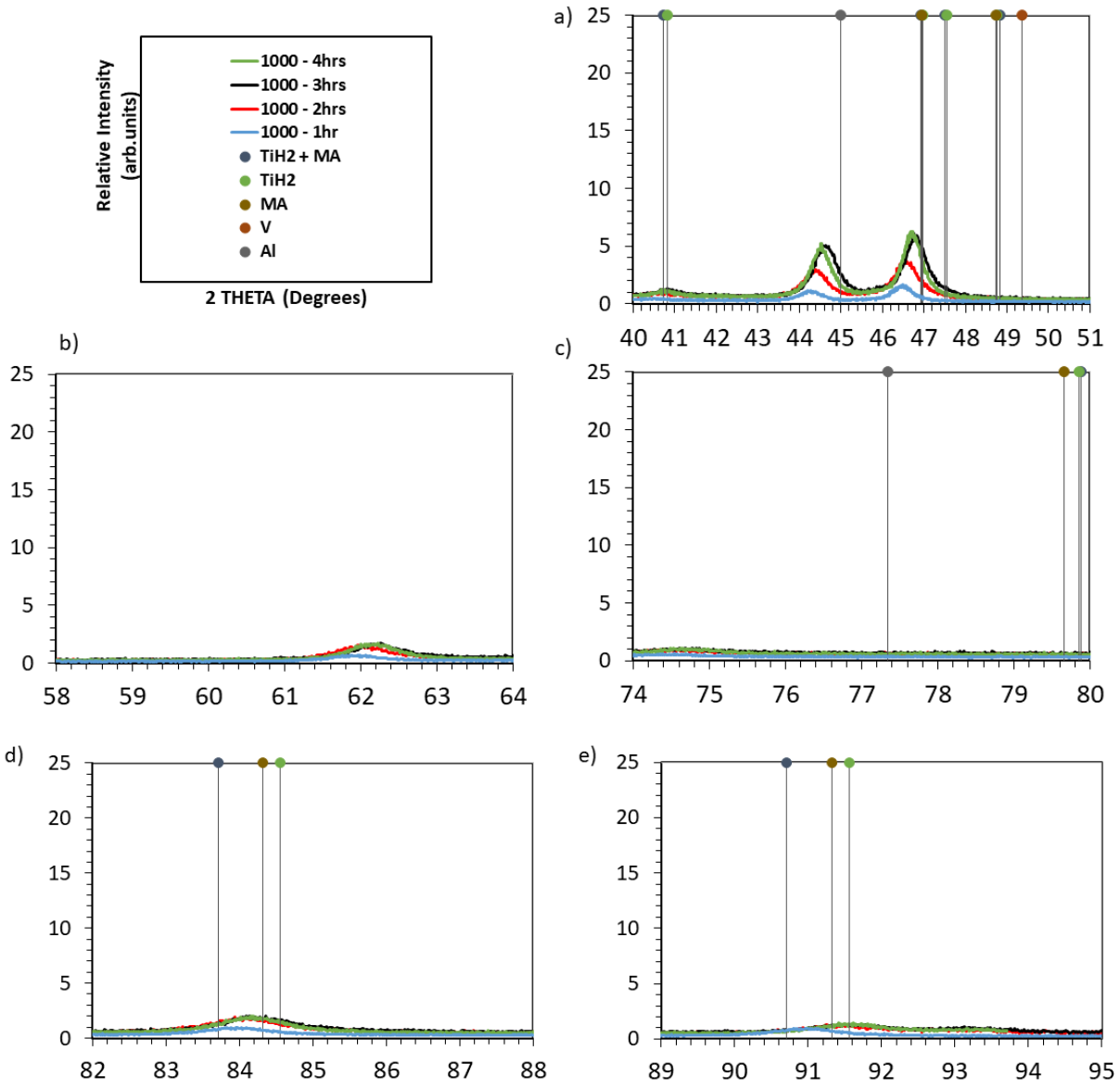

Figure A1: XRD spectrum for; TiH_2 + MA blend compacts sintered at 1000°C for 1hour, 2 hours, 3hours and 4 hours respectively and TiH_2 + MA powder blend, TiH_2 base powder, MA (60AL-40V master alloy), Al powder and V powder peaks represented by lines on a split 2 Theta of a) 40-51° b) 58-64° c) 74-80° d) 82-88 ° e) 89-95°.

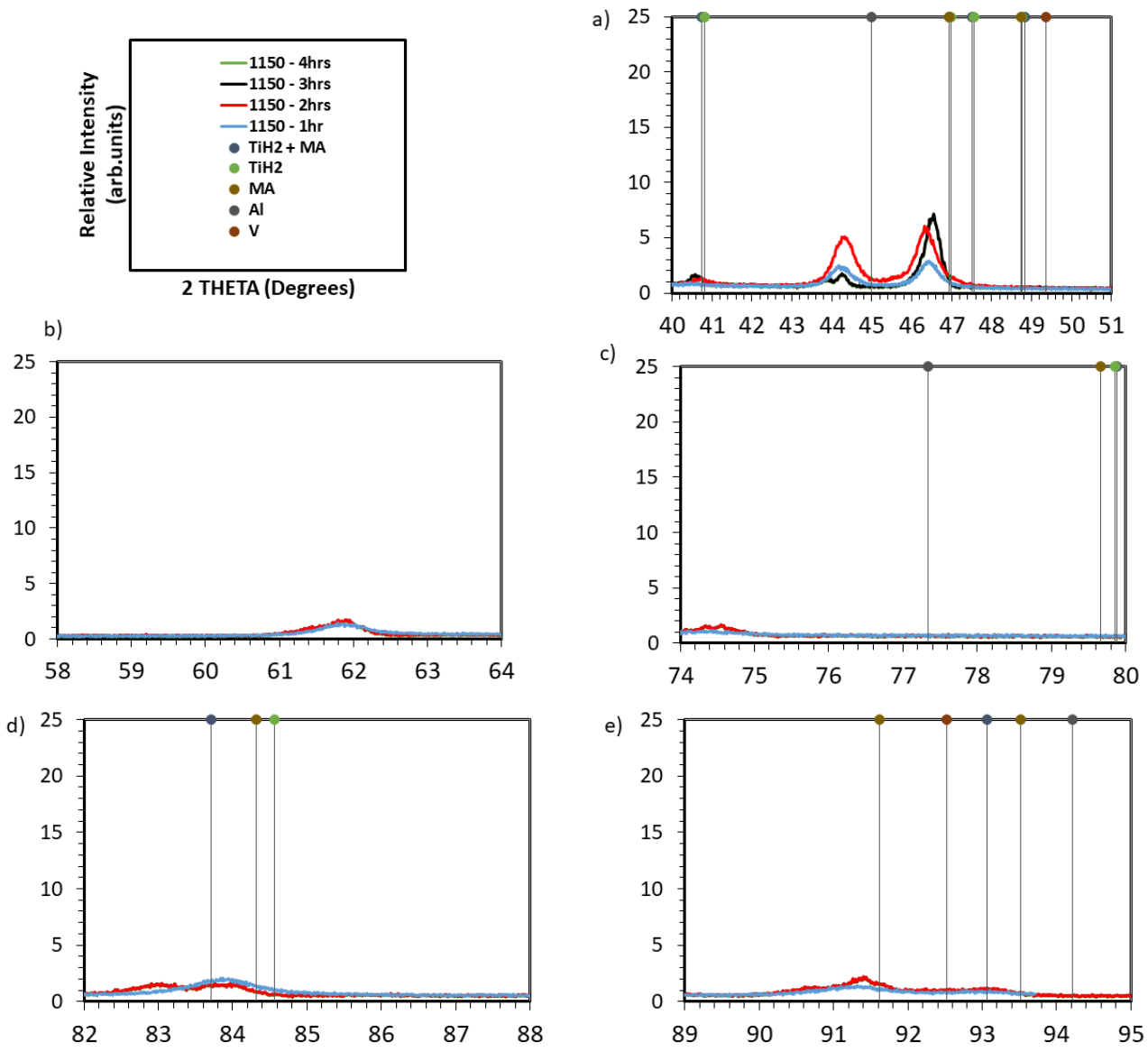

Figure A2: XRD spectrum for; TiH_2 + MA blend compacts sintered at 1150^{o}C for 1hour, 2 hours, 3hours and 4 hours respectively and TiH_2 + MA powder blend, TiH_2 base powder, MA (60AL-40V master alloy), Al powder and V powder peaks represented by lines on a split 2 Theta of a) 40-51° b) 58-64° c) 74-80° d) 82-88 ° e) 89-95°.

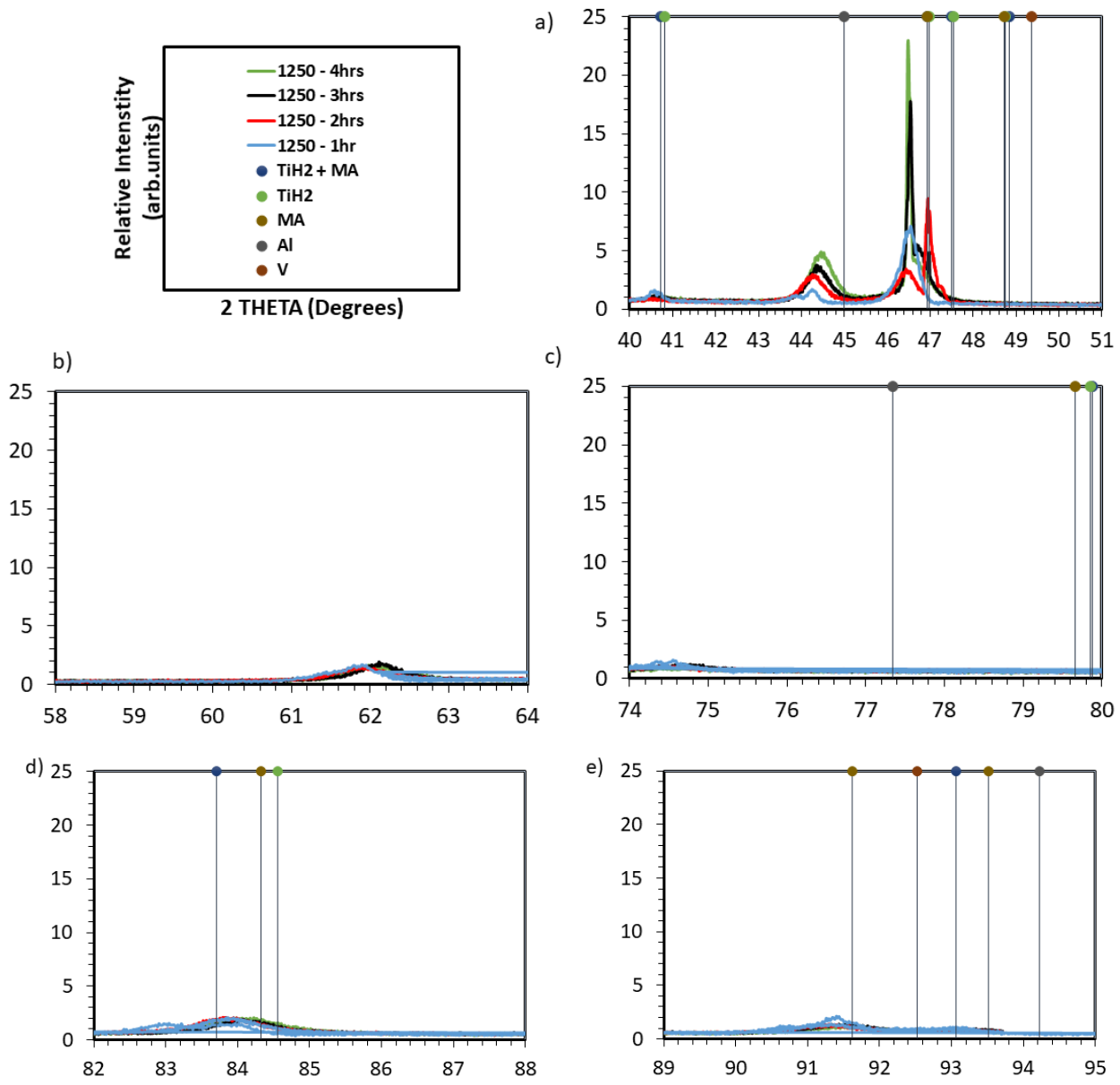

Figure A3: XRD spectrum for; TiH_2 + MA blend compacts sintered at 1250^{o}C for 1hour, 2 hours, 3hours and 4 hours respectively and TiH_2 + MA powder blend, TiH_2 base powder, MA (60AL-40V master alloy), Al powder and V powder peaks represented by lines on a split 2 Theta of a) 40-51° b) 58-64° c) 74-80° d) 82-88 ° e) 89-95°.

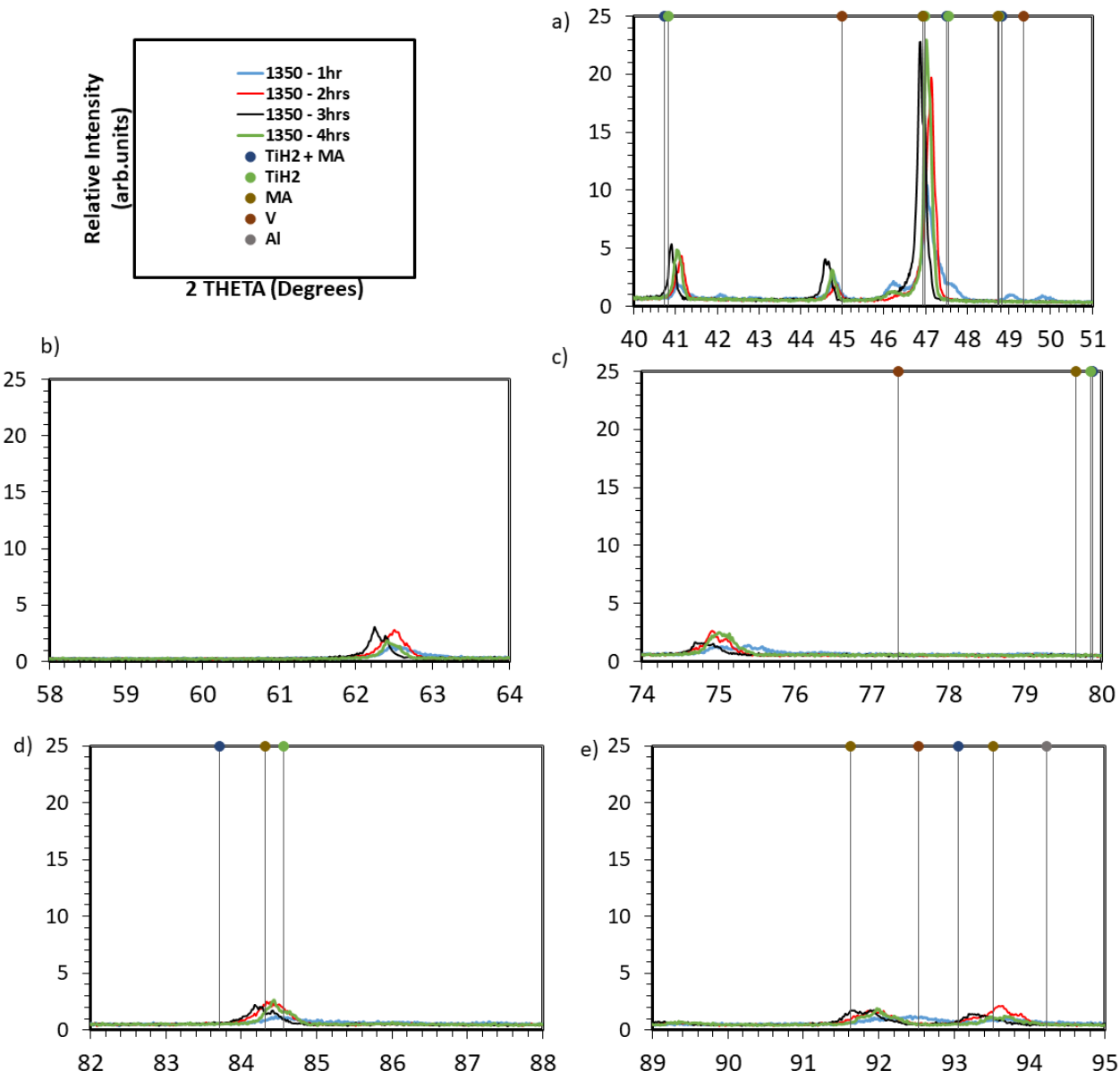

Figure A4: XRD spectrum for; TiH_2 + MA blend compacts sintered at 1350°C for 1hour, 2 hours, 3hours and 4 hours respectively and TiH_2 + MA powder blend, TiH_2 base powder, MA (60AL-40V master alloy), Al powder and V powder peaks represented by lines on a split 2 Theta of a) 40-51° b) 58-64° c) 74-80° d) 82-88 ° e) 89-95°.

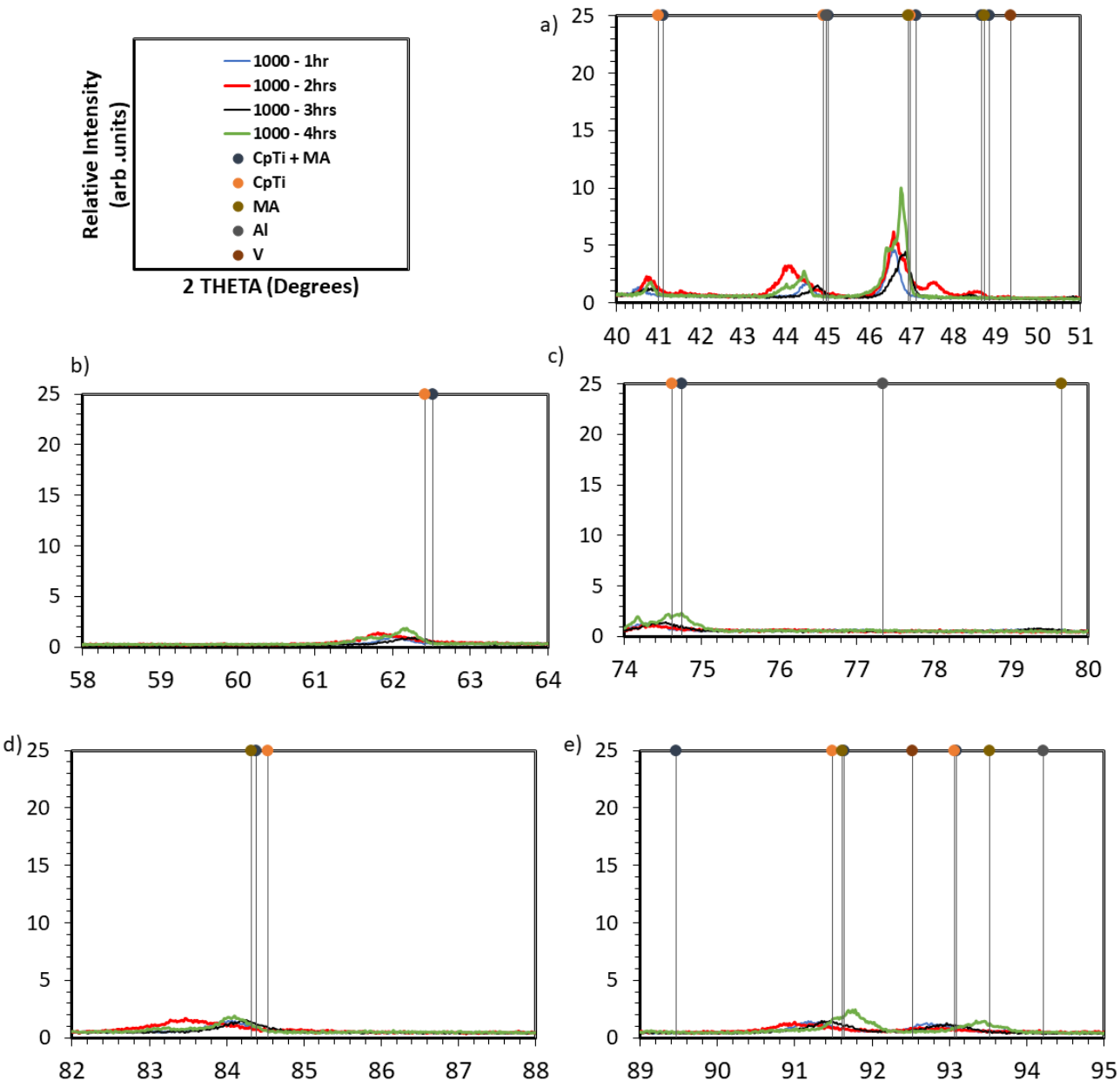

Figure A5: XRD spectrum for; CpTi+ MA blend compacts sintered at 1000^{o}C for 1hour, 2 hours, 3hours and 4 hours respectively and CpTi + MA powder blend, CpTi base powder, MA (60AL-40V master alloy), Al powder and V powder peaks represented by lines on a split 2 Theta of a) 40-51° b) 58-64° c) 74-80° d) 82-88 ° e) 89-95°.

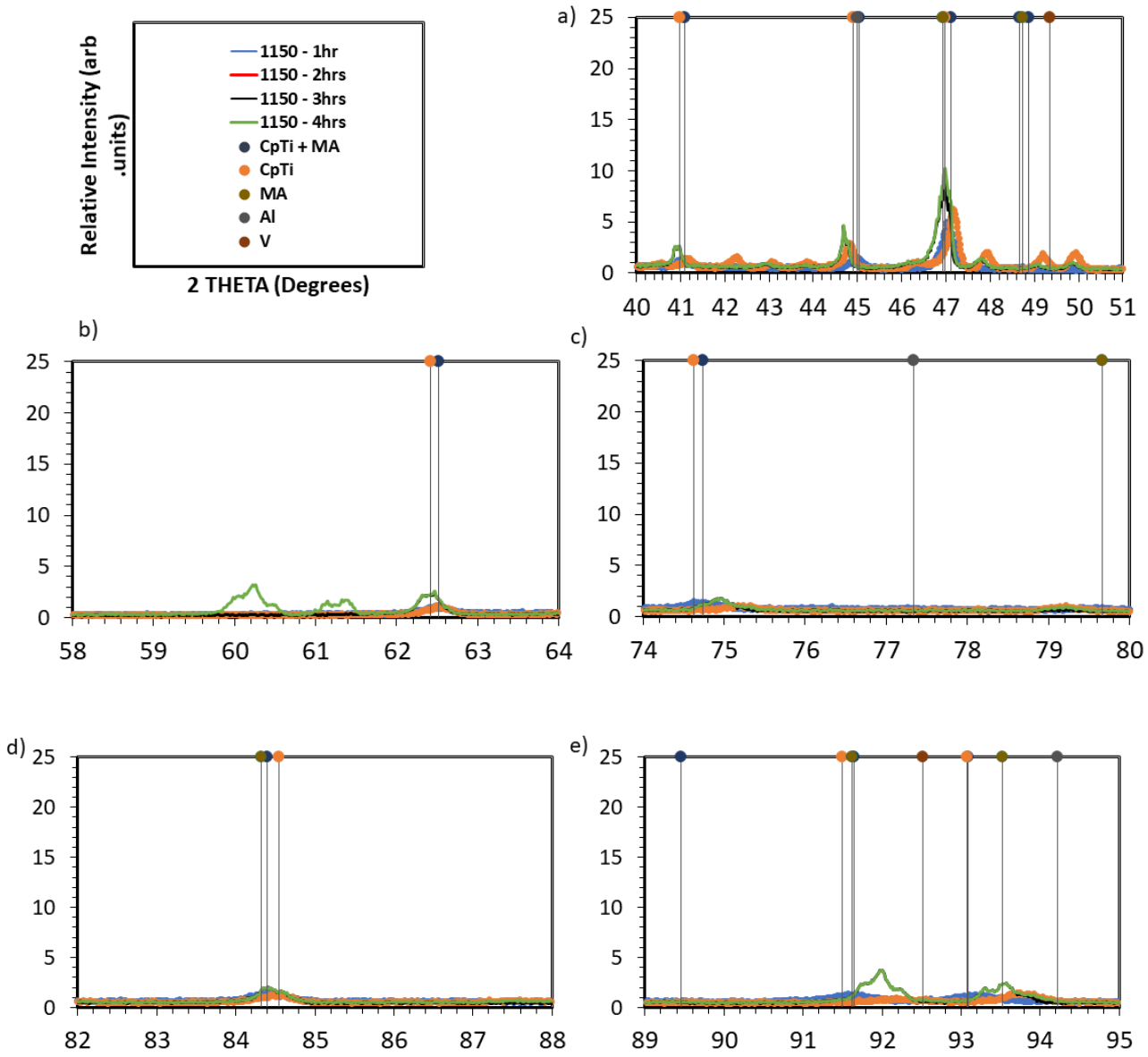

Figure A6: XRD spectrum for; CpTi+ MA blend compacts sintered at 1150^{o}C for 1hour, 2 hours, 3hours and 4 hours respectively and CpTi + MA powder blend, CpTi base powder, MA (60AL-40V master alloy), Al powder and V powder peaks represented by lines on a split 2 Theta of a) 40-51° b) 58-64° c) 74-80° d) 82-88 ° e) 89-95°.

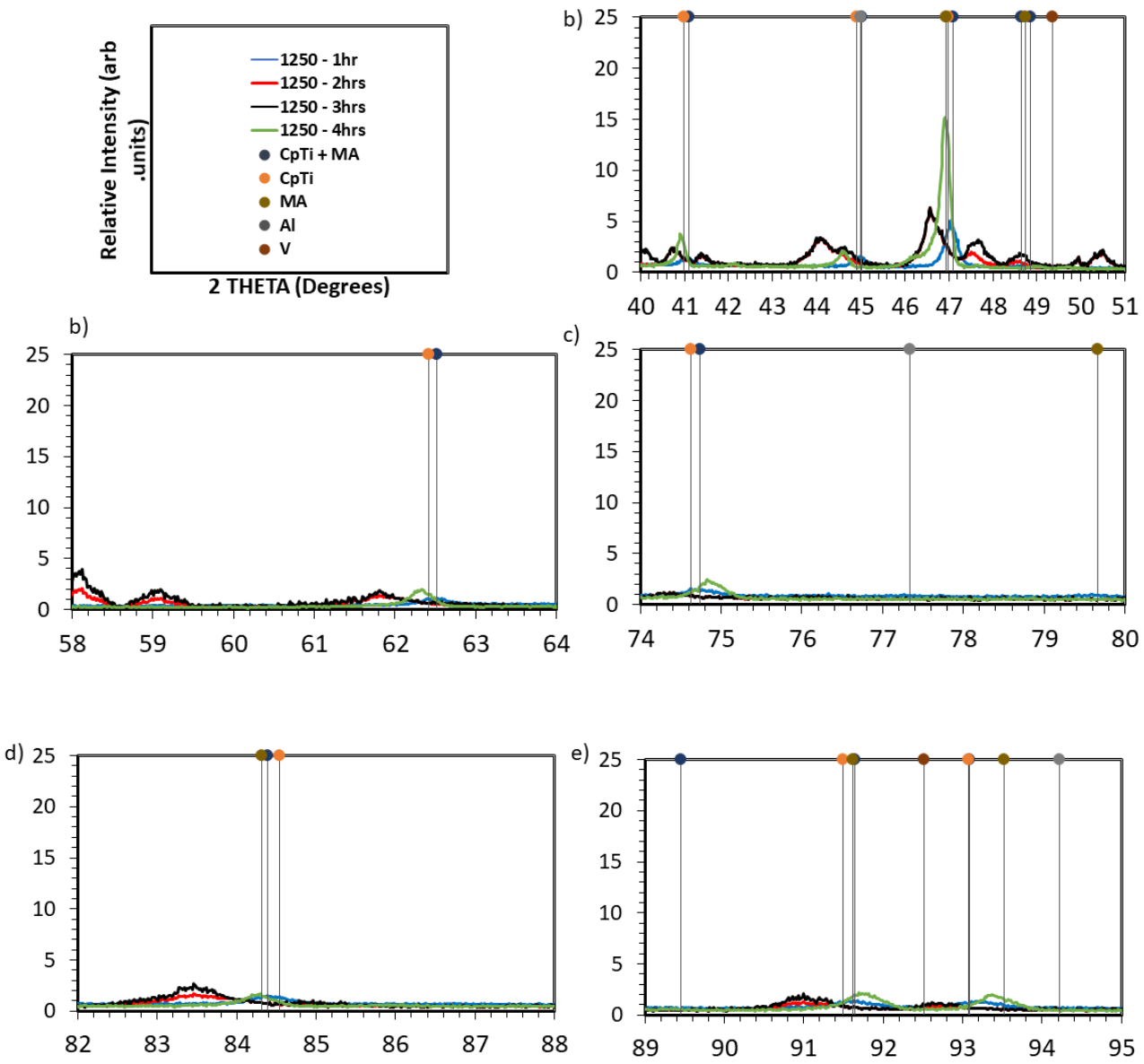

Figure A7: XRD spectrum for; CpTi+ MA blend compacts sintered at 1250^{o}C for 1hour, 2 hours, 3hours and 4 hours respectively and CpTi + MA powder blend, CpTi base powder, MA (60AL-40V master alloy), Al powder and V powder peaks represented by lines on a split 2 Theta of a) 40-51° b) 58-64° c) 74-80° d) 82-88 ° e) 89-95°.

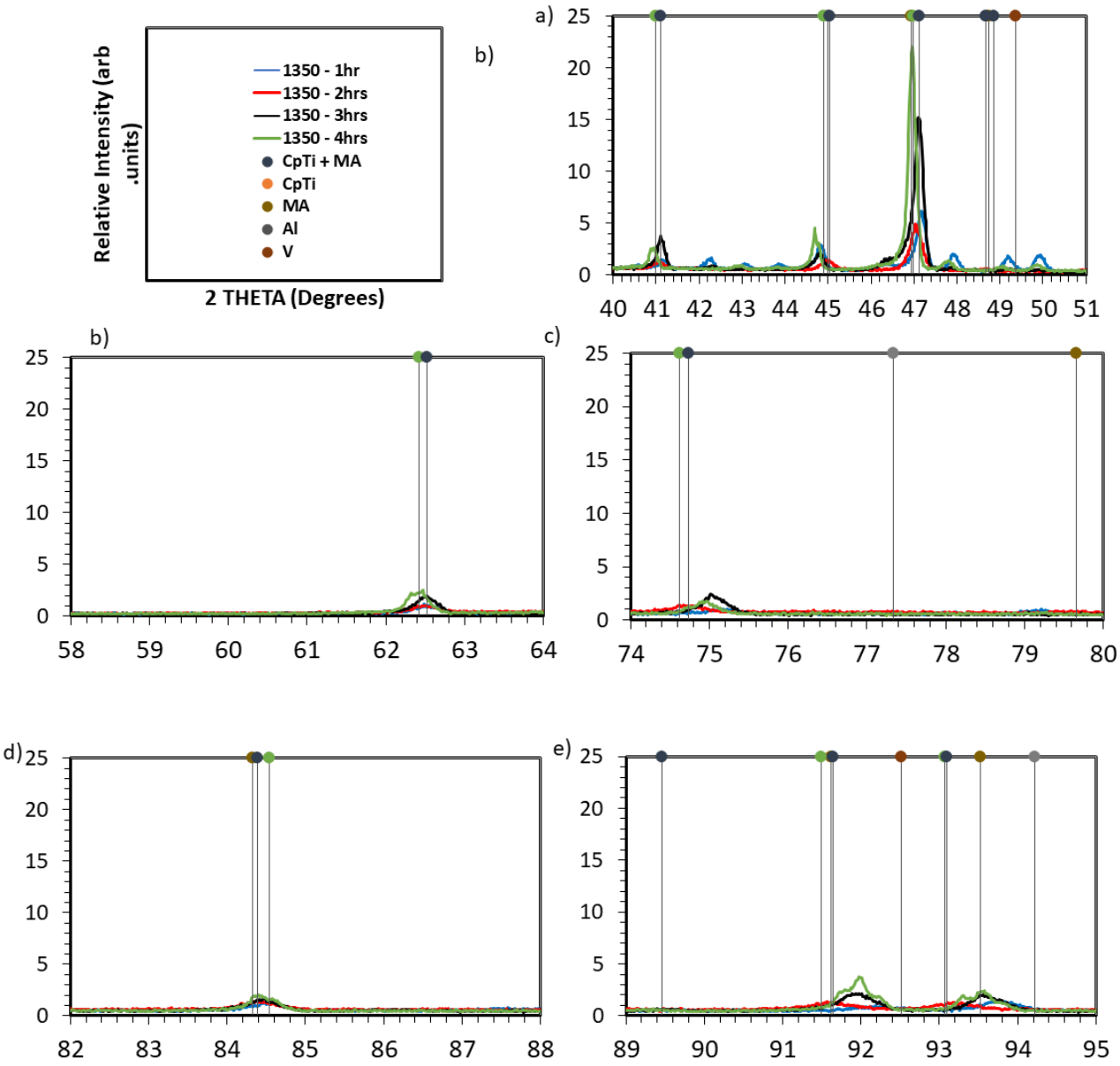

Figure A8: XRD spectrum for; CpTi+ MA blend compacts sintered at 1350^{o}C for 1hour, 2 hours, 3hours and 4 hours respectively and CpTi + MA powder blend, CpTi base powder, MA (60AL-40V master alloy), Al powder and V powder peaks represented by lines on a split 2 Theta of a) 40-51° b) 58-64° c) 74-80° d) 82-88 ° e) 89-95°.

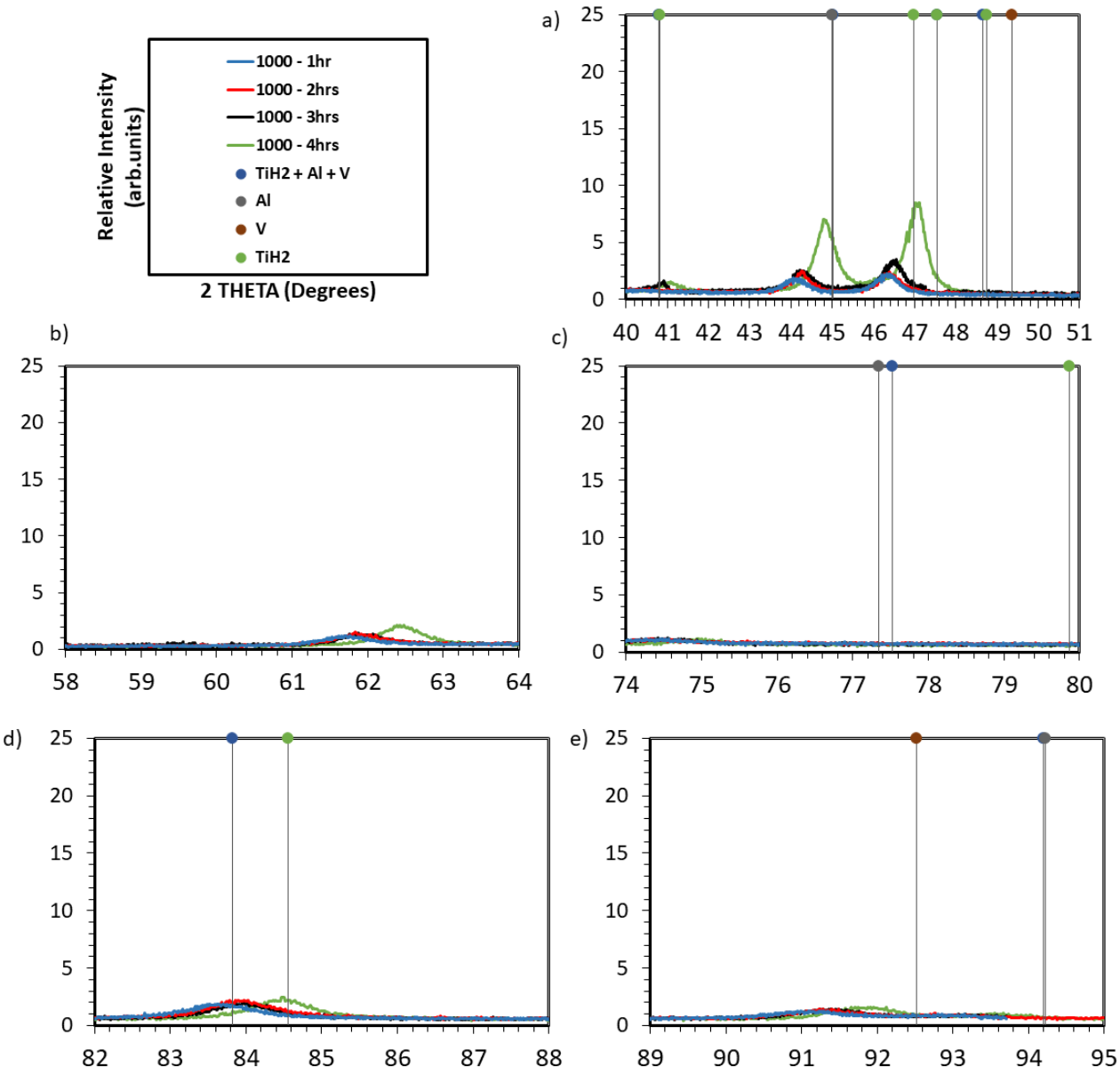

Figure A9: XRD spectrum for; TiH_2 + Al +V blend compacts sintered at 1000^{o}C for 1hour, 2 hours, 3hours and 4 hours respectively and TiH_2 + Al + V powder blend, TiH_2 base powder, Al powder and V powder peaks represented by lines on a split 2 Theta of a) 40-51° b) 58-64° c) 74-80° d) 82-88 ° e) 89-95°.

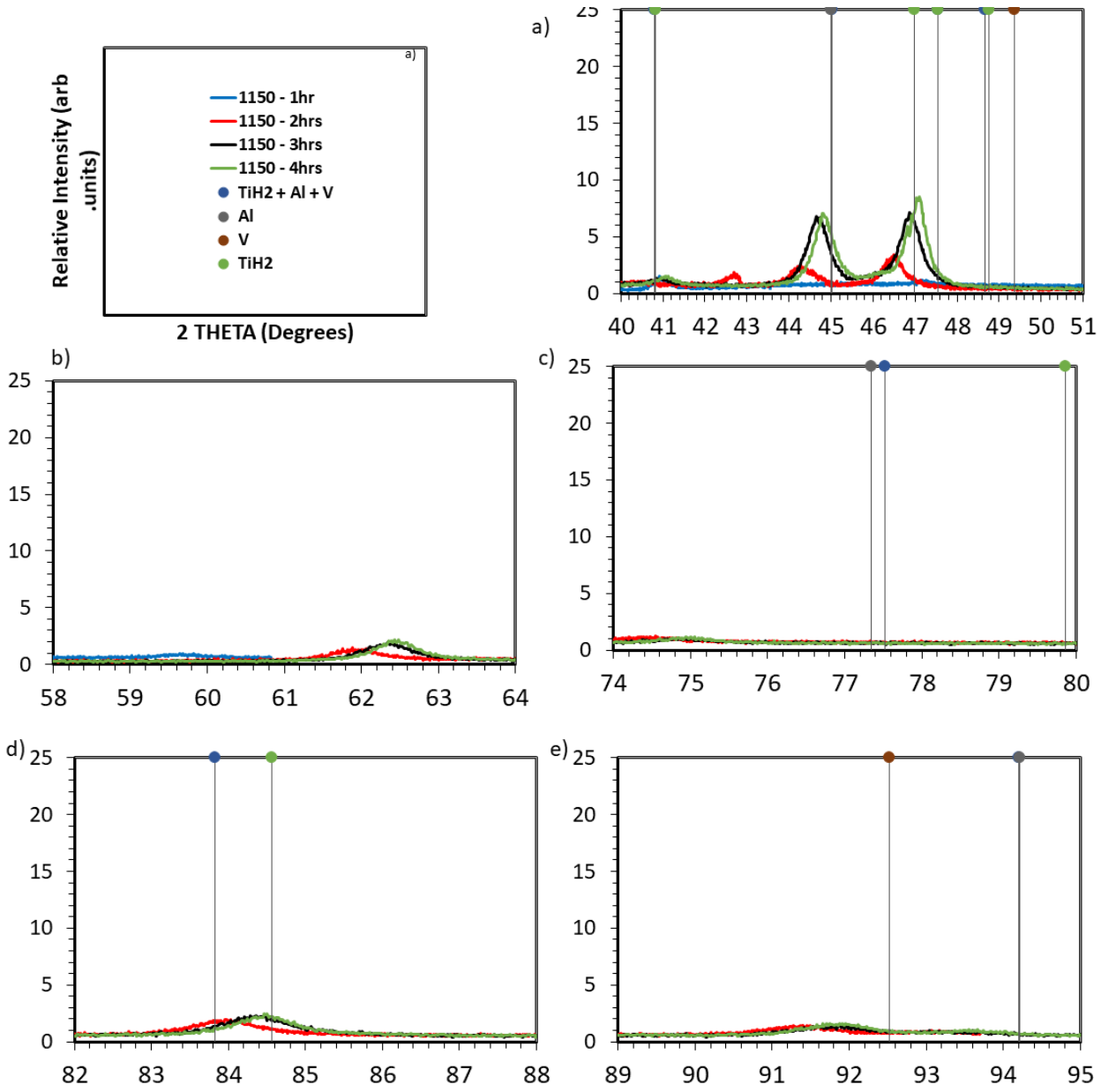

Figure A10: XRD spectrum for; TiH_2 + Al +V blend compacts sintered at 1150^{o}C for 1hour, 2 hours, 3hours and 4 hours respectively and TiH_2 + Al + V powder blend, TiH_2 base powder, Al powder and V powder peaks represented by lines on a split 2 Theta of a) 40-51° b) 58-64° c) 74-80° d) 82-88 ° e) 89-95°.

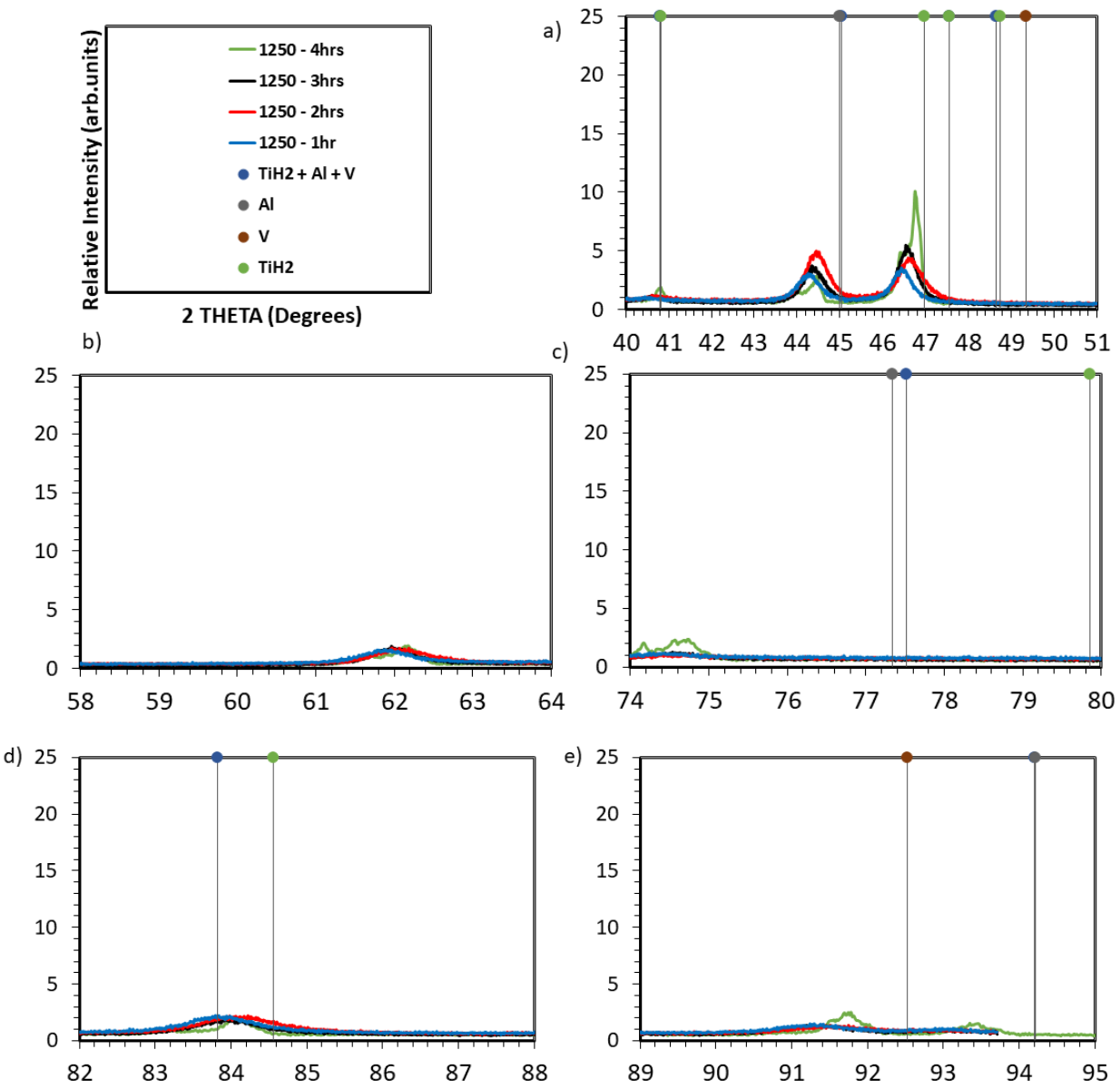

Figure A11: XRD spectrum for; TiH_2 + Al +V blend compacts sintered at 1250^{o}C for 1hour, 2 hours, 3hours and 4 hours respectively and TiH_2 + Al + V powder blend, TiH_2 base powder, Al powder and V powder peaks represented by lines on a split 2 Theta of a) 40-51° b) 58-64° c) 74-80° d) 82-88 ° e) 89-95°.

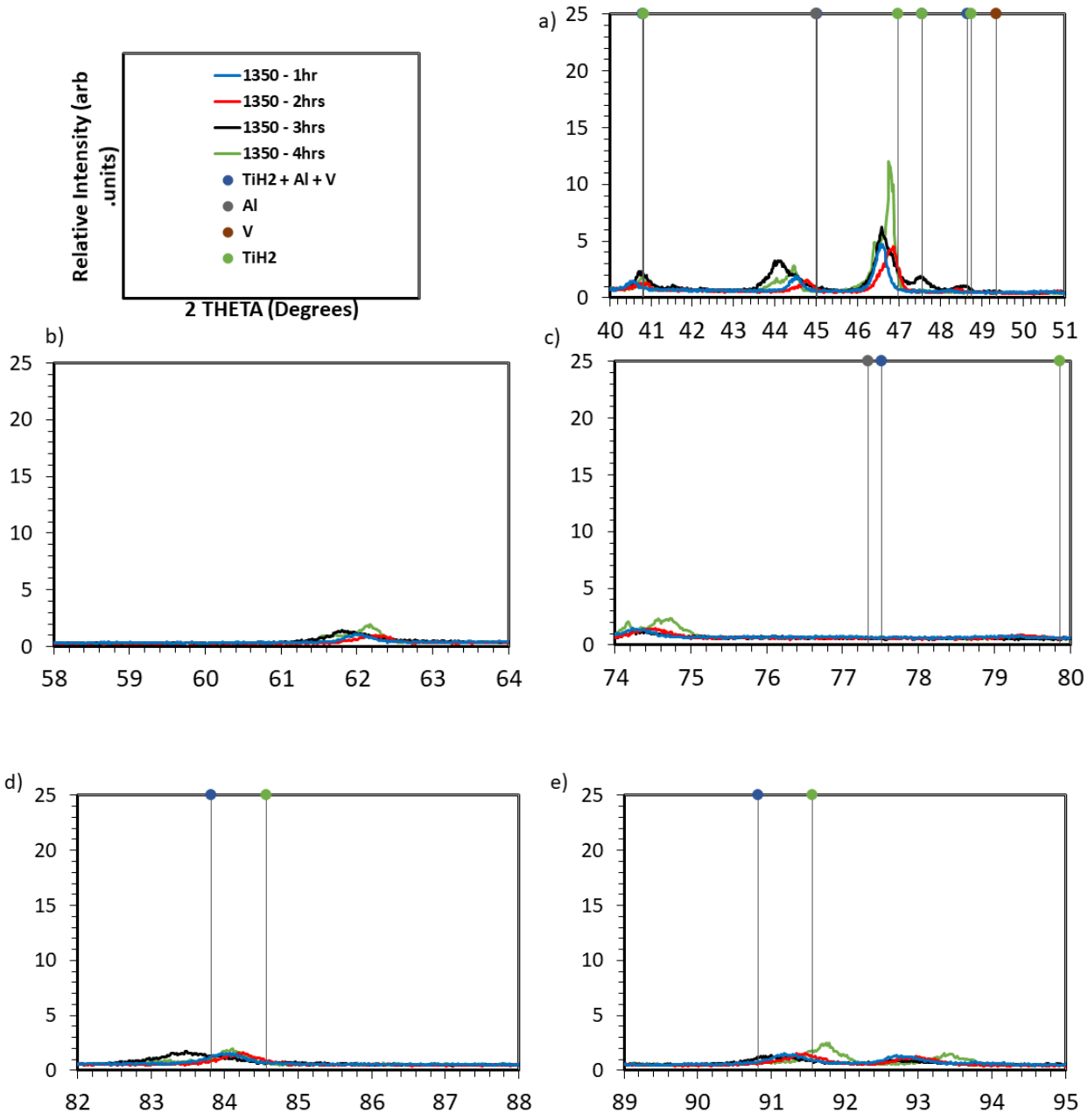

Figure A12: XRD spectrum for; TiH_2 + Al +V blend compacts sintered at 1350°C for 1hour, 2 hours, 3hours and 4 hours respectively and TiH_2 + Al + V powder blend, TiH_2 base powder, Al powder and V powder peaks represented by lines on a split 2 Theta of a) 40-51° b) 58-64° c) 74-80° d) 82-88 ° e) 89-95°.